REPORT

Final Summary Report

22 September 1967

THEORETICAL STUDIES ON THE RELATIONSHIP BETWEEN
THE THERMIONIC WORK FUNCTIONS OF REFRACTORY-METAL
INTERMETALLIC COMPOUNDS AND THEIR ELECTRONIC
AND CRYSTAL STRUCTURES

UNIVERSITY OF DENVER
DENVER RESEARCH INSTITUTE

N 67-36970

(ACCESSION NUMBER)   (THRU)

137

(PAGES)   (CODE)   26

CR#88549

(NASA CR OR TMX OR AD NUMBER)   (CATEGORY)

FACILITY FORM 602

THEORETICAL STUDIES ON THE RELATIONSHIP BETWEEN THE THERMIONIC WORK FUNCTIONS OF REFRACTORY-METAL INTERMETALLIC COMPOUNDS AND THEIR ELECTRONIC AND CRYSTAL STRUCTURES

Final Summary Report

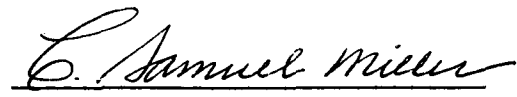- Submitted to -
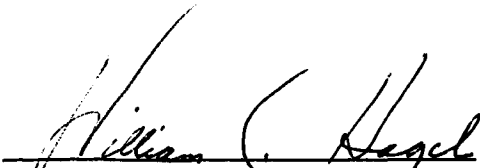
- Submitted by -

University of Denver
Denver Research Institute
Denver, Colorado

22 September 1967

APPROVED FOR THE
DIRECTOR BY:

William C. Hagel, Head
Metallurgy Division

PREPARED BY:

C. Samuel Miller
Graduate Research Assistant

ACKNOWLEDGEMENT

TABLE OF CONTENTS

LIST OF TABLES

LIST OF FIGURES

ABSTRACT

The Group VIA-Re binary systems are characterized by the presence of several intermediate phases. The σ phase is present in all of the systems, but the α-Mn phases occur in only the Mo-Re and W-Re systems. The occurrence of these intermediate phases appears to be governed largely by electronic factors and is predictable on the basis of electron/atom ratio.

The thermionic work functions of the intermediate phase materials were experimentally determined. A correlation between the work function and the screening of the outermost electrons in the Group VIA metals was found.

As might be expected for purely metallic substances, the work functions were relatively high, in the range 4.5 to 5.0 eV, and in each case were bracketed by the work functions of the pure constituents.

A discontinuous change in the average work function with composition is proposed, based on a thermodynamical treatment of the electron vapor.

CHAPTER I

INTRODUCTION

Statement of the Problem

In a study of materials for thermionic converter applications, Goodman and Homonoff[1] summarized the physical and chemical properties which determine the performance of a given emitter or collector in a thermionic converter as follows:

1. The apparent work function

2. The vapor pressure and rate of vaporization

3. The thermodynamic stability

4. The emittance

5. The thermal conductivity

The first of the above properties is of fundamental importance, since it is the difference between emitter and collector work functions which determines the output voltage of the converter. The work function and Richardson A of the emitter determine the current supplied by the converter.

The second and third properties criteria of Goodman and Homonoff are significant when one considers that a thermionic converter is a heat engine, limited by the Carnot efficiency. Although the theoretical efficiency is increased by employing high emitter temperatures, vaporization and thermodynamic stability problems associated with emitter materials become increasingly troublesome with increased temperature.

The last two material-property criteria are associated with radiative and conductive heat losses by the emitter. Not only is heat lost by such mechanisms not available for excitation of electrons from

the emitter, but the radiant energy may further decrease converter efficiency by heating the collector.

Upon consideration of various classes of materials available for converter applications with respect to the Carnot efficiency and the above property criteria, the Group VIA metals or their alloys are strongly suggested.

Tungsten and thoriated tungsten have long been used as thermionic emitters in electron tubes. Rhenium, a Group VIIA metal, and thoriated rhenium have been the subjects of more recent interest, since rhenium has emission properties at least the equal of tungsten and is much more resistant to the destructive "water-cycle" reaction commonly observed with tungsten.

Molybdenum and chromium are of interest, although used less frequently for electron-emission sources because of their lower melting points.

Because of the increased Carnot efficiency at high temperatures, refractory carbides, borides and nitrides have received considerable attention. Somewhat less interest has been shown in other intermetallic compounds such as the silicides and beryllides. For the above-mentioned compounds, polycrystalline specimens were utilized, having been prepared by painting, or by cataphoretic deposition of the finely divided material onto a tungsten substrate[2].

In the study here described, a rather different class of materials, whose thermionic properties have apparently been heretofore uninvestigated, was considered with a view toward possible thermionic converter applications. Specifically these materials are intermediate phases in the binary systems Cr-Re, Mo-Re and W-Re. These materials would seem to satisfy most of the other criteria of Goodman and

Homonoff for thermionic converters, with the possible exception of the Cr-Re material, which has a rather high vapor pressure.

All three of the Group VIA - Re binary systems are characterized by the presence of a σ phase of nominal composition Re_3M_2, where M is the VIA metal, or more properly $Re_{18}M_{12}$,[3] since the σ-phase has a unit cell of 30 atoms. The Mo-Re and W-Re systems are further characterized by the presence of another intermediate phase of nominal composition Re_3M, having the α-Mn structure with 58 atoms per unit cell.

The objectives of the investigation were as follows:

1. To prepare the intermediate-phase materials from the pure elements of the three binary systems, developing such equipment, processes and experimental techniques as might be required.

2. To fabricate specimens suitable for incorporation as emitters in a thermionic diode and to experimentally measure the thermionic emission properties of each of the materials.

3. To make use of the isotypic behavior of the three binary VIA-Re systems and differences between the σ and α-Mn structures within a single system for the purpose of establishing correlations of the work functions with other physical and chemical properties.

4. To evaluate the materials for possible thermionic-converter application with respect to their thermionic-emission characteristics.

Goodman and Homonoff have reviewed attempts by various investigators to make rigorous theoretical calculations of the work functions of metals. Such calculations have been successful only for the alkali and alkaline-earth elements.

As Hume-Rothery[4] pointed out, there is presently no satisfactory theory for the transition metals or their alloys. For these materials, investigators have been limited largely to semi-empirical correlations between various experimentally determined physical and chemical properties.

Such comparisons are not without value of course, and have frequently been used as a basis for predictions of other related properties, or of similar behavior in other metal systems.

Review of Previous Investigations

Chromium, molybdenum and tungsten comprise Group VIA of the periodic table and are members of the first, second and third long periods, respectively. Dickinson and Richardson[5] studied the phase equilibria of the binary systems Mo-Re and W-Re. Similar studies of these two systems, and the Cr-Re system as well, were made by Savitskii and Tylkina[6]. Although there are minor discrepancies between the proposed phase diagrams, there is general agreement that the Group VIA elements all combine with rhenium to form intermediate phases of fairly broad compositional extent, centered at about the nominal composition Re_3M_2 where M is the Group VIA constituent.

X-ray investigations revealed these intermediate phases were of the tetragonal σ-phase structure, $P4_2/mnm$, having 30 atoms per unit cell arranged in a "rumpled" hexagonal array as shown in Figures 1 and 2. Such phases are fairly common in other binary systems and occurs frequently in high-strength steels where they seriously impair the mechanical properties.
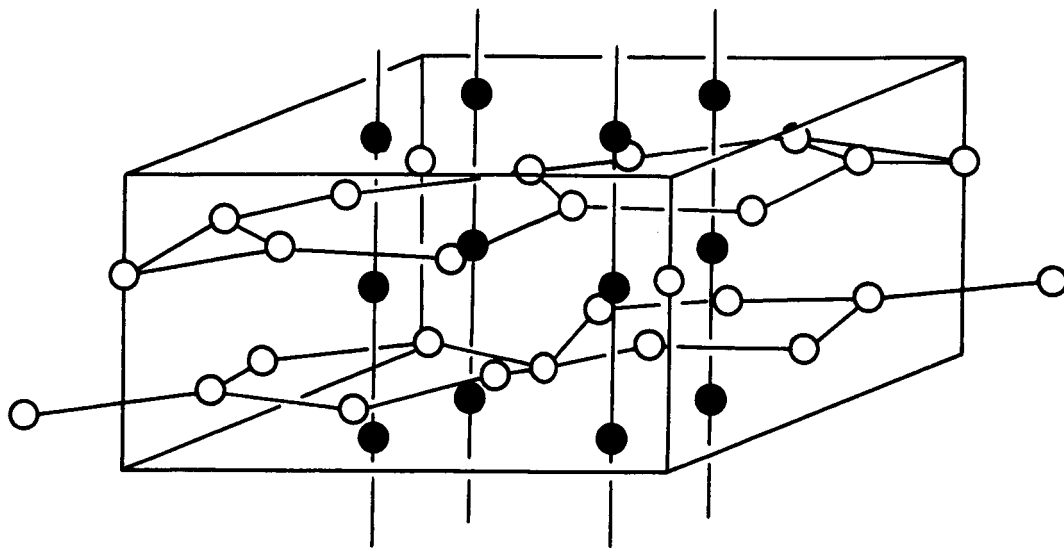
Figure 1.   Crystal Structure of the σ Phase
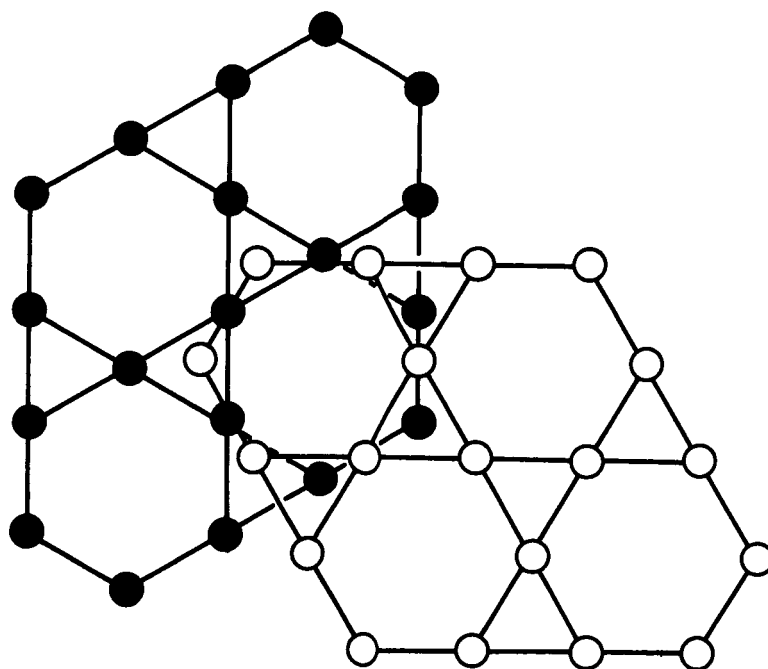
Figure 2.   Arrangement of Atoms in the "Rumpled" Hexagonal Layers
of the σ-Phase Structure

The Mo-Re and W-Re binary systems are further characterized by the appearance of another intermediate phase at the nominal composition Re$_3$M. This phase is much narrower in compositional extent than the σ phases and posses the cubic σ-Mn structure I$\overline{4}$3m with 58 atoms per unit cell. Re$_3$M is not present in the Cr-Re system.

The proposed phase diagrams of Savitskii and Tylkina for the three binary systems are shown in Figures 3, 4 and 5.

Numerous work-function determinations of pure elements during the period 1924-1949 have been summarized by Michaelson[7]. The following discussion concerning elemental work functions is the result of the author's critical review of the original papers cited by Michaelson and of several more recent investigations. The materials of interest are, of course, the three Group VIA elements, chromium, molybdenum, and tungsten, and the Group VIIA element, rhenium.

The work function of chromium has been measured by Wahlin[8] who reported a value of 4.60 eV for electrodeposited chromium. However, recent measurements have been made by Paddock and Magee[9] who reported a value of 4.42 ± .07 eV for high-purity chromium wire. The latter investigators speculated that the discrepancy between the two values could be caused either by Wahlin's introduction of hydrogen into the system for reduction of oxide surface layers or by differences in surface structure between the drawn wire sample and the electrodeposited layer of Wahlin. The preferred orientation of electrodeposited chromium in the [100] and [111] directions is well known, having been investigated earlier by Wood[10], and was cited by Paddock and Magee as a possible reason for the observed discrepancy. Their value of 4.42 eV is in better agreement with the photoelectric work function of 4.37 eV[11], and the work function determined by the contact potential-difference method, 4.38 eV[12].
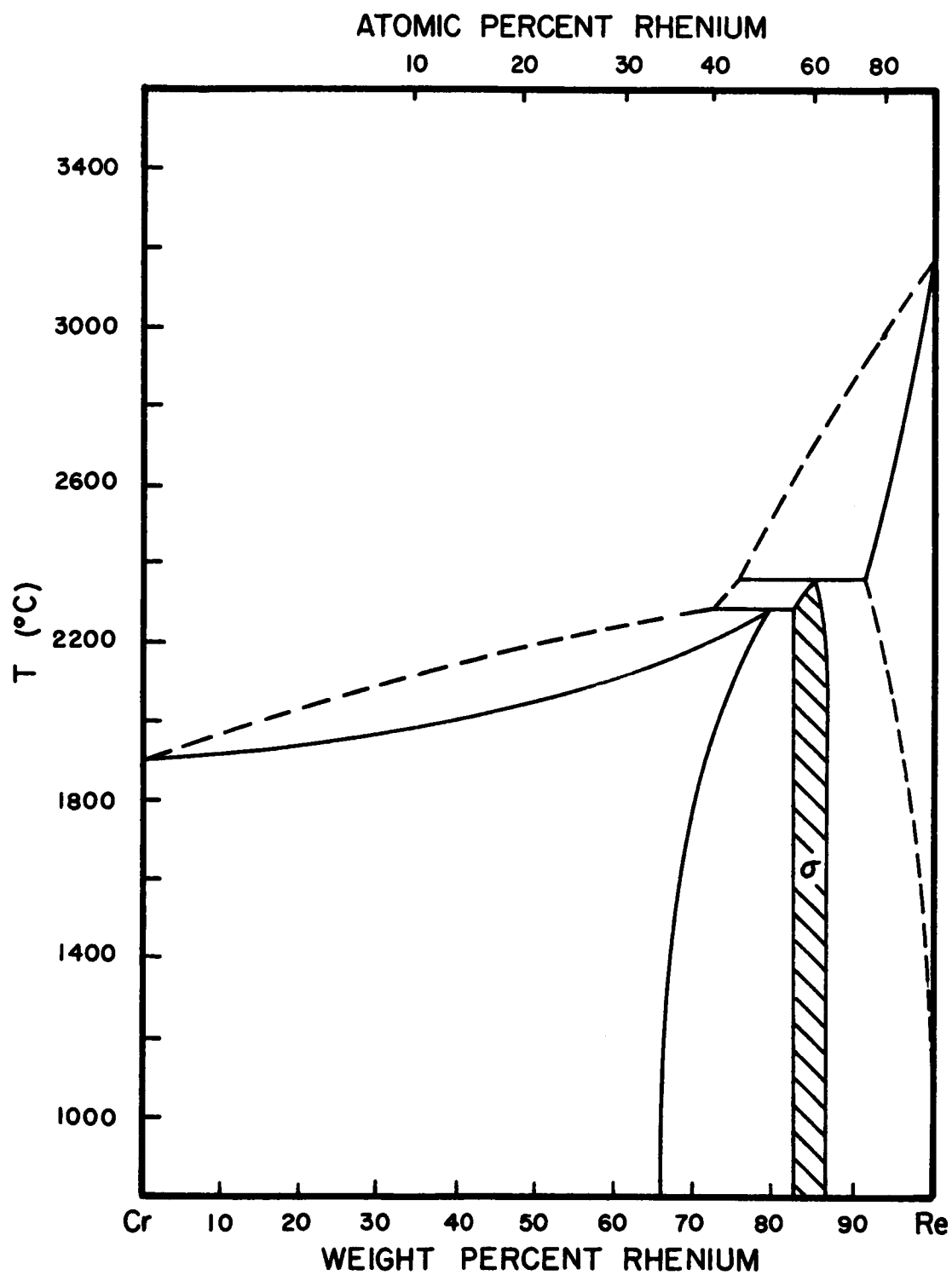
Figure 3.   Chromium-Rhenium Phase Diagram Proposed by Savitskii
and Tylkina
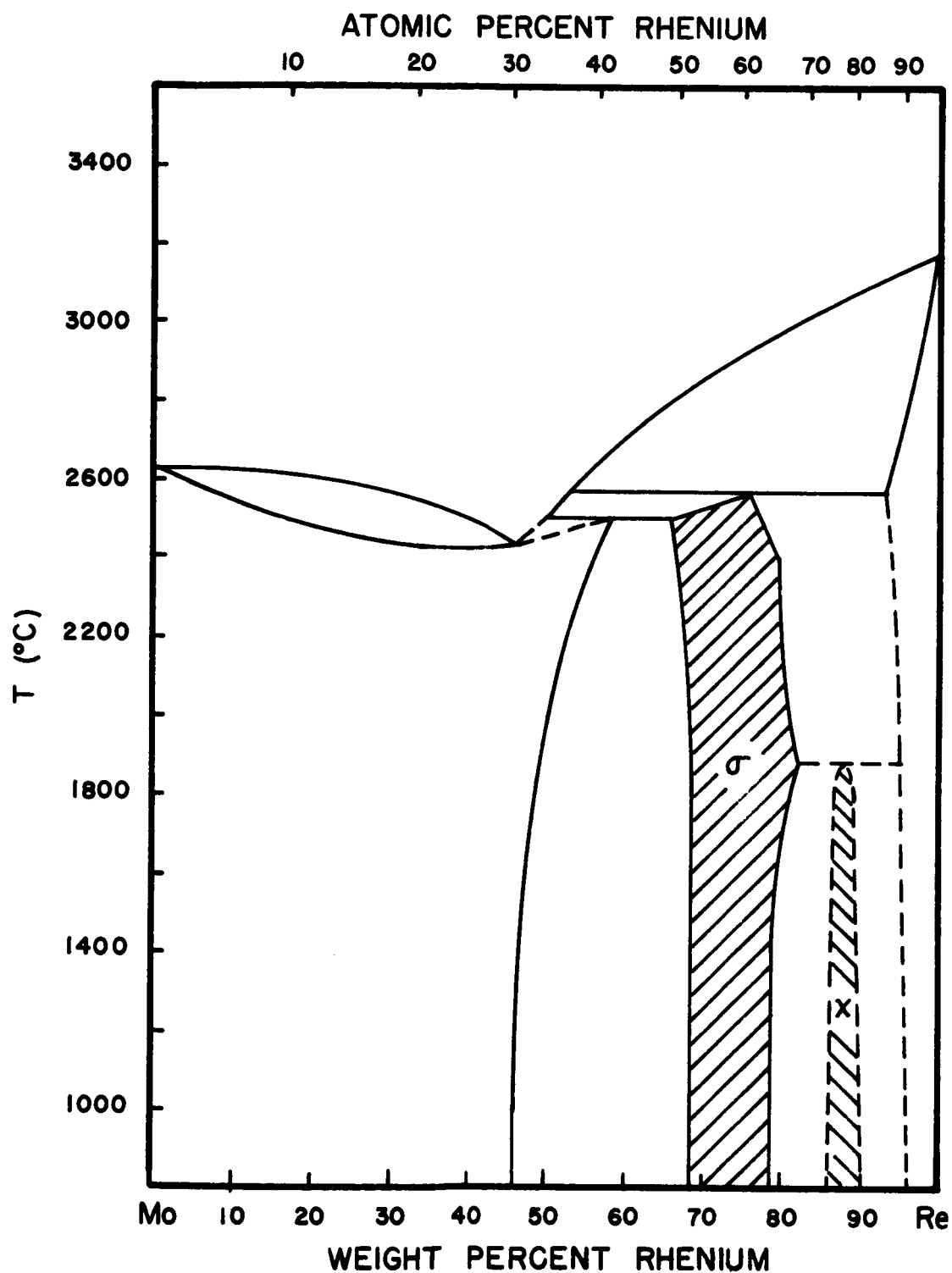
Figure 4.   Molybdenum-Rhenium Phase Diagram Proposed by Savitskii and Tylkina
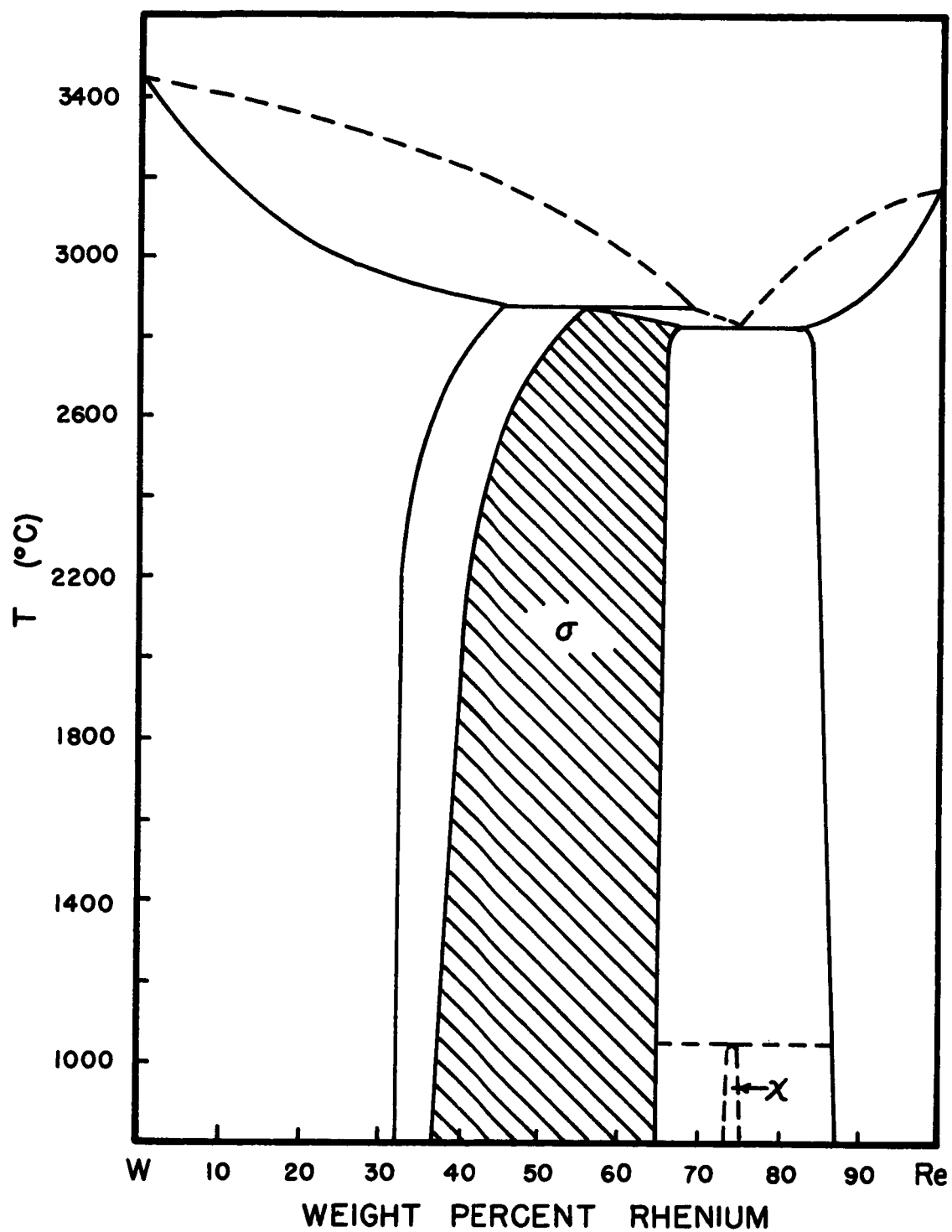
Figure 5.   Tungsten-Rhenium Phase Diagram Proposed by Savitskii and Tylkina

The work function of molybdenum has been the subject of numerous investigations[7]. Thermionic work functions reported vary between 4.15 and 4.44 eV; the differences are due in most cases to preferred orientation and possibly, since most of the work was done before 1940, to insufficiently high vacuum, with the attendant contamination of the surface layers by gaseous impurities.

The high-temperature properties of tungsten, and the extensive commercial and technological exploitation of these properties, have made tungsten the subject of more thermionic-emission investigations than any other metal. It is one of the few metals which has been studied in sufficient detail to determine the work functions for particular crystallographic orientations[7]. These values range between 4.25 and 4.69 eV, depending upon orientation. Nichols[13] reported the average work function for polycrystalline wires to be 4.53 eV. This value was recently verified by Jerner[14], who reported a value of 4.52 ± 0.09 eV, with a similar apparatus utilized for the present study.

The thermionic work function of rhenium was first determined by Agte et al.[15] who reported a value of 5.1 eV. In more recent work with rhenium electrodeposited on a tungsten substrate, Levi and Esperson[16] obtained a value of 4.74 eV. The failure of earlier investigators to make the Schottky correction and the large crystals formed by vapor-phase decomposition of rhenium salts were cited by Levi and Esperson as possible reasons for the high value obtained in the early work. Husmann[17] reported a value of 4.86 eV for porous rhenium.

The work functions of refractory metals have been exhaustively studied primarily because of their remarkable mechanical properties at high temperature. Similarly, the literature is replete with

thermionic-emission data on oxides and other materials having extensive commercial applicability. On the other hand, thermionic-emission studies of purely intermetallic compounds, particularly Group VIA-Re intermetallic compounds, have not received commensurate attention. Husmann[17] has studied tungsten-rhenium alloys in the tungsten-rich region of the binary system (compositions less than 26% Re). The author is unaware of any other investigations of the thermionic-emission characteristics of intermediate phases in the binary systems Cr-Re, Mo-Re and W-Re.

CHAPTER II

THEORETICAL ASPECTS OF THERMIONIC EMISSION

The Richardson-Dushman Equation

Consider a rectangular potential well of linear dimension, a, and depth, U. If the top of the well is defined as the zero of potential energy, the energy at the bottom of the potential well must be -U.

At 0°K, the maximum energy of electrons in the well is the Fermi energy, E_F. At temperatures greater than 0°K, some of the electrons gain enough additional energy to escape; this additional energy is defined as the work function, ϕ.

$$\phi = U - E_F \tag{2-1}$$

Since $E_F - U$ is the partial molal free energy of electrons, also known as the chemical potential, μ, then

$$\phi = -\mu. \tag{2-2}$$

We now assume a thermodynamic system composed of the solid emitter material in thermal equilibrium with a classical vapor of electrons. According to Herring and Nichols[18], the electron vapor behaves ideally at practically any attainable vapor density, with the potential energy between electrons being much less than kT.

If the vapor and solid phases are in thermal equilibrium, their chemical potentials must be identical.

$$\mu_{solid} = \mu_{vapor} \tag{2-3}$$

The statistical expression for the chemical potential of electrons in the vapor is given by

$$\mu = \frac{F - H_0^0}{N} = -kT \ln \frac{Q}{N}, \tag{2-4}$$

where N is the number of particles and Q is the total partition function, in this case the product of the one-dimensional translation and spin-partition functions.

$$Q = Q_{spin} Q_{trans} = 2 \sum_j g_j \exp \left[- \frac{\epsilon_j}{kT} \right] \qquad (2-5)$$

For ϵ_j in the above expression, we substitute the solution obtained in the familiar rectangular well problem.

$$\epsilon_j = \frac{n^2 h^2}{8 \, ma^2} \qquad (2-6)$$

Hence,

$$Q = 2 \sum (1) \exp \left[- \frac{n^2 h^2}{8 \, ma^2} \right]. \qquad (2-7)$$

If $h^2/8 \, ma^2 << 1$, the energy levels will be very close together and the summation can be replaced by an integral.

$$Q = 2 \int_{n=0}^{\infty} \exp \left[- \frac{n^2 h^2}{8 \, ma^2} \right] dn$$

$$= \frac{2(2\pi mkT)^{\frac{1}{2}} a}{h} \qquad (2-8)$$

Generalizing to three dimensions, one obtains the following result:

$$Q = Q_{spin} Q_x Q_y Q_z = \frac{2(2\pi mkT)^{3/2} V}{h^3} \qquad (2-9)$$

Substituting for Q in equation (2-4),

$$\mu = -kT \, \ln \left[\frac{2(2\pi mkT)^{3/2} V}{h^3 N} \right]. \qquad (2-10)$$

Since the electron vapor can be considered an ideal gas to a very good approximation,

$$\frac{V}{N} = \frac{kT}{P}. \qquad (2-11)$$

The chemical potential is now given by

$$\mu = -kT \ln \left[\frac{2(2\pi mkT)^{3/2} kT}{h^3 P} \right]. \tag{2-12}$$

Recalling that $\mu = -\phi$, and solving for P one obtains

$$P = \frac{2kT}{h^3} (2\pi mkT)^{3/2} \exp \left[-\frac{\phi}{kT} \right]. \tag{2-13}$$

In the kinetic theory of gases, the number of particles, z, striking a unit surface per unit time is given by

$$z = \frac{P}{(2\pi mkT)^{\frac{1}{2}}}$$

$$= \frac{4\pi mk^2 T^2}{h^3} \exp \left[-\frac{\phi}{kT} \right]. \tag{2-14}$$

Because the gas and solid are in equilibrium, the number of particles striking the solid surface per unit time is equal to the number leaving the surface.

Since the particles are electrons, with a negative charge, one can prevent their return to the emitter surface by placing a collector of appropriate shape in the vicinity. The result is a net flow of electrons, which of course comprises the emission current per unit of emitter area.

$$j = ze = \frac{4\pi mk^2 e T^2}{h^3} \exp \left[-\frac{\phi}{kT} \right] \tag{2-15}$$

where e is the electronic charge. By grouping the constants and rearranging slightly, one obtains

$$\frac{j}{T^2} = \frac{4\pi mk^2 e}{h^3} \exp \left[-\frac{\phi}{kT} \right]. \tag{2-16}$$

This is the well-known Richardson-Dushman equation. The factor $4\pi mk^2 e/h^3$ is numerically equal to 120 Amps/cm^2°K^2, and is frequently given the symbol A_0.

Stout[19] has pointed out that, ". . . although one can derive other thermionic emission equations from special models of electron emitters, and can evaluate constants of such models from emission results. The Richardson-Dushman equation remains the universal emission equation, independent of the kind of emitter, be it metal, monolayer or semi-conductor." This versatility comes about because the equation is derived from thermodynamical considerations, in which the electron vapor is assumed to be in equilibrium with the solid. The great advantage of this approach is that one is able to deal with processes taking place in the vapor without having to describe the solid in great detail.

The Work Function

Although the phenomenon of thermionic emission of electrons from solids is generally considered to be well understood, there has been widespread misinterpretation of experimental measurements, due in part, as Hensley[20] has pointed out, to the indiscriminate use of the term "work function." The "true" work function refers to the energy required to remove an electron from the surface of the solid to rest at infinity as in Figure 6.

The "true" work function is primarily a theoretical concept, for use in discussions involving a detailed model of the surface. For a practical surface, the true work function would be non-uniform and temperature dependent. Information obtained from experimental measurements is usually insufficient for its unique determination. Correct mathematical description of all but a few alkali-metal surfaces has proven most elusive, together with the fact that the imprecise definition of the vacuum level outside the surface leaves a degree of ambiguity in even the definition of the true work function. Hence, it is necessary to formulate additional definitions for experimentally determined work
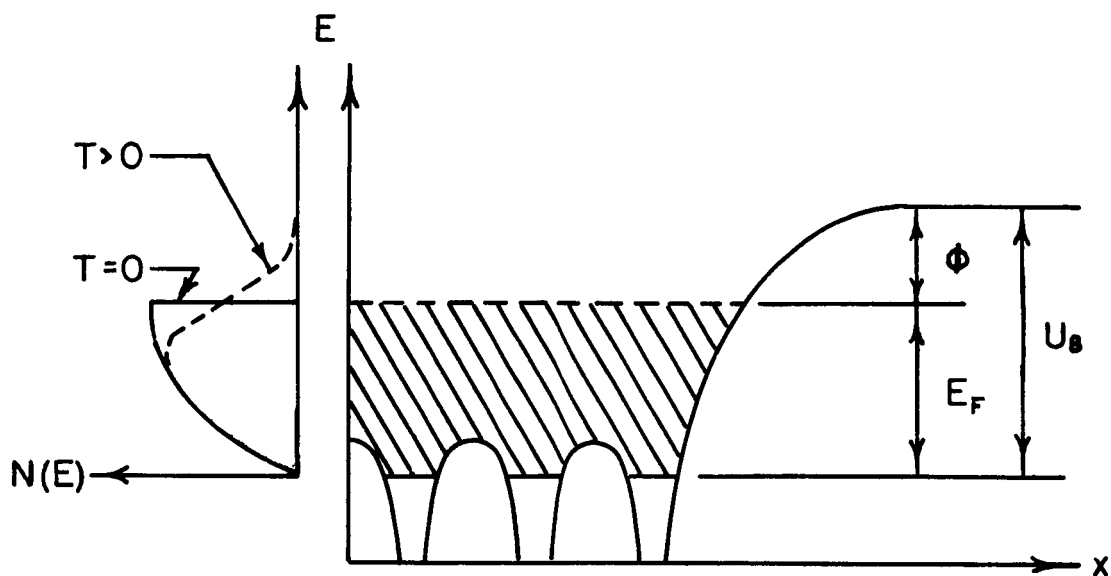
Figure 6.   Potential energy of Electron Near Atoms at the Surface of an
Emitter.   The Fermi Districution of Electrons in the Metal
is Shown at the Left

functions, which hopefully approximate the true work function to the extent that scientific comparison and speculation are possible. Hensley[20] suggests that experimentally determined work functions be preceded by a descriptive adjective to indicate the method by which they are obtained.

The "effective" work function ϕ_e is defined as the work function obtained by direct substitution of temperature and emission current density into the Richardson-Dushman equation (2-16), assuming no reflection of escaping electrons at the surface and taking the constant A to be A_0, 120 Amp/cm^2°K^2.

$$\phi_e = 2.303 \; kT \; \log \left[\frac{A_0 T^2}{j} \right] \qquad (2\text{-}17)$$

The "Richardson" work function ϕ_R, sometimes called the "apparent" work function is traditionally defined from the slope of a "Richardson plot" of $\log j/T^2$ vs $1/T$. The intercept of the plot is then $2.303 \log A_R$, where A_R is the so-called Richardson A, and is generally different from the theoretical A_0 of 120 Amp/cm^2°K^2 for reasons which are discussed in the following sections.

Effect of Electric Fields on the Work Function

Since the work function is the difference in energy between the height of the surface potential barrier and the Fermi energy, any change in the height of the potential barrier will be manifest as a change in the work function. As the negatively charged electron escapes the surface, it experiences an electrostatic attraction due to the net positive charge it left in the emitter, given to a good approximation by

$$F(x) = \frac{1}{4\pi\epsilon_0} \; \frac{e^2}{(2x)^2}, \qquad (2\text{-}18)$$

where x is the distance of the electron from the surface. The potential energy associated with this force is then given by

$$U(x) = \int_x^\infty F(x)dx = -\frac{e^2}{16\pi\epsilon_0 x} \; . \tag{2-19}$$

In the absence of an externally applied electric field, the electrons, influenced by the force given by equation (2-18), remain in the vicinity of the emitter as a space charge. This concentration of negatively charged electrons influences other electrons subsequently emitted, so that only a small fraction of the escaping electrons find their way to the collector, where they constitute the measured thermionic current.

In practice, the retarding effect of the space charge is eliminated by the application of an external accelerating electric field, E, which produces a constant force of magnitude eE on the electrons escaping from the emitter surface. The potential energy associated with the external field is therefore given by

$$U(x) = -eEx. \tag{2-20}$$

The effective potential energy is found by simply reducing the potential energy due to the "image" force, equation (2-19), by the potential energy associated with the external field, equation (2-20).

$$U(x) = -\frac{e^2}{16\pi\epsilon_0 x} - eEx \tag{2-21}$$

At a particular distance, $x = x_0$ from the emitter surface, the force on an electron due to the external field will be equal to the opposing image force.

$$\frac{e^2}{16\pi\epsilon_0 x_0^2} = eE \; , \tag{2-22}$$

from which

$$x_0 = \left(\frac{e}{16\pi\epsilon_0 E}\right)^{\frac{1}{2}} \; . \tag{2-23}$$

Substituting this result, x_0, for x in equation (2-21), yields the amount by which the barrier height is effectively reduced by application of the external field.

$$U(x_0) = -e \left(\frac{eE}{4\pi\epsilon_0} \right)^{\frac{1}{2}} \qquad (2-24)$$

Since the work function is the difference between the height of the potential barrier and the Fermi energy, equation (2-24) can also be regarded as the effective reduction of the work function due to the external field. Such reduction of the surface potential barrier by external fields is now known as the Schottky effect, after its discoverer, W. Schottky[22]. A schematic representation of the effect is shown in Figure 7.

With the modification of the work function by the external field, the Richardson-Dushman equation is similarly modified.

$$j = AT^2 \exp \left[-\frac{(\phi - e\sqrt{eE/4\pi\epsilon_0})}{kT} \right]$$

$$= AT^2 \exp \left[-\frac{\phi}{kT} \right] \exp \left[\frac{\sqrt{eE/4\pi\epsilon_0}}{kT} \right] \qquad (2-25)$$

The factor $\exp[\sqrt{eE/4\pi\epsilon_0}/kT]$ expresses the increase in the current density due to the external field, the remainder of the expression being regarded as the current density, j_0, that would be measured in the absence of an electric field, if such measurement was not precluded by the space charge discussed previously.

$$j = j_0 \exp \left[\frac{\sqrt{eE/4\pi\epsilon_0}}{kT} \right] \qquad (2-26)$$

In experimental determinations of work functions, including those of the present study, equation (2-26) is more useful in logarithmic form.

$$\log j = \log j_0 + \frac{\sqrt{eE/4\pi\epsilon_0}}{kT}$$

$$= \log j_0 + \frac{1.913}{T} E^{\frac{1}{2}} \qquad (2-27)$$
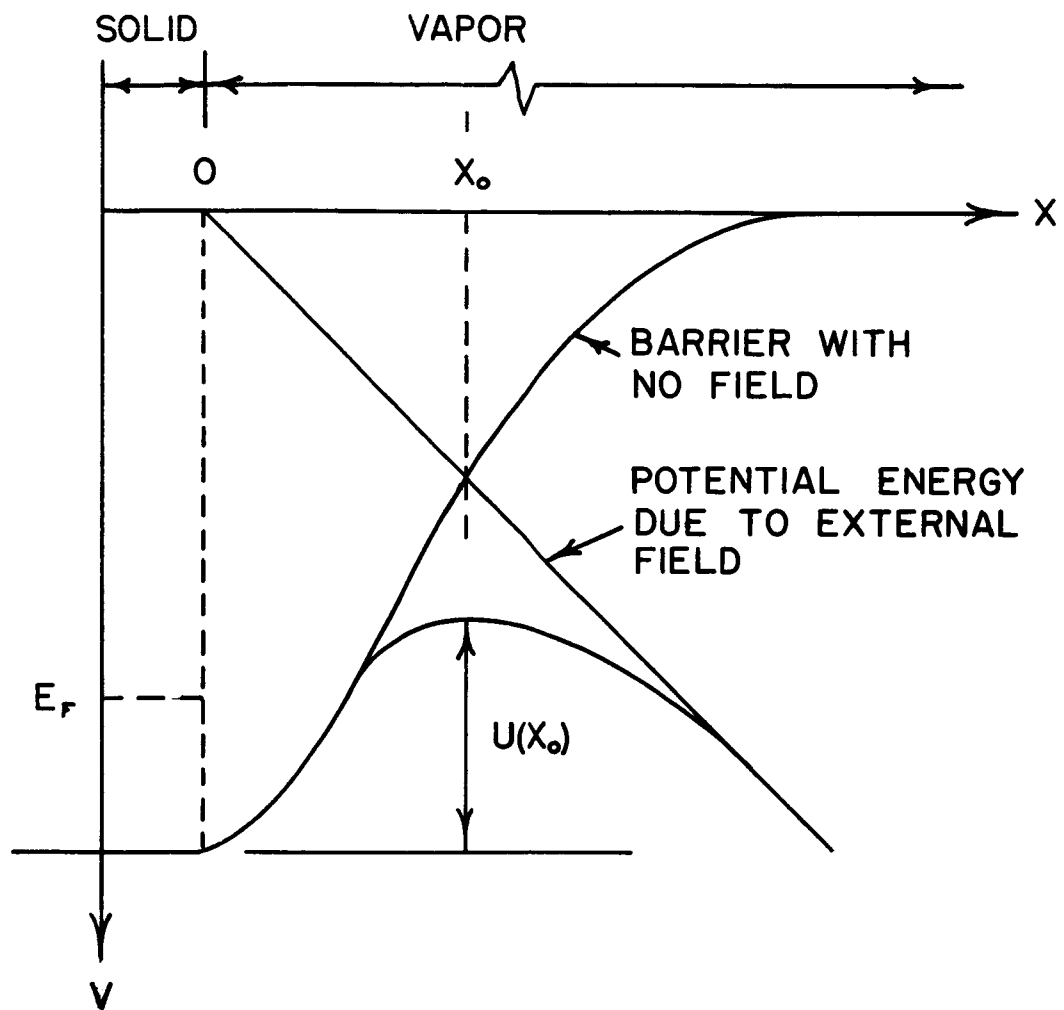
Figure 7. Reduction of Surface Potential Barrier by an External Electric Field

A plot of log j vs $E^{\frac{1}{2}}$, called a Schottky plot, is typically of the shape of the three such plots illustrated in Figure 8.

Since equation (2-27) is the equation of a straight line, of the form $y = b + mx$, the intercept, obtained by extrapolation of the linear portion of the Schottky plot to $E^{\frac{1}{2}} = 0$, yields the value of log j_0. The slope of the linear portion of the plot is inversely proportional to T.

The values of log j_0, obtained from the Schottky plots are now used in the Richardson-Dushman equation, written for convenience in logarithmic form.

$$\log j_0 - 2 \log T = \log A_R - \frac{\phi_R}{2.303k} \left(\frac{1}{T}\right) \qquad (2-28)$$

The form of equation (2-28), suggests a plot of log j - 2 log T vs $\frac{1}{T}$, again a straight line, having a slope $-\phi_R/2.303k$, from which ϕ_R is easily evaluated. Such a plot is shown in Figure 9.

The intercept of the Richardson plot yields the logarithm of A_R, which is associated with the temperature dependence of the work function, as discussed in the following two sections.

Hensley[20] claims that such plots are of little value and prefers to calculate the effective work function, ϕ_e, at a single value of the electric field just sufficient to overcome the space charge. He estimates the required potential difference between emitter and collector from the Langmuir-Child Law[24]. Jerner[14] and Paddock[25,9] have made limited use of Hensley's method in the interest of expedience, but both investigators expressed reservations regarding its use, as did Haas[26]. In the present work, Hensley's method was not used for the reasons discussed in the following sections.
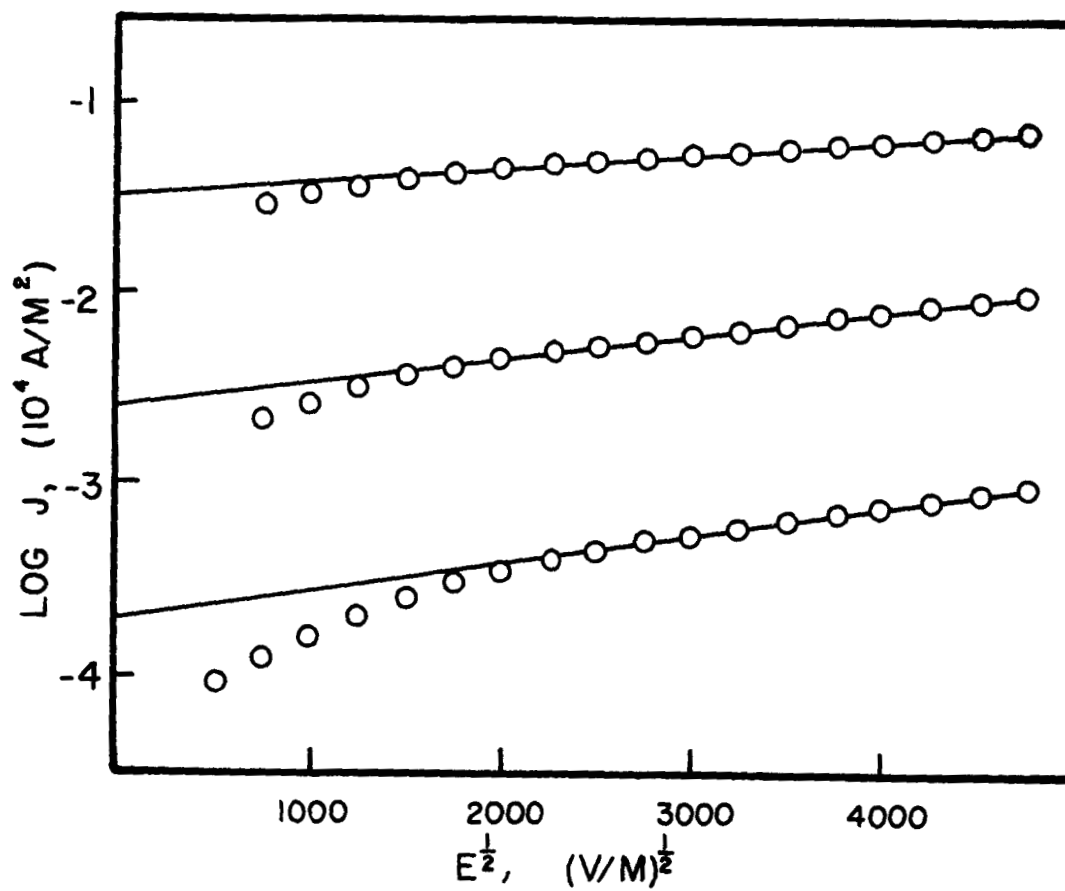
Figure 8.   Schottky Plots for a Uranium Carbide Emitter at Three
Temperatures
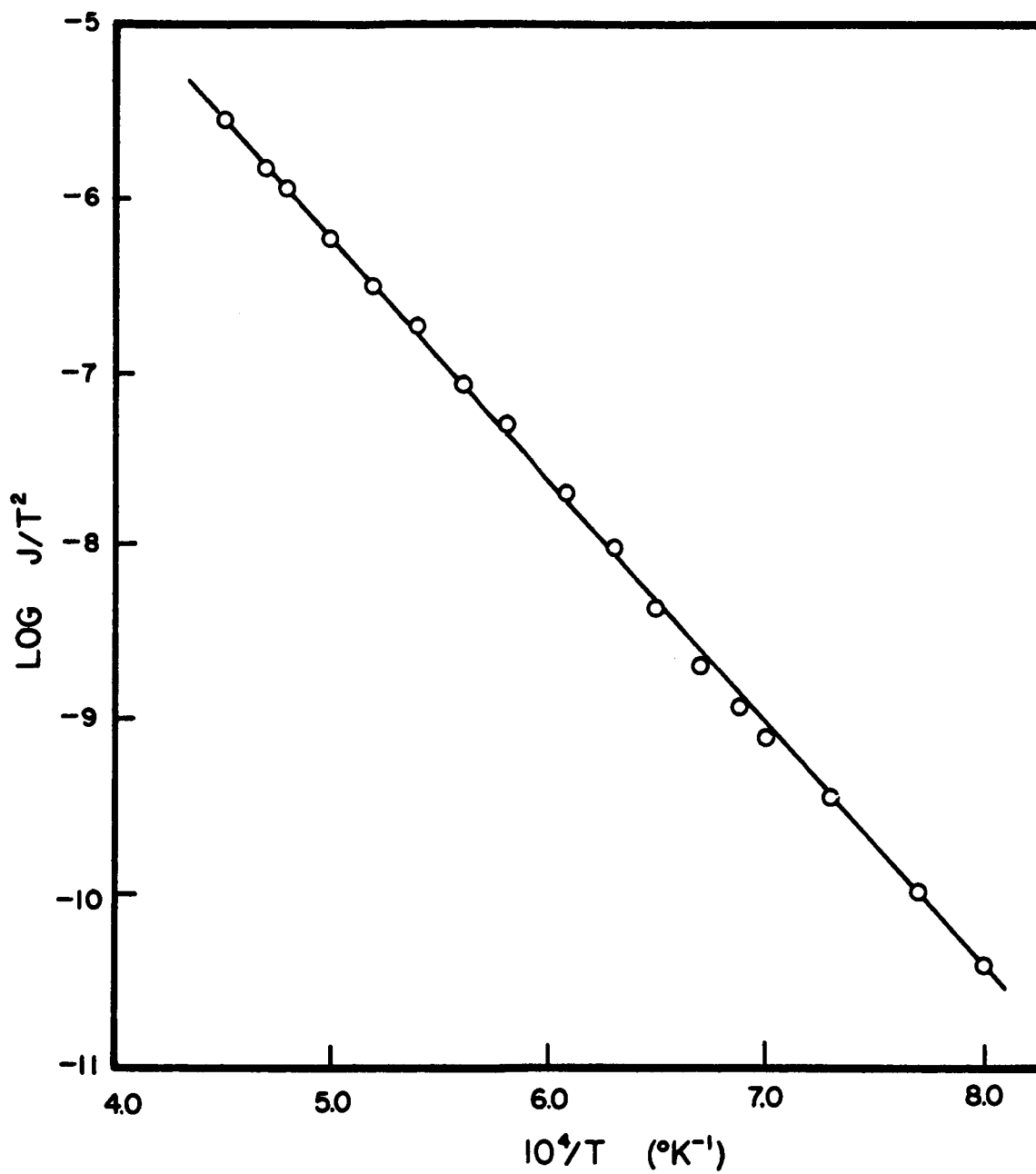
Figure 9. Richardson Plot of Thermionic Emission Data for Uranium Carbide

The Patch Effect

The work function of an emitter is dependent on the crystallographic orientation of the emitting surface. In a metal such as tungsten, atoms at the surface may have only 4, 5, or 6 nearest neighbors as compared with the 8 nearest neighbors of their interior counterparts, depending on orientation. The mirror-image model, assumed earlier in the discussion of the Schottky effect, does not account for these differences in orientation, and so is only approximately correct.

In polycrystalline materials, the emitting surface may include patches of various orientations, and hence various work functions. Indeed, if the thermionic diode utilizes cylindrical geometry, as is common practice in order to obtain suitable accelerating fields with a modest potential source, even a single crystal specimen will present a surface of varying orientation about its circumference.

Juenker[27] has plotted the work function of tungsten as a function of orientation, using the data of Smith[28] and field emission data of Müller[29], however, theoretical prediction of such work functions is beyond the capability of the present technology. Juenker has proposed a qualitative interpretation of experimental data based on the two-patch "checkerboard" model. The model assumes two crystallographic orientations, one having a low work function ϕ_L and the other a high work function ϕ_H.

Figure 10 shows the two patch potentials and the superposition of the mirror-image potential on each.

Electron emission in a weakly accelerating field is chiefly from the low function patches with a small, nearly constant contribution from the higher work-function patches, the result being characteristic of some "average" work function $\overline{\phi} \cong 1/2 \; (\phi_H + \phi_L)$. At much higher fields, both types of patches contribute to the emission current, but the current
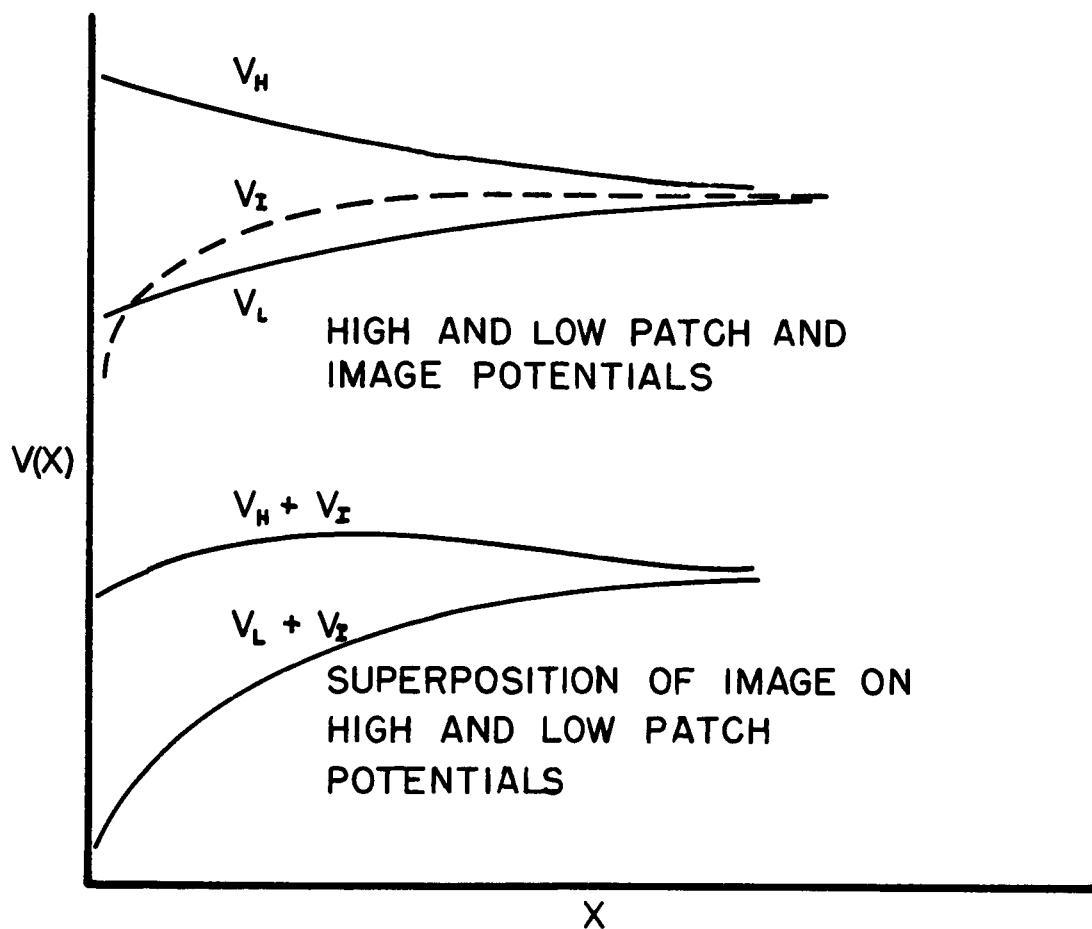
Figure 10. Superposition of Image Potential on Patch Potentials of High and Low-Work Function Patches

is characteristic of the low work function ϕ_L. Patch effects are fre-
quently manifest in Schottky plots of sigmoidal shape, as illustrated
schematically in Figure 11.
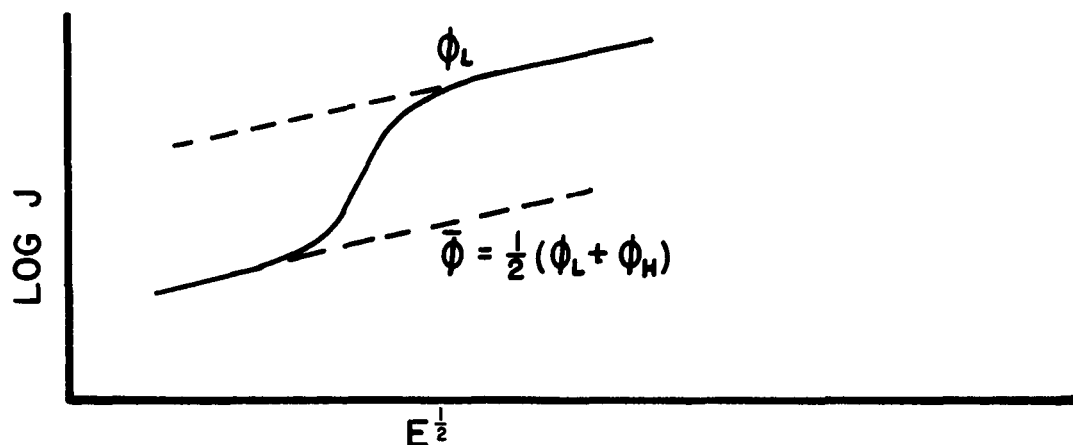
Figure 11. Schematic Representation of a Schottky Plot
for a Hypothetical Two-Path Emitter

The anomalous region is shown in an arbitrary position in
Figure 11. $E_p \cong \delta\phi/\Delta y$ where $\delta\phi$ is the difference between the two
work functions and Δy is the patch width. Such curves are rather
common in course-grained materials such as tantalum. For fine-
grained metals, such as molybdenum, patch breaks in the Schottky
curve may be more numerous and complicated[27].

Temperature Dependence of the Work Function

In the Richardson-Dushman equation (2-16), it will be recalled
that ϕ_t, the "true" work function, is defined as the difference in energy
between the Fermi level, E_F, and the surface potential barrier. A_0 is
$4\pi mk^2 e/h^3$, a universal constant numerically equal to 120 $Amp/cm^2{}^\circ K^2$.
However, experimental determinations of the work function by the
Richardson plot method, including invocation of the Schottky theory to

account for the effect of the accelerating field, yield values of A_R which are, in general, not equal to the theoretical value of 120 Amp/cm^2°K^2. The discrepancy occurs because several important aspects of thermionic emission are not taken into account by the Richardson-Dushman equation:

1. The surface potential barrier and the Fermi level, which define the true work function, are both temperature-dependent.

2. The theoretical evaluation of the current density is seldom correct, because of surface inhomogeneities called "patches" discussed in the previous section. In general, patch effects are themselves temperature dependent and thus contribute to the temperature dependence of the work function.

The temperature dependence of the surface potential energy, also known as the electron affinity, is not well understood, and only semi-quantitative explanations are presently available. Wigner and Bardeen[30] and later Herrmann and Wagener[31] considered the formation of a surface dipole layer on a hypothetical clean surface in their quantum-mechanical calculations of the work function. The calculations achieved only limited success, notably for the alkali metals. Nevertheless, there is little doubt that such dipole layers exist. Their modification due to thermal expansion is presently believed to be an important contributor to the temperature coefficient of the surface potential barrier. Herring and Nichols[18] made a semi-quantitative estimate of the magnitude of the effect, and concluded that the temperature coefficient for a metal such as tungsten would be of the order of only 1/2 k, which is much too small to account for the temperature coefficient observed experimentally. Contributions from other factors such as roughening of the surface by thermal vibrations, or increased extension of the electron cloud outside the solid

surface due to the thermal energies of the electrons are thought to be even smaller. Homonoff and Ruby[32] conclude that the temperature coefficient of the surface potential barrier from all causes makes only a small contribution to the temperature dependence at the work function in any case.

The temperature dependence of the Fermi level is somewhat more quantitative and direct, and calculations, for some metals at least, yield values in better agreement with experiment.

The Fermi energy is given by:

$$E_F = E_{F^0} \left[1 - \frac{\pi^2}{12} \left(\frac{kT}{E_{F^0}} \right)^2 + \ldots \right] . \tag{2-29}$$

E_{F^0} is the Fermi energy at the absolute zero, and given by the quantum free electron theory:

$$E_{F^0} = \frac{h^2}{8m} \left(\frac{3N}{\pi V} \right)^{\frac{2}{3}} \tag{2-30}$$

where N/V is the number of electrons per unit volume of the metal.

The correction factor $\left[1 - \frac{\pi^2}{12} (kT/E_{F^0})^2 + \ldots \right]$ does not account for the observed temperature dependence of the work function. As Homonoff and Ruby[32] point out, E_f for tungsten is changed by only .004 eV as the temperature is increased to 2000 K, an effect which may be dismissed as negligible. A much better agreement is obtained by considering the linear coefficient of expansion, β, which causes the volume, V, in equation (2-30) to change as follows:

$$V = V_0 (1 + \beta T)^3 , \tag{2-31}$$

where V is the volume at any temperature, T, and V_0 the volume at the absolute zero.

Substituting for V in the expression for E_F in equation (2-29), and neglecting the second order correction, one obtains

$$E_F = \frac{h^2}{8m} \left[\frac{3N}{\pi V(1+\beta T)^3} \right]^{\frac{2}{3}}$$

$$= E_{F^\circ} \left[\frac{1}{(1+\beta T)^2} \right]$$

$$\cong E_{F^\circ} (1-2\beta T). \qquad (2-32)$$

The change in E_F for polycrystalline tungsten, $2\beta T$, is now about 0.14 eV at 2000°K, the temperature coefficient being -7×10^{-5} eV/°K, which agrees well with the experimental value given by Homonoff and Ruby[32] -6×10^{-5} eV/°K. Unfortunately, such agreement is not achieved for all metals because Wohlfarth[33] has shown that equation (2-32) does not correctly describe the temperature dependence of the Fermi energy if the highest energy bands overlap, or if E_F is very close to the top or bottom of the bands.

Furthermore, equation (2-32) predicts that E_F is always decreased by an increase in temperature, which would correspond to a positive temperature coefficient of the work function in all cases. Experimentally, one occasionally observes negative temperature coefficients[32].

Another factor generally considered temperature independent, may nevertheless affect the value of A_R and hence be inadvertently attributed to the temperature dependence. This is the so-called reflection coefficient which is discussed by Hensley[20] and by Herring and Nichols[18]. A fraction, r, of the total number of electrons having the required energy fail to escape from the surface because they undergo quantum-mechanical reflections at the surface potential barrier. The fraction which do succeed in surmounting the barrier is therefore (1-r), a quantity referred to as the transmission coefficient, and often included in the Richardson-Dushman equation as

$$\frac{j}{T^2} = A(1-r) \exp\left[-\frac{\phi}{kT}\right] \qquad (2-33)$$

Although the reflection coefficient may be of importance in some materials, Herring and Nichols have pointed out that for clean metallic emitters it is ordinarily less than 0.05, and therefore usually neglected. When one considers that the situation is further complicated by such factors as crystal faceting, poisoning of the emitter surface by impurities, and preferential adsorption of gaseous impurities by patches of particular orientation, all of which are temperature dependent processes, the complexity of the problem becomes forcefully apparent. Consequently, in experimental determinations of work functions, it is common practice to simply combine the numerous and complex effects into a single temperature coefficient of the work function, α. The true work function is considered to be approximated by the sum of the temperature-independent apparent work function and a linear term which expresses the temperature dependence.

$$\phi_t = \phi_R + \alpha T \qquad (2-34)$$

Substitution of this expression into the Richardson-Dushman equation yields the following result:

$$\frac{j_0}{T^2} = A_0 \exp\left[-\frac{\alpha}{k}\right] \exp\left[-\frac{\phi_R}{kT}\right], \qquad (2-35)$$

where the product $A_0 e^{-\alpha/k}$ is now presumed to be equal to the Richardson constant A_R. The temperature dependence is therefore given by

$$\alpha = 2.303k \log \frac{A_0}{A_R}. \qquad (2-36)$$

While the effective work function, ϕ_e, may well approximate the true work function, because it is temperature dependent, the Richardson-slope method is considered preferable by many investigators because it

does take into account, although not individually, the effects of the elec-
tric fields, of patches and the uncertainty of the effective emitting area.
It is presently believed, according to Homonoff and Ruby[32], that the
Richardson-slope method yields the best values of the work function
obtainable by direct thermionic-emission measurement.

For the present study, choice of the Richardson slope method
over the effective work function method proposed by Hensley[20] can best
be justified by pointing out several of the disadvantages of the latter
method related to the effects of the undesirable but necessary electric
fields.

Recall that Hensley's method requires a field just sufficient to
overcome the effect of the space charge, the cathode-anode voltage
having been estimated by the Langmuir-Child Law. For the cylindrical
diode geometry of the study here described, the appropriate Langmuir-
Child equation is

$$j = \frac{14.6 \times 10^{-6} V^{\frac{1}{2}}}{r_a \beta^2} , \qquad (2-37)$$

where V is the cathode-anode voltage, r_a is the radius of the anode and
β is a constant approximately equal to unity for ratios of anode-cathode
radii greater than 10. Since r_a appears in the Langmuir-Child equation,
it is immediately apparent that comparison with data of other investiga-
tors poses a minor problem, unless the anode radii are identical.
Furthermore, inspection of a series of Schottky plots reveals that the
field below which log j deviates from the linear portion of the plot
increases with decreasing temperature, whereas the Langmuir-Child
equation is independent of temperature. Preliminary calculations of V
for the diode of the present study, which has an anode radius of 0.953 cm,
were made at various temperatures using the data of Haas and Jensen[12]

for uranium carbide, and of Jerner[14] for pure polycrystalline tungsten. In each case, the cathode-anode voltage predicted by the Langmuir-Child Law was lower than the voltage at which the experimentally determined current densities departed from the linear portion of the Schottky plots for measurements at low temperatures.

Of course, it is possible to increase the field arbitrarily to a sufficiently high value, but desirable comparison with data of other investigators is further sacrificed.

On the other hand, the zero-field values resulting from invocation of the Schottky theory used in the Richardson slope method are unambiguous and standard and permit easy comparison. Furthermore, the Schottky plots may themselves provide useful information. For example, the shift of the anomalous region during a series of runs might indicate, as in the case of experiments by Paddock and Magee[9], that extensive grain growth had occurred.

Current Density and Electric Field Strength in a Cylindrical Diode

The current density is obtained by dividing the emission current by the area of the emitting surface. For the cylindrical diode of the present study, this area is simply the product of the emitter circumference, $2\pi r_c$, and the length of the central anode, ℓ. Hence, for an emission current I, the current density is given by

$$j = \frac{I}{2\pi r_c \ell} . \tag{2-38}$$

The relationship between the cathode-anode potential and the electric field strength is obtained in the conventional way, by use of Gauss' Theorem and symmetry arguments. The cylindrical cathode of radius r_c is surrounded by a concentric anode of radius r_a. If the anode

is positive with respect to the cathode, the electric field is directed, by convention, from the anode to the cathode as shown in Figure 12.

(a)   **(b)**
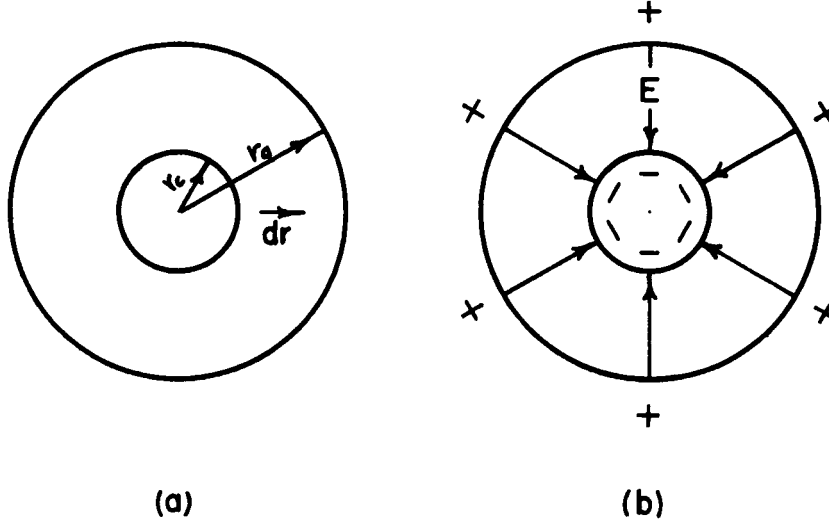
Figure 12.   Cylindrical Diode Configuration
and the Radial Electric Field

A hypothetical Gaussian surface is constructed in the form of a concentric cylinder of radius r_c, the radius of the cathode, with length, ℓ, the length of the collector anode, so that it encloses a length, ℓ, of the cathode having a charge, -q at any instant in time. Gauss' Theorem then states that the scalar product of the field and the area, taken over the entire area of the closed Gaussian surface, is proportional to the enclosed charge. Mathematically,

$$\epsilon_0 \oint \vec{E} \cdot \vec{ds} = -q \,, \tag{2-39}$$

where ϵ_0 is the permitivity in vacuum, and $\vec{ds}$ is an element of area having a direction normal to the surface. For this particular case, $\vec{ds}$ is always anti-parallel to the field which, by convention, is directed from positive to negative. Since there are no axial field components, the end caps of the Gaussian surface make no contribution to the vector integral, and integration over the curved portion remaining gives the following result:

$$\epsilon_0 \, E \, (2\pi r_c \ell) = q \tag{2-40}$$

from which,

$$E = \frac{q}{2\pi\epsilon_0 \ell r_c} \,. \tag{2-41}$$

The difference in potential between anode and cathode is also defined in terms of a vector integral:

$$V = -\int_{r_c}^{r_a} \vec{E} \cdot \vec{dr} \tag{2-42}$$

Here $\vec{dr}$ is a segment of the radius vector along which the integration is to be performed. Substituting for $\vec{E}$ in the equation, we have

$$V = -\int_{r_c}^{r_a} \left(\frac{\vec{q}}{2\pi\epsilon_0 r_c \ell} \right) \cdot \vec{dr} \,. \tag{2-43}$$

Recalling once more that $\vec{E}$ is directed inward, and is therefore anti-parallel to $\vec{dr}$, the following result is obtained:

$$V = \frac{q}{2\pi\epsilon_0 \ell} \, \ell n \, \frac{r_a}{r_c} \tag{2-44}$$

Upon inspection of the expression for V, it is apparent that the factor $q/2\pi\epsilon_0 \ell$ is, except for a factor $1/r_c$, identical with the expression for E. Hence:

$$\frac{V}{r_c} = E \, \ell n \, \frac{r_a}{r_c} \,, \tag{2-45}$$

from which

$$E = \left[\frac{1}{2.303 \, r_c \, \log \, (r_a/r_c)} \right] V \,. \tag{2-46}$$

The foregoing is usually derived in more general form[34] by constructing the Gaussian surface of a general radius r, intermediate

between the cathode and anode radii. Such generality is unnecessary for the present investigation, however, since the electric field of particular interest is that which is present at the emitter surface.

In practice there are end effects which would cause the electric field to have non-radial components. For this reason, guard anodes are located longitudinally above and below the central anode so as to preserve the wholly radial character of the field in the region of the central anode. The diode is more completely described in the following chapter.

CHAPTER III

EQUIPMENT AND EXPERIMENTAL PROCEDURE

Preparation of Intermediate-Phase Materials

For the reasons discussed in the following section on specimen preparation, it was necessary to first prepare the intermediate-phase materials from the appropriate elements, and then reduce the materials by grinding to the smallest practical particle size. Figure 13 illustrates the various processes developed to accomplish this objective.

All of the intermediate phases were prepared from the pure elements obtained from the suppliers in the form of fine powders. Minus-300 mesh powders of molybdenum and tungsten were procured from Sylvania Electric Products, Chemical and Metallurgical Division, Towanda, Pennsylvania. The rhenium was obtained as minus -300 mesh powder from Chase Brass and Copper Company, Rhenium Division, Waterbury, Connecticut. Spectrographic analyses provided with the powders are shown in Table I.

The chromium was obtained in the form of chunks of fairly large crystals of iodide-process material from D. T. Klodt of the Denver Research Institute. No chemical analysis was available, but Klodt indicated that the chromium was of the highest obtainable purity. The chromium crystals were reduced to minus-200 mesh particles with a mortar and pestle.

The desired compositions were obtained by blending the various powders in the correct proportions in a glass vial turned by a small roller mill. A steel die was then used to press the materials into powder compacts which served as charge in the subsequent arc-melting operation.
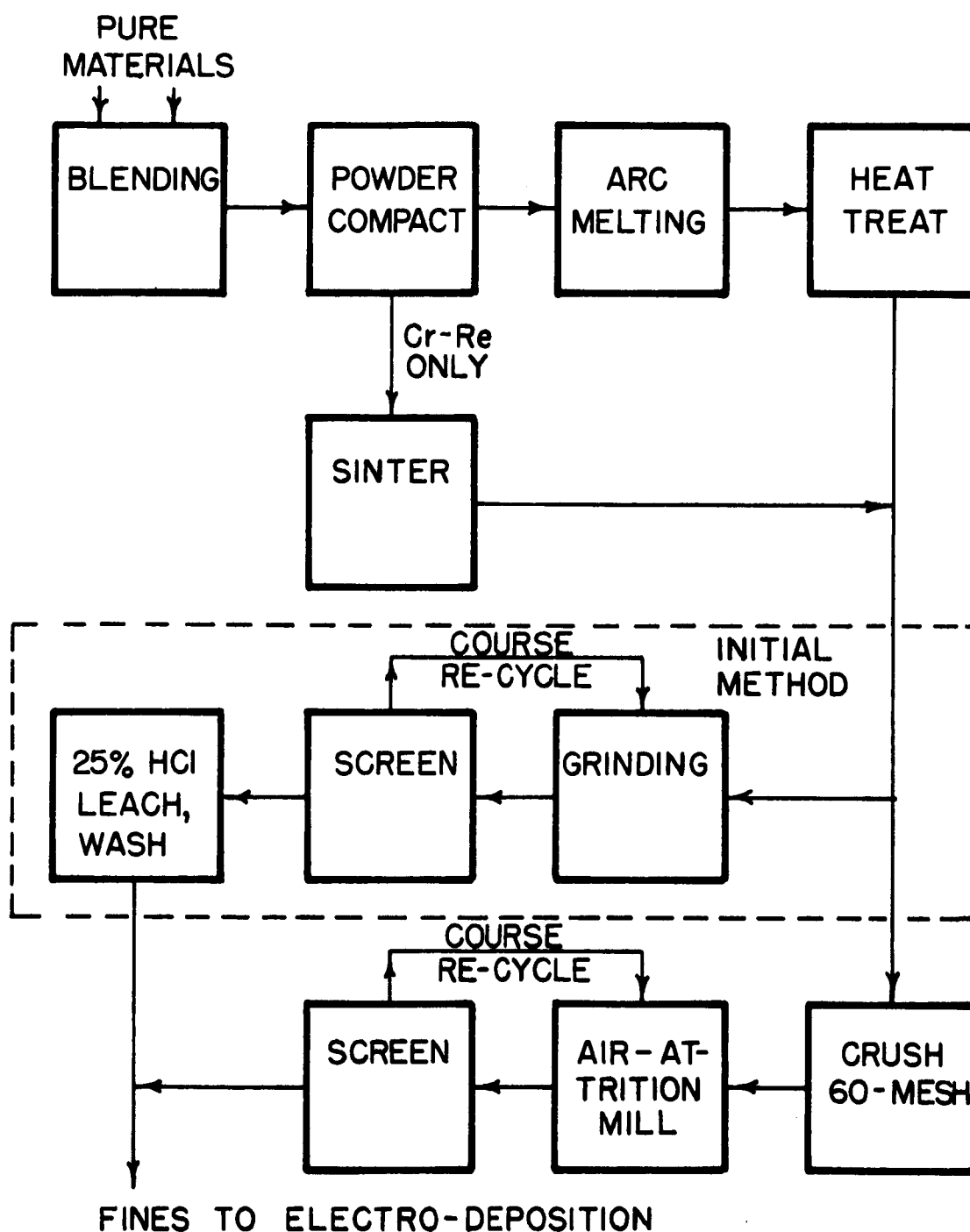
Figure 13. Preparation of Intermediate-Phase Materials for Electro-
phoretic Deposition

TABLE I

SPECTROGRAPHIC ANALYSES OF MOLYBDENUM, TUNGSTEN
AND RHENIUM POWDERS USED IN PREPARATION OF
REFRACTORY INTERMEDIATE-PHASE MATERIALS

	Indicated Impurity (ppm)		
Impurity	Molybdenum	Tungsten	Rhenium
Al	7	< 20	<1
Ca	--	--	<1
Cr	38	< 20	<1
Cu	5	< 20	<1
Fe	6	--	15
Mg	4	--	<1
Mn	1	< 20	--
Mo	--	< 20	<1
Ni	26	< 20	<1
Nb	--	<100	--
Pb	9	--	--
Si	19	<150	<1
Ta	--	< 50	--
Ti	--	< 20	--
C	--	< 30	--
H	--	< 1	--
N	--	< 5	--
O	--	< 10	--

The high vapor pressure of chromium precluded arc melting of the Cr-Re intermediate phase material. Instead, the powder compacts were sealed in a tantalum tube and heat treated in a vacuum furnace for two hours at 1800C. This powder-metallurgy technique proved to be a successful way to circumventing the vapor pressure problem. Since the material is subsequently ground into fine powder, porosity is not a problem.

The Mo-Re and W-Re green powder compacts were melted in a D.C. arc furnace, utilizing a water-cooled copper crucible and a water-cooled tungsten electrode. Power was supplied by a Lincoln arc-welding generator with a continuous rating of 900 Amps. The furnace is provided with a manifold which permits either vacuum or inert-gas melting. The Mo-Re and W-Re alloys of the present study were melted in a purified argon atmosphere. A 30-gram charge typically required a current of about 300 Amps for which the voltage was about 16-18 Volts. The furnace also features a manipulating rod; upon cooling, the button-like charges are turned over and remelted repeatedly to insure homogeneity.

Metallographic and X-ray analyses of the as-cast "buttons" revealed that all of the materials contained more than one phase. Heat treatments were developed to bring about the desired transformations to the single-phase. The schedules for the various compositions are given by Table II. The effectiveness of these heat treatments in converting the as-cast alloys to single-phase materials is indicated by Figures 14 through 17. X-ray diffraction analyses were also utilized to verify the presence of a single phase.

TABLE II

HEAT TREATMENT OF ARC-CAST MATERIALS TO
OBTAIN A SINGLE PHASE

Composition Stoichiometric	Nominal (w/o)	Structure Type	Heat Treatment Temp (°C)	Time (Hr)
Re_3Mo_2	74Re-26Mo	σ	2300	0.75
Re_3Mo	85Re-15Mo	a-Mn	1850	4.0
Re_3W_2	55Re-45W	σ	2300	0.75
Re_3W	74Re-26W	a-Mn	1850	4.0
Re_3Cr_2*	85Re-15Cr	σ	1800	2.0

---

* The Re_3Cr_2 was not arc cast. It was prepared by sintering the green powder compact in a sealed tantalum tube to preclude excessive loss of chromium normally experienced in arc melting.
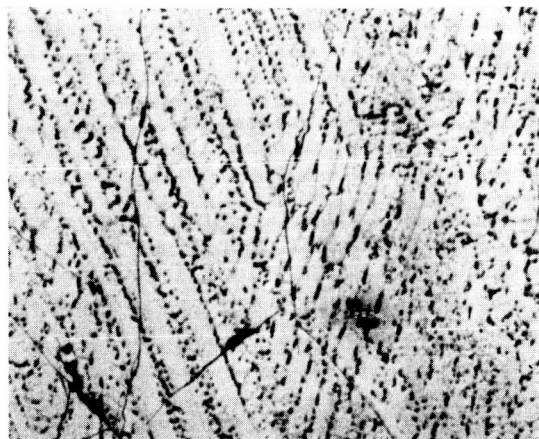
	a		b
Re₃Mo₂		Re₃Mo₂	H. T. 2300 C -3/4 HR
9HF -1HNO Etch	250X	K₃Fe(CN)₆	250X

Figure 14.   Effect of Heat Treatment on Re₃Mo₂

	a		b
Re₃Mo	As Cast	Re₃Mo	H. T. 1850 C -4 HR
9HF -1HNO Etch	250X	K₃Fe(CN)₆ Etch	250X

Figure 15.   Effect of Heat Treatment on Re₃Mo

a

Re_3Mo_2 As Cast Re_3Mo_2 H. T. 2300 C -3/4 HR
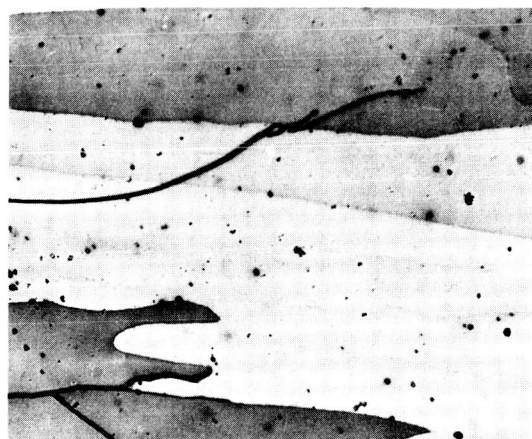
9HF -1HNO Etch   250X $K_3Fe(CN)_6$ 250X

Figure 14.   Effect of Heat Treatment on Re_3Mo_2

a

Re_3Mo As Cast Re_3Mo H. T. 1850 C -4 HR

9HF -1HNO Etch   250X $K_3Fe(CN)_6$ Etch   250X

Figure 15.   Effect of Heat Treatment on Re_3Mo

a		b	
Re₃W₂	As Cast	Re₃W₂	H. T. 2300 C-3/4 HR
9HF-1HNO₃ Etch	250 X	K₃Fe(CN)₆ Etch	250 X

Figure 16.   Effect of Heat Treatment on Re_3W_2
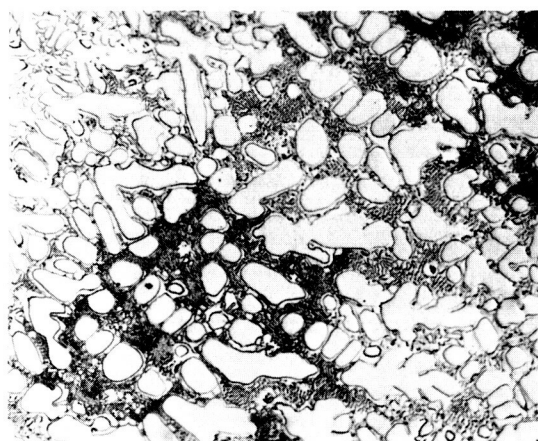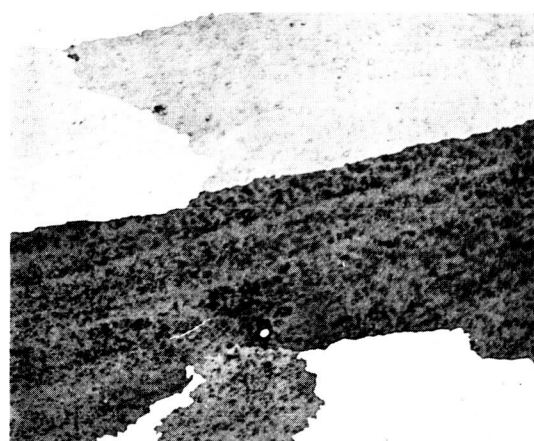
a		b	
Re₃W	As Cast	Re₃W	H. T. 1850 C-4 HR
9HF-1HNO₃ Etch	250 X	K₃Fe(CN)₆ Etch	250 X

Figure 17.   Effect of Heat Treatment on Re_3W

A vacuum furnace was designed and built especially for heat treating the arc-cast materials. It is also used for measuring the spectral emittance as described in a following section.

In preparing the a-Mn phase materials, it was noted that the peritectoid temperatures proposed by Savitskii and Tylkina[6] seemed much too low, particularly in the case of the tungsten-rhenium system. Although an extensive investigation of the phase boundaries was not undertaken, Table II shows that the temperature at which these phases are formed is at least 1850C, in agreement with the results of Dickinson and Richardson[5].

Figure 18 shows the furnace as set up for heat treating. The heating element is a 1-1/8 inch O.D. tantalum tube which is held vertically between two water-cooled copper electrodes. The left side of the modular enclosure houses the vacuum column which includes a 600 liter-per-second diffusion pump, a liquid nitrogen-cooled baffle and a four-inch vacuum valve. The mechanical backing and roughing pump is located directly under the furnace in the right side of the modular enclosure. The enclosure also houses the water-distribution and collection systems, the relay bank and solenoid valves. A pressure switch shuts down the furnace in case of water failure and floods the system with helium. With the 1-1/8 inch diameter element, the furnace is capable of temperatures of over 2000C for extended periods. An automatic liquid-level control is provided to keep the baffle filled with liquid nitrogen for heat treatments of long duration. At 2000C, pressure is typically in the 1×10^{-6} to 5×10^{-7} Torr range.

Pressures greater than 10^{-3} Torr are measured with an NRC thermocouple gage. Pressures less than 10^{-4} Torr are measured with a Varian UHV-12P ion gage in conjunction with a Varian 971-0003 ion-gage control unit.
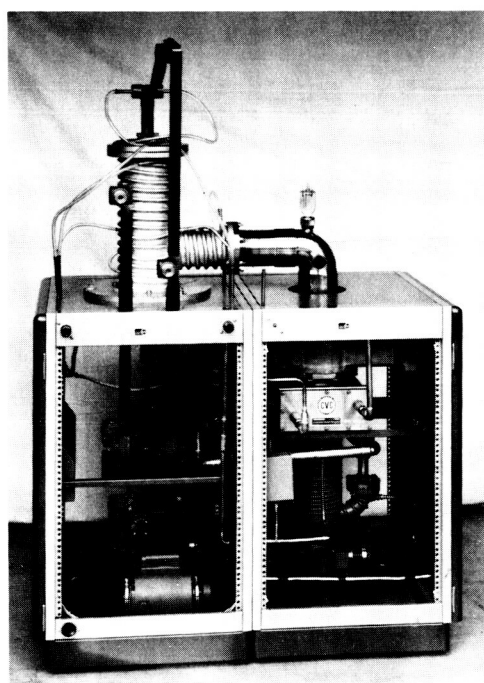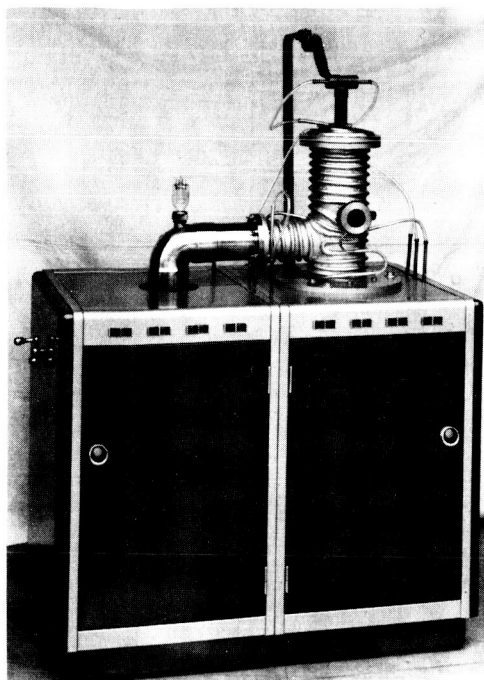
Figure 18. High-Temperature Vacuum Furnace for Heat Treatment and Measurement of Spectral Emittance

The versatility of the furnace is further enhanced by several sets of auxilliary electrodes which receive heating elements of 3/4-inch and 1/4-inch O.D. The 3/4-inch elements greatly augment the temperature capability of the furnace. The 1/4-inch elements are used in the measurement of spectral emittance.

The arc-melted buttons, having been heat-treated to obtain a single phase, were extremely brittle and easily broken up with a steel mortar and pestle. Initially, the materials were ground to minus-400 mesh in the mortar and pestle, and then leached with 25 percent HCl to remove the impurities, primarily iron.

Table III shows semi-quantitative spectrographic analyses, made without standards, for iron in two W-Re compounds before and after the leaching operation. The acid leach is effective in reducing the iron-impurity level to about 10 ppm, the limit of detection of the spectrograph.

TABLE III

SPECTROGRAPHIC ANALYSES FOR IRON IN W-RE
INTERMETALLIC COMPOUNDS

Compound	Condition	Iron Present (ppm)
W_2Re_3	as ground, (minus-400 mesh)	50
	ground and leached (25% HCl)	10
WRe_3	as ground (minus-400 mesh)	40
	ground and leached	< 10

Although the leaching process was considered to be moderately successful in removing impurities, it was never completely satisfactory from the electrophoretic-deposition aspect. The smallest and most

desirable particles were extremely difficult to retain through the three leachings and three washings. The remainder of the particles, although all minus-400 mesh, were still considered too coarse for ideal deposition, especially in view of the relatively high densities of the materials. For these reasons, a Helme air-attrition mill was used for subsequent grinding operations.

The air-attrition mill utilizes a cyclone-classifier principle such that particles smaller than a given size, in this case less than five microns, are removed from the mill, and the larger particles are recycled. Again, the materials of interest posed a serious problem, because they fracture as fairly coarse flakes rather than spherical particles. Since the flakes' behavior in the airstream is not the same as spheres, they were not all recycled properly and a substantial fraction of these large particles was found in the collecting jar. The material in the collection jar was therefore put through a 325-mesh screen and the coarse particles were recycled, as shown previously in Figure 13.

Specimen Fabrication

Early in the research program, a diode of cylindrical geometry with a wire-like emitter was chosen. Such geometry effectively circumvents the edge effects of parallel-plate geometry and provides a substantially higher electric field for the same applied potential. Fabrication of the wire-like emitters from the intermediate-phase materials of this program presents several unique problems. A number of fabrication methods were investigated, and several are believed to merit the following brief discussion:

A direct casting technique attracted considerable attention in the early phases of the project. The process is a modification of one described by Abrahamson and Grant[35] in which an evacuated tube of

fused silica is thrust into the molten alloy within the arc-melting fur-
nace. The metal is drawn up into the tube where it freezes. The tube
can then be carefully crushed and broken away, leaving a cylindrical
specimen of the same diameter as the bore of the tube. Many specimens
3 mm in diameter and about 7 cm in length were cast in this way, but
attempts to increase the length-to-diameter ratio proved unfruitful.
Experiments with fused-silica tubes of smaller bore and various wall
thicknesses were unsuccessful due to the rapid freezing of the smaller
sections before the molten metal reached significant height in the tube.
Attempts to reduce the 3 mm diameter specimens to smaller diameter
by grinding and electrochemical machining were similarly unsuccessful.

One of the most attractive and unique methods for producing the
desired specimens was reduction of the gaseous hexafluorides or
carbonyls of the metals on the heated tungsten substrate. Leitten[36]
and Holzl[37] have been successful in developing processes for the deposi-
tion of pure materials by this technique. When contacted about the
possibility of deposition of the intermediate phases of the present
investigation however, both investigators indicated that such work was
considerably beyond their present capability.

The fabrication process finally chosen was the electrophoretic
deposition of the finely-ground intermediate-phase materials on a
tungsten-wire substrate. The fine particles are suspended in an organic
media and are driven to the substrate by a potential applied between the
substrate and the container wall.

The electrophoretic-deposition work was performed by Indelco,
Inc., of Beverly, Massachusetts. After the deposition of the particles
from the organic media, the coated specimens were sintered for 30

minutes at 1700C except for the Cr-Re alloy which was sintered for 30 minutes at 1575C. An atmosphere of $75H_2$-$25N_2$ was used for all specimens.

Initially, a coating two mils thick was applied to a five-mil diameter tungsten substrate, bringing the overall diameter of the specimen to about nine mils. Several diodes incorporating these cathodes were made; however, temperature variations of several hundred degrees were encountered due to the large volume of the nonuniformly conducting coating with respect to the volume of the substrate. This problem was effectively countered by using substrates of ten-mil diameter. Substrate diameters of over ten-mils substantially increase the diode design problems, particularly those associated with the helical spring. The spring serves to keep the emitter straight and concentric with the collector over the required range of temperature. Power requirements and excessive anode heating also pose rather formidable problems if the substrate diameter exceeds ten mils.

Fabrication of Thermionic Diodes

The thermionic diodes were fabricated by International Telephone and Telegraph Co., Electron Tube Division, Easton, Pennsylvania. Figure 19 shows the completed diode which is 2-1/2 inches in diameter and 10 inches high. The appendages at the sides of the tube accommodate a Varian UHV-12P ion gage for pressure measurement and a getter for removing gasious impurities from the tube during pump-down. The tube elements are supported by a pair of sapphire rods projecting vertically upward from the tube base. The cathode is attached securely to a cross member at the top and kept tight by a spring at the bottom. The filament is surrounded by five anodes 7/8 inch in
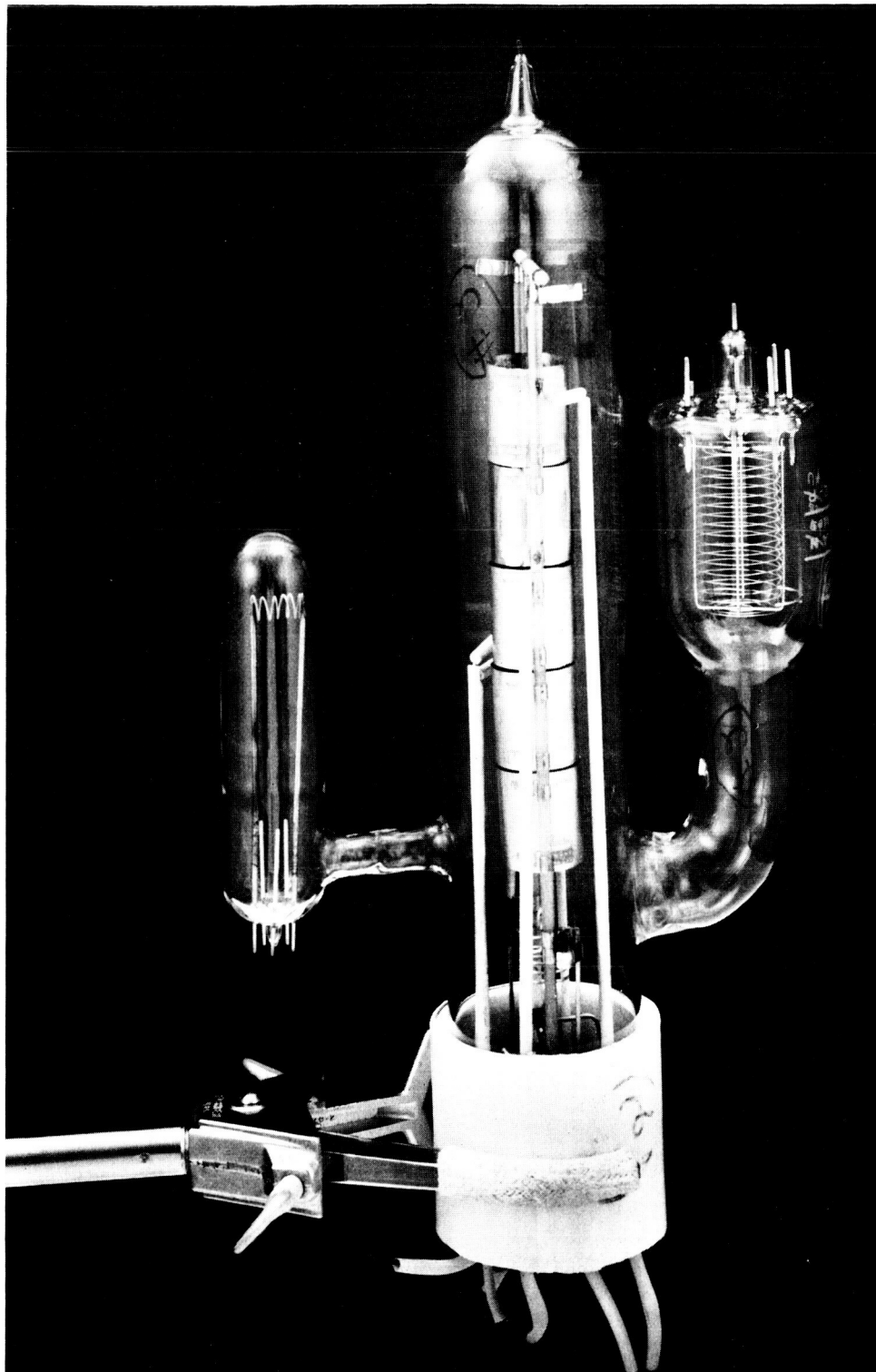
Figure 19. The Thermionic Diode. Appendages Contain an Ion Gage for Pressure Measurement and a Getter to Remove Gaseous Impurities During Pump-Down

diameter and one inch long. The anodes are also supported by the sapphire rods and are provided with individual leads through the press at the bottom of the diode.

The spring must be designed to account for thermal expansion of the filament from ambient temperatures to the incandescent temperatures at which the measurements are made; it must also serve as a conductor for the filament current. The design of such springs is discussed in some detail by Blodgett and Langmuir[38] and by Tawney[39]. The helical spring design of Langmuir and Blodgett was chosen for the present diode. The spring finally used was wound of 30-mil tungsten wire and had a helix diameter of 0.625 inches. Six turns were required to preclude exceeding the elastic limit of the tungsten at the 2000C temperature.

Measurement of the Emission Current

As discussed in a previous section, the work function is determined by measuring the emission current as a function of the electric field at various temperatures, invoking the Schottky theory to calculate the current density in the absence of all fields. The zero-field current densities are then used in a Richardson plot from which the work function and the constant A_R are obtained.

A dynamic system of measurement was originally assembled, in which the electric field was provided by a high-voltage pulse generator, and the corresponding current pulses measured with a Tektronix 535-A oscilloscope, after the method of Haas and Harris[40]. The pulse generator shown in Figure 20 was built and tested, but repeated attempts to detect the current pulse with the diode in place failed. When the diode was replaced by an appropriate resistor, a current pulse of the expected
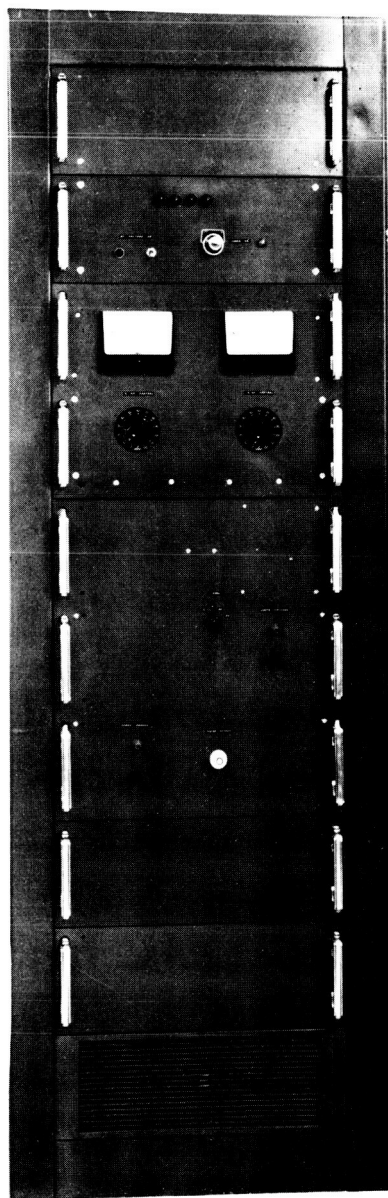
Figure 20. High-Voltage Pulse Generator Designed for Dynamic Measurement of Thermionic Emission Properties

value was detected, as shown in Table IV. Failure to detect the pulse in the diode is believed to be the result of distributed capacitance in the tube. Rather than to remanufacture the diodes, which had already been responsible for much of the difficulty and delay encountered on the project, the dynamic measurements were abandoned in favor of the less troublesome D. C. measurements.

TABLE IV

COMPARISON OF EXPECTED AND MEASURED VALUES OF THE
CURRENT PULSE WITH THE DIODE REPLACED BY
A 6. 5 MEGOHM RESISTOR

Potential (KV)	Current (Amps $\times$ 10^4)	
	Calculated	Measured
1	1. 54	1. 57
2	3. 08	3. 15
5	7. 70	7. 85
10	15. 4	15. 7
15	23. 1	23. 5

In the present system, a D. C. potential, continuously variable from 0 to 1000 volts and regulated to within one percent, is provided by a Keithley 240 regulated power supply. The desired voltage can be obtained to within one percent simply by placing the decade switches on the supply in the correct position. A Simpson 260 volt-ohm-milliammeter was also used to monitor the D. C. potential.

A Keithley 414 micro-microammeter is used to measure the current. For the diode geometry and materials of the present study, the emission currents typically varied from 10^{-12} Amps to as much as

10^{-2} Amps and required the full range of scales provided by the 414 instrument.

The filament is heated to the desired temperature by an alternating current. A stabiline line voltage regulator holds the line voltage fluctuations to less than 0.1 percent. The desired filament voltage is obtained by a Variac auto transformer in conjunction with a center-tapped step-down transformer, shown schematically in Figure 21. The secondary winding of the transformer has high-voltage insulation, thus permitting the negative D.C. potential to be applied at the center tap. The anodes are held at near-ground potential.

The emission current is measured only at the center anode. The other anodes are guards and serve only to prevent axial components of the electric field in the region of the central anode. The radial symmetry of the field is preserved if the guard anodes and the central anode are at the same potential. Since the center anode is not electrically tied to the guards, this condition is assured by adjusting the variable resistor, R_1, until the galvanometer between the central anode and the guards indicates a null.

The diodes were allowed to outgas for several hours at 1700C, a temperature higher than the maximum temperature at which the measurements were made. A 1000-volt potential was maintained between filament and anodes during this outgasing period. The anode current due to the resulting field provides additional heating and outgasing of the anodes. Pressure decreases steadily during this period as gaseous impurities initially expelled from the emitter and the anodes condense on cooler less-critical portions of the tube. The pressure
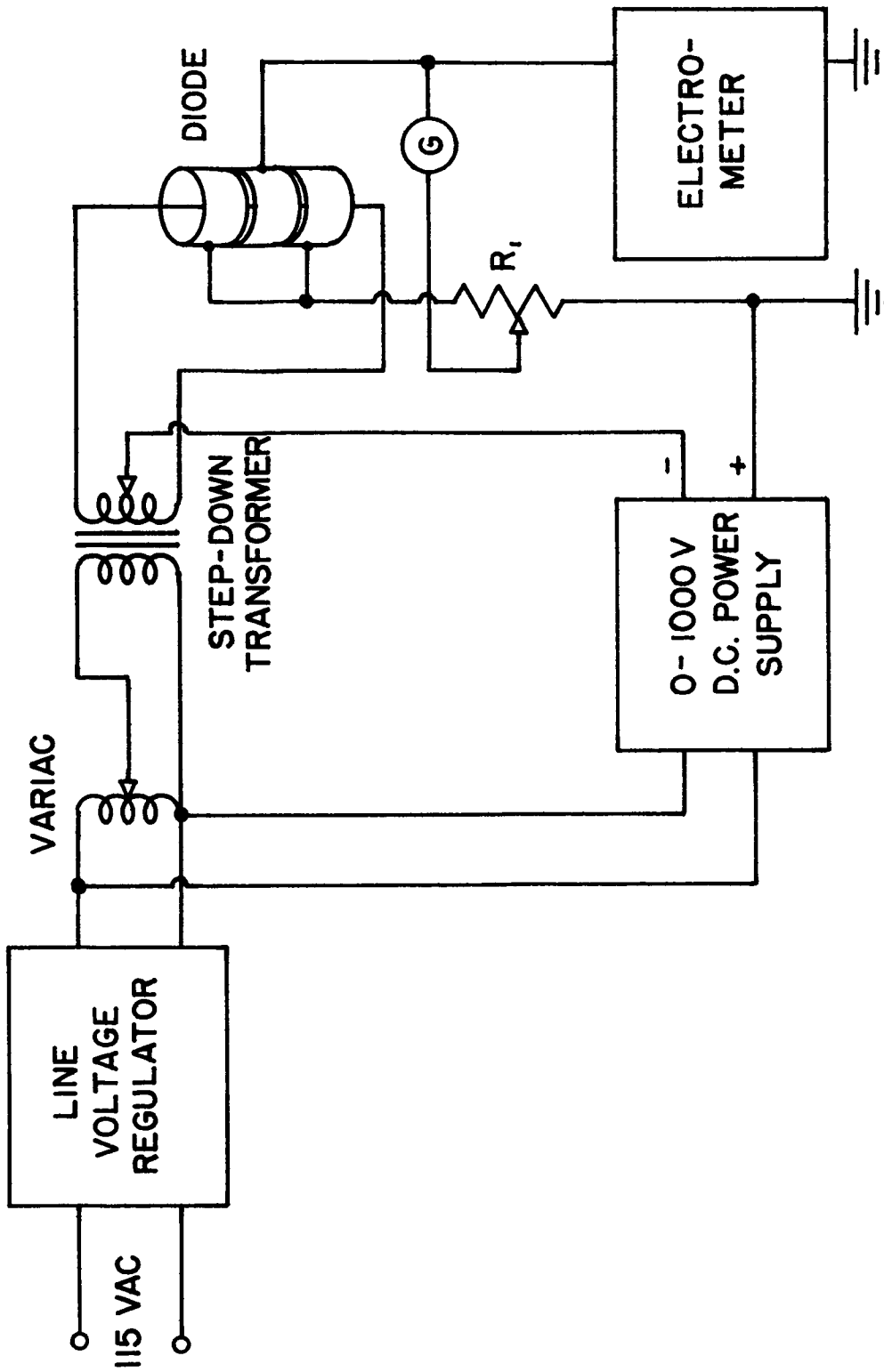
Figure 21. Apparatus for Emission Current Measurement (Schematic)

reaches a constant value after several hours at temperature. The pressure depends on the temperature, of course, but was always less than 1×10^{-8} Torr at 1700C.

All the intermediate-phase materials of the present study undergo phase transformations at temperatures between 1800 and 2000C. The temperature for outgasing was therefore limited to 1600C for the Cr-Re material and 1700C for the remainder of the materials. When corrected for sight-port transmittance and spectral emittance, the resulting temperatures are still less than 1850C, thus assuring that no phase transformations occur. Then, since surfaces are more easily kept clean at the higher temperatures, the measurements are made in order of decreasing temperature in increments of 25 degrees. Current was measured at least four times at each temperature; twice after the voltage was decreased from its former value and twice after being increased. The agreement was almost always within one percent. However, at the lower temperatures, the values were found to vary moderately unless sufficient time was allowed upon reaching the decreased temperature before measurements were begun. When the variation exceeded 5 percent the measurements were repeated at that temperature. Since the variations were always observed at the lower temperatures, they were attributed to contaminants on the emitter surface; measurements at these temperatures were considered less reliable than those made at the higher temperatures.

Temperature Measurement and Correction

Temperature measurements for the present investigation were made with a Pyro micro-optical pyrometer, model 95. The instrument is capable of measuring temperatures of targets less than 0.003 cm in diameter. A set of six objective lenses, supplied with the pyrometer,

provides for almost any conceivable distance between objective and target. In the temperature interval 1200 to 2100K, the effective wavelength of the instrument is 0.660 micron. The three non-linear, overlapping scales have smallest scale divisions of 5 degrees. The emitter temperature of the thermionic diodes was measured by focusing the pyrometer on the emitter by sighting through the 0.16 cm spaces separating the center anodes from the nearest guard anodes above and below it.

The temperatures measured in this way are, of course, not the absolute temperatures used in the calculation of the work function, and must be corrected for the spectral emittance of the cathode and the transmittance of the glass envelope through which the light must pass. Failure to make such corrections results in large systematic error in the temperature used to calculate the thermionic work function.

The spectral normal emittances of the materials were determined by the Worthing-tube method[41]. Specimens were prepared from tantalum tubing, 1/4-inch O.D. and 0.010-inch wall thickness, cut into 9-1/2 inch lengths. A 1/16-inch hole was drilled through the wall at the center of the tube, and the central portion of the tube coated with the finely ground material of interest. The coating can be applied electrophoretically or by carefully painting on a suspension of the powdered material in sucrose benzoate. The organic materials in the suspension can be driven off by heat treating in vacuum for two hours at 200C, after which the temperature is increased to 1500C for an additional two hours in order to sinter the coating in place. The tube is held between two water-cooled copper electrodes in the vacuum furnace described previously in another section. The ends of these

electrodes are drilled to a depth of 1.27 cm, thus decreasing the effective specimen length to 21.6 cm. Nevertheless, no discernable temperature gradients were observed on an uncoated tantalum tube within the central 13 cm of the specimen's length.

The spectral emittance is determined by measuring the temperature of the coated surface in the central section of the tube, and comparing it with the blackbody temperature within the tube, as seen through the 1/16 inch hole in the tube wall. The spectral emittance is found from the Wein Radiation Law.

$$W_\lambda = c_1 \lambda^{-5} e^{-c_2/\lambda T} \tag{3-1}$$

where W is the energy emitted at wavelength λ, per unit time, C_1 and C_2 are the first and second radiation constants and T is the absolute temperature in degrees K. The power radiated by the surface is related to that radiated by a blackbody by $t \epsilon_{\lambda, T}$

$$\exp\left[-\frac{c_2}{\lambda T_S}\right] = t \epsilon_{\lambda, T} \exp\left[-\frac{c_2}{\lambda T_{BB}}\right] \tag{3-2}$$

where T_S and T_{BB} are the observed temperatures at the surface and within the tube, respectively, $\epsilon_{\lambda, T}$ is the spectral emittance, and t is the transmittance of the fused-silica sight port. Written in logarithmic form, the equation is

$$2.303 \left(\log t + \log \epsilon_{\lambda, T}\right) = \frac{c_2}{\lambda} \left(\frac{1}{T_{BB}} - \frac{1}{T_S}\right). \tag{3-3}$$

Since both temperatures are observed through the same sight port, no transmittance correction is necessary for the calculation of $\epsilon_{\lambda, T}$. Values of c_2 and λ used for these calculations are 14,388 micron-°K and 0.660 micron, respectively.

Emittances determined in this way are, of course, themselves temperature dependent. Their values are shown in the emission tables of Chapter IV for the appropriate temperatures.

Strictly speaking, there is a temperature gradient due to conductive heat transfer through the tube wall, for which a correction should be made in the emittance calculation. The difference in temperature between inside and outside walls of a tube are given by Angell[42].

$$T_{in} - T_{out} = \frac{EI}{2k} \left[r^2 \log \frac{R}{r} - \left(\frac{R^2 - r^2}{2} \right) \right] \qquad (3-4)$$

Where T_{in} and T_{out} are the temperatures of the inside and outside walls of the tube, at radii r and R from the tube axis, respectively. E is the applied voltage per unit length of the tube, I is the current density in the tube, and K is the thermal conductivity of the tube material at the inside wall temperature T_{in}.

For the present investigation, however, the thin-wall tubing and conductivity are such that the correction amounts to only 0.08 degree, and can therefore be neglected. The temperatures observed in the thermionic diodes may now be corrected, using the appropriate spectral emittances determined by the method just described. The sight-port transmittance correction, not necessary for the calculation of the emittance, is now required.

The absorption of radiation by the fused-silica sight-port is assumed negligible so that the transmittance, t, is given by

$$t = (1 - r')^2, \qquad (3-5)$$

where r' is the reflectance of the sight-port. The reflectance is

related to the refractive index of the fused silica by Fresnel's equation.

$$r' = \frac{(n-1)^2}{(n+1)^2}$$
(3-6)

where n is the index of refraction. Taking n to be 1.5, r' is 0.04, from which the transmittance of the sight-port is found to be 0.92.

The observed temperatures, T_S, of the diodes were corrected by a computer solution of equation (3-3) for T_{BB}. The emission tables of the following chapter show the observed temperature, the spectral emittance and the corrected temperature.

CHAPTER IV

RESULTS

It is the purpose of this chapter to summarize the values of the thermionic work functions and the emission constants obtained in the present study for the materials shown in the following table.

TABLE V

COMPOSITION AND STRUCTURE OF REFRACTORY INTERMEDIATE PHASES

Composition Stoichiometric	Nominal (Wt. Pct.)	Crystal Type
Re_3Cr_2	85Re-15Cr	σ
Re_3Mo_2	74Re-26Mo	σ
Re_3Mo	85Re-15Mo	α-Mn
Re_3W_2	55Re-45W	σ
Re_3W	73Re-27W	α-Mn
W	100W	BCC

Determination of the thermionic emission properties required the independent measurement of current, cathode-anode potential and temperature, as discussed in the previous chapter. In the following discussions of each of the materials, the first table of each section shows the observed values.

The emission current density and electric field strengths are linear functions of the current and applied voltage, respectively. The constants of proportionality depend only on the diode geometry, according to the equations (2-38) and (2-46), reproduced here for convenience.

$$j = \frac{1}{A} I = \left(\frac{1}{2\pi r_c \ell}\right) I \tag{2-38}$$

$$E = \left[\frac{1}{2.303 \, r_c \, \log \left(r_a/r_c\right)}\right] V \tag{2-46}$$

where r_c is the radius of the emitter and r_a is the radius of the collector. The Schottky plots constructed for the purpose of determining the current density in the absence of an electric field are shown as log I vs. $V^{\frac{1}{2}}$. The intercept corresponds to the logarithm of current, rather than current density, at zero field and permits easy comparison with the experimental values shown in the tables preceding each plot.

Table VI summarizes the calculations of the constants of proportionality for the various emitters, which varied slightly in diameter due to minor variations in coating thickness. The diodes were otherwise identical, each having anodes of radius 1.11 cm and length 2.54 cm.

Having determined from the Schottky plots those points which describe the linear portions, the appropriate conversions for current density and electric field strength were applied and the zero-field current density found by computer extrapolation of the linear region to zero field for each temperature. The values thus obtained, and the reciprocal temperature corrected for spectral emittance and sight-port transmission, are used to construct the Richardson plots. Therefore, each of the following sections contains a table showing these data. The Richardson plot is located immediately following this tabular data from which it was constructed.

Tungsten

The first material to be measured in the study was pure poly-
crystalline tungsten. The specimen was made up in a prototype diode
to serve as a test of the diode design and the measurement capabilities
of the system.

Figure 22 shows the Schottky plots, constructed from the data
of Table VII, which were recorded at observed temperatures between
1090 and 1710C in the course of two runs on two separate days. Both
sets of data were combined in Table VIII to construct the Richardson
Plot shown in Figure 23.

A computer fit of these data yielded a work function of 4.60
± 0.17 eV for the combined runs, whereas if they are taken separately,
the work functions are 4.42 and 4.65 for the first and second runs
respectively. The 4.60 combined value is higher by 0.08 eV than the
4.52 ± .09 eV reported by Jerner[14], although the experimental uncer-
tainties associated with the two values are mutually inclusive.

It is believed that Jerner's value is most nearly correct, and
that the present value is neither particularly good nor representative of
measurements on the remainder of the materials. As mentioned pre-
viously, the measurements were made using a prototype diode, which
failed upon cooling from the 1710C temperature.

The tungsten measurement, while not particularly necessary to
the present study, was useful in bringing to light several minor
problems which were easily corrected:

1. The tension spring in the diodes was redesigned with a
   lower stiffness to allow for thermal expansion without
   exceeding the yield strength of the filament at high
   temperatures.

2. Departure of the Schottky plots from the saturation region at potentials as high as 100 Volts resulted in extrapolations from as few as four points. The 0-400 Volt power supply was replaced by a 0-1000 Volt supply in order to extend the linear region.

TABLE VII

VARIATION OF EMISSION CURRENT WITH TEMPERATURE AND EMITTER-COLLECTOR POTENTIAL FOR POLYCRYSTALLINE TUNGSTEN

Emitter Diameter 0.0254 cm   E = 17.60 V $j = 4.937\ I$

T_{OBS} (°C)	1710	1608	1485	1468	1350
$\epsilon_{\lambda,T}$	0.440	0.442	0.445	0.446	0.448
T_{BB} (°K)	2161	2039	1894	1874	1738
Current (Amps)	$I \times 10^3$	$I \times 10^3$	$I \times 10^4$	$I \times 10^4$	$I \times 10^5$
Potential (Volts)					
400	9.60	2.10	1.84	1.68	2.52
300	9.20	3.03	1.78	1.63	2.40
200	8.60	1.94	1.70	1.56	2.28
100	7.70	1.81	1.60	1.48	2.08
75	7.20	1.73	--	1.46	--
50	6.70	1.65	1.46	1.42	1.91
40	6.38	1.58	1.43	1.39	1.82
30	5.85	1.50	1.40	1.36	1.71
25	5.53	1.46	1.39	1.33	1.63
16	3.55	1.32	1.35	1.25	1.43
9	1.54	1.07	1.30	1.14	1.20
5	0.730	0.620	1.24	1.02	0.980
4	0.550	0.454	1.19	0.980	0.895
3	0.399	0.320	1.10	0.870	0.783
2	0.270	0.196	0.830	0.670	0.620
1	0.155	0.140	0.440	0.400	0.350
0	0.062	0.040	0.109	0.140	0.052

TABLE VII (Continued)

T_{OBS} (°C)	1207	1167	1090
$\epsilon_{\lambda, T}$	0.450	0.451	0.455
T_{BB} (°K)	1574	1529	1442
Current (Amps)	$I \times 10^7$	$I \times 10^7$	$I \times 10^8$
Potential (Volts)			
400	9.60	1.76	1.41
300	9.35	1.69	1.33
200	8.90	1.60	1.24
100	8.35	1.50	1.13
75	--	1.47	--
50	7.78	1.43	1.05
40	7.62	1.40	1.03
30	7.50	1.38	1.01
25	7.40	1.35	1.00
16	7.20	1.31	0.965
9	6.65	1.24	0.920
5	5.80	1.17	0.885
4	5.30	1.15	0.870
3	4.80	1.12	0.850
2	4.05	1.04	0.810
1	2.98	0.750	0.680
0	0.910	0.290	0.250
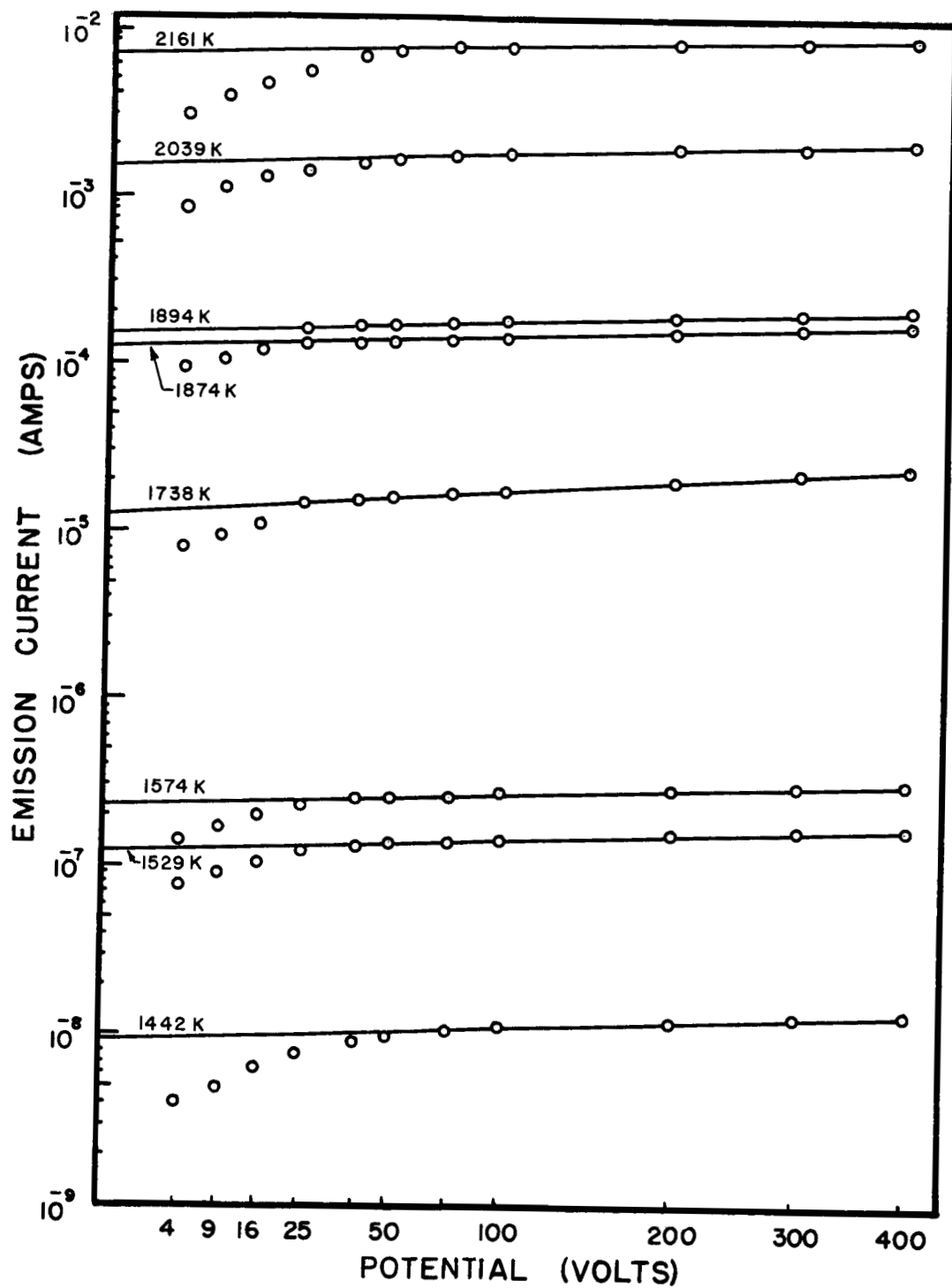
Figure 22. Variation of Emission Current with Emitter-Anode Potential
for Polycrystalline Tungsten

TABLE VIII

FUNCTIONS OF ZERO-FIELD CURRENT DENSITY AND TEMPERATURE FOR CONSTRUCTION OF RICHARDSON PLOT FOR POLYCRYSTALLINE TUNGSTEN

T_{BB} (°K)	$10^4/T_{BB}$ (°K^{-1})	$\log j_0$	$\log j_0 - 2 \log T_{BB}$
2161	4.628	$\bar{2}.50515$	$\bar{9}.83454$
2039	4.904	$\bar{3}.88081$	$\bar{9}.26043$
1894	5.279	$\bar{4}.83759$	$\overline{10}.28122$
1874	5.335	$\bar{4}.77815$	$\overline{10}.23104$
1738	5.775	$\bar{5}.93702$	$\overline{11}.45568$
1574	6.352	$\bar{6}.55388$	$\overline{12}.15832$
1529	6.541	$\bar{7}.79239$	$\overline{13}.42226$
1441	6.937	$\bar{8}.65321$	$\overline{15}.33418$
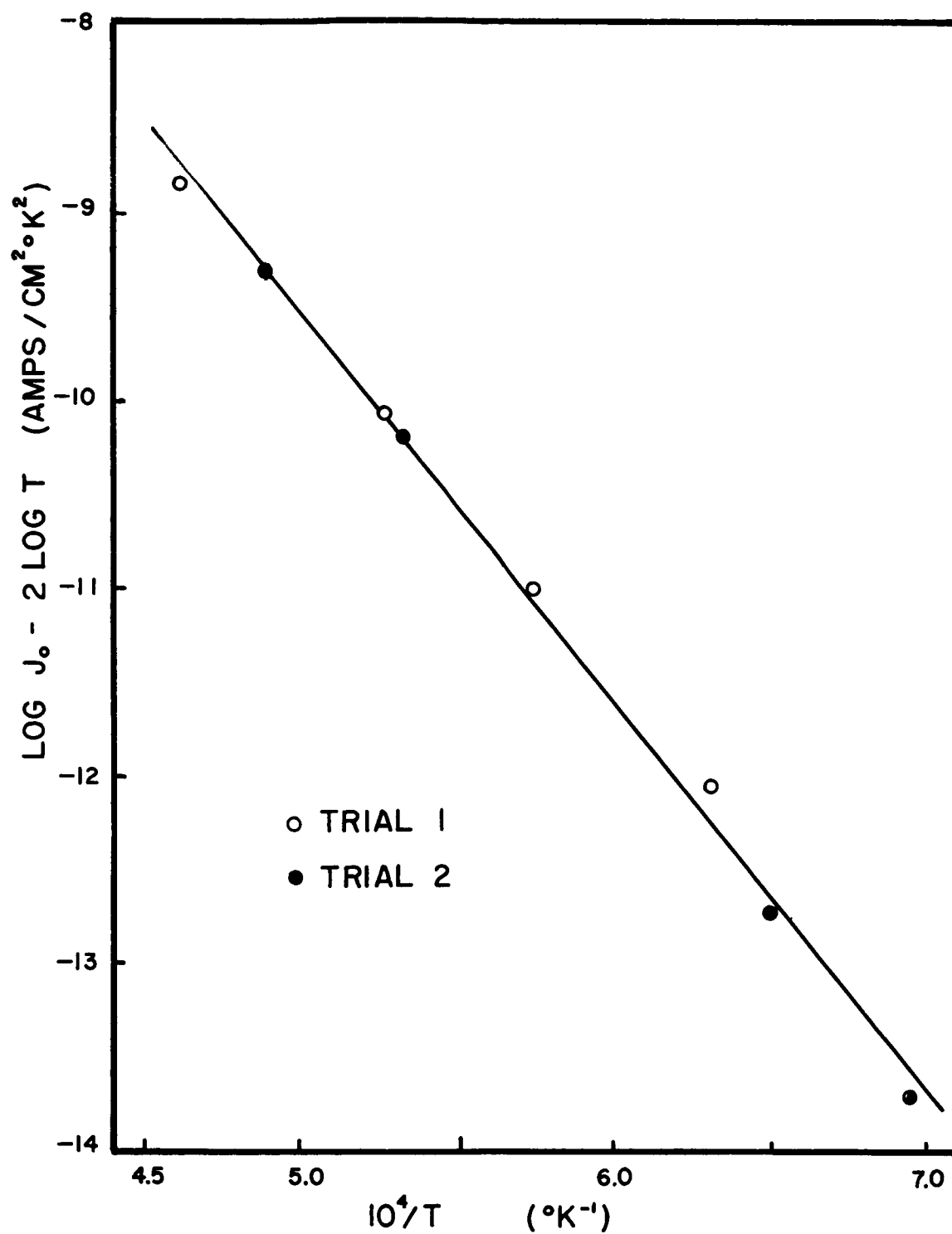
Figure 23. Richardson Plot for Polycrystalline Tungsten

Re$_3$Cr$_2$

Schottky plots for the Re$_3$Cr$_2$ intermediate phase material are shown in Figure 24, and the corresponding Richardson plot appears in Figure 25, constructed from Tables IX and X, respectively.

As mentioned previously, this material required development of special powder-metallurgy processes and heat treatment in a sealed tube to prevent loss of chromium. Anticipating further difficulties because of the high vapor pressure of chromium, the maximum temperature at which the runs were made was limited to 1400C observed or about 1750K when corrections for emittance and sight-port were applied. Except for this precaution however, the measurements were made in the same manner as for the other materials, and no difficulties were encountered.

The work function, obtained from the slope of the Richardson plot, is 4.57 ± 0.10 eV. This is slightly lower than the value reported for pure chromium, 4.60 eV by Wahlin[8], but above the value of Michaelson[7], 4.51 eV.

The work function of the σ phase nearly equal to that of the pure Group VIA constituent is unlike those of σ phases in the other two systems, Mo-Re and W-Re, in which the work functions of the σ phases are substantially higher. However, this may be due to the work function of pure chromium which, as explained in the following chapter, is somewhat higher than one might expect on the basis of screening of the outermost electrons.

TABLE IX

VARIATION OF EMISSION CURRENT WITH TEMPERATURE
AND EMITTER-COLLECTOR POTENTIAL FOR Re_3Cr_2

Emitter Diameter 0.0343 cm   E = 1398 V   j = 3.657 I

T_{OBS} (°C)	1400	1375	1350	1325	1300
$\epsilon\lambda, T$	0.622	0.626	0.630	0.635	0.639
T_{BB} (°K)	1748	1720	1692	1664	1634
Current (Amps)	$I \times 10^7$	$I \times 10^7$	$I \times 10^7$	$I \times 10^8$	$I \times 10^8$
Potential (Volts)					
1000	3.29	2.10	1.11	7.19	4.26
900	3.24	2.04	1.08	6.88	4.07
800	3.14	1.98	1.05	6.58	3.86
700	3.06	1.90	9.48	6.28	3.64
600	2.94	1.82	9.01	5.94	3.42
500	2.81	1.73	8.53	5.57	3.18
400	2.66	1.64	8.02	5.21	2.88
300	2.49	1.53	7.42	4.78	2.60
200	2.29	1.39	6.76	4.32	2.31
100	2.04	1.24	5.88	3.76	1.95
75	1.96	1.19	5.63	3.59	1.84
50	1.85	1.14	5.29	3.39	1.72
40	1.81	1.12	5.15	3.29	1.66
30	1.76	1.08	4.98	3.20	1.60
25	1.73	1.06	4.90	3.12	1.56
16	1.69	1.00	4.70	2.90	1.49
9	1.61	0.928	4.48	2.01	1.12
0	0.797	0.519	2.48	1.37	0.676

TABLE IX (Continued)

T_{OBS} (°C)	1275	1250	1225
$\epsilon_{\lambda, T}$	0.643	0.648	0.652
T_{BB} (°K)	1608	1580	1553
Current (Amps)	$I \times 10^8$	$I \times 10^8$	$I \times 10^8$

Potential (Volts)

1000	2.43	2.04	1.48
900	2.30	1.92	1.37
800	2.14	1.78	1.26
700	2.00	1.64	1.08
600	1.84	1.50	0.992
500	1.68	1.36	0.871
400	1.52	1.22	0.752
300	1.35	1.07	0.625
200	1.17	0.887	0.495
100	0.939	0.707	0.358
75	0.980	0.660	0.322
50	0.816	0.602	0.263
40	0.785	0.578	0.247
30	0.751	0.552	0.230
25	0.730	0.539	0.222
16	0.693	0.507	0.205
9	0.654	0.479	0.189
0	0.379	0.262	0.110
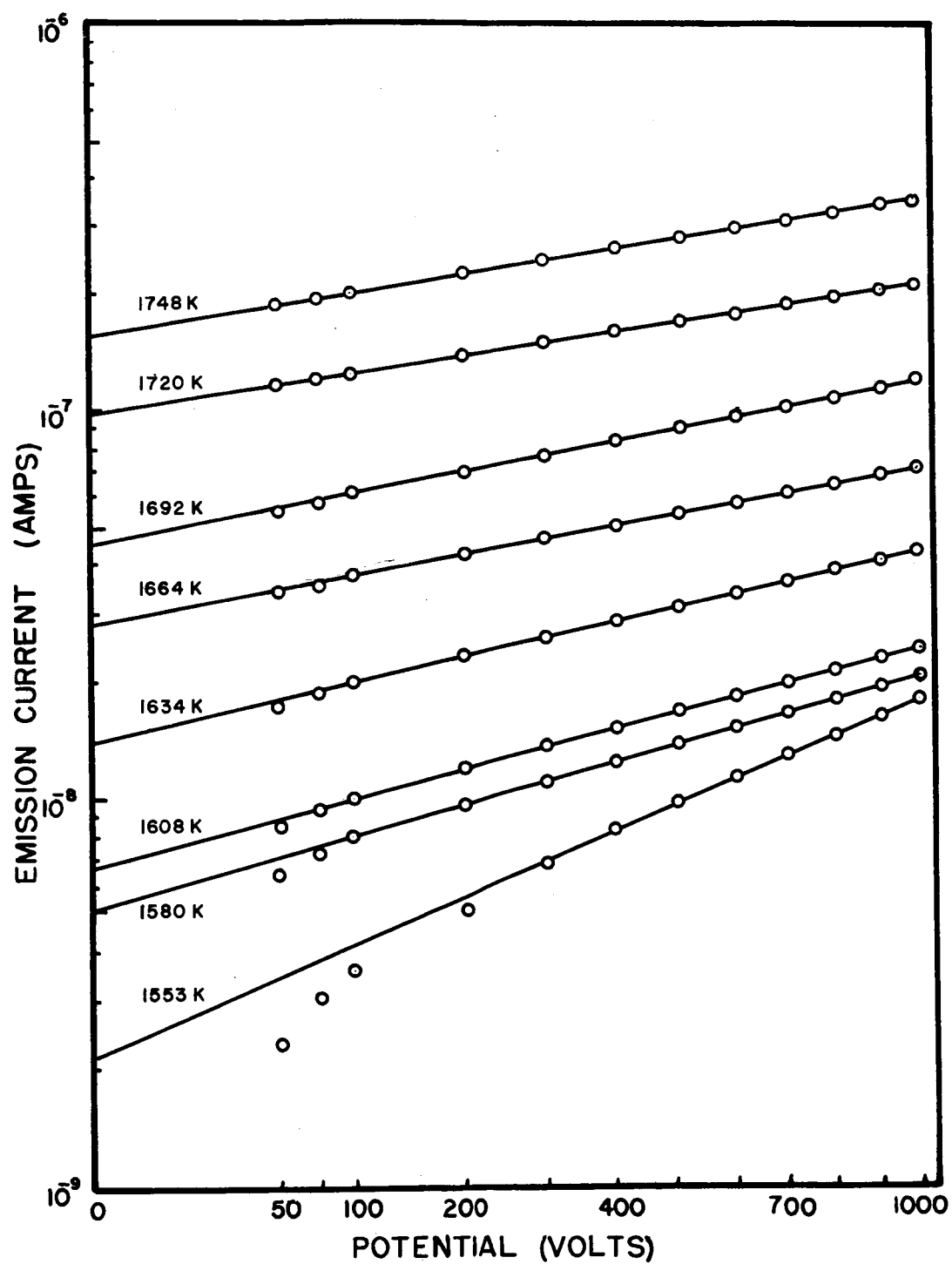
Figure 24. Variation of Emission Current with Emitter-Anode Potential for Re_3Cr_2

TABLE X

FUNCTIONS OF ZERO-FIELD CURRENT DENSITY
AND TEMPERATURE FOR CONSTRUCTION OF
RICHARDSON PLOT FOR Re_3Cr_2

T_{BB} (°K)	$10^4/T_{BB}$ (°K^{-1})	log j_0	log j_0 - 2 log T_{BB}
1748	5.721	$\overline{7}$.76805	$\overline{13}$.28163
1720	5.815	$\overline{7}$.54907	$\overline{13}$.07675
1692	5.011	$\overline{7}$.20500	$\overline{14}$.74695
1664	6.011	$\overline{7}$.01580	$\overline{14}$.57233
1636	6.114	$\overline{8}$.71545	$\overline{14}$.28664
1608	6.219	$\overline{8}$.37827	$\overline{15}$.96432
1580	6.329	$\overline{8}$.26367	$\overline{15}$.86490
1553	6.441	$\overline{9}$.92935	$\overline{15}$.54587
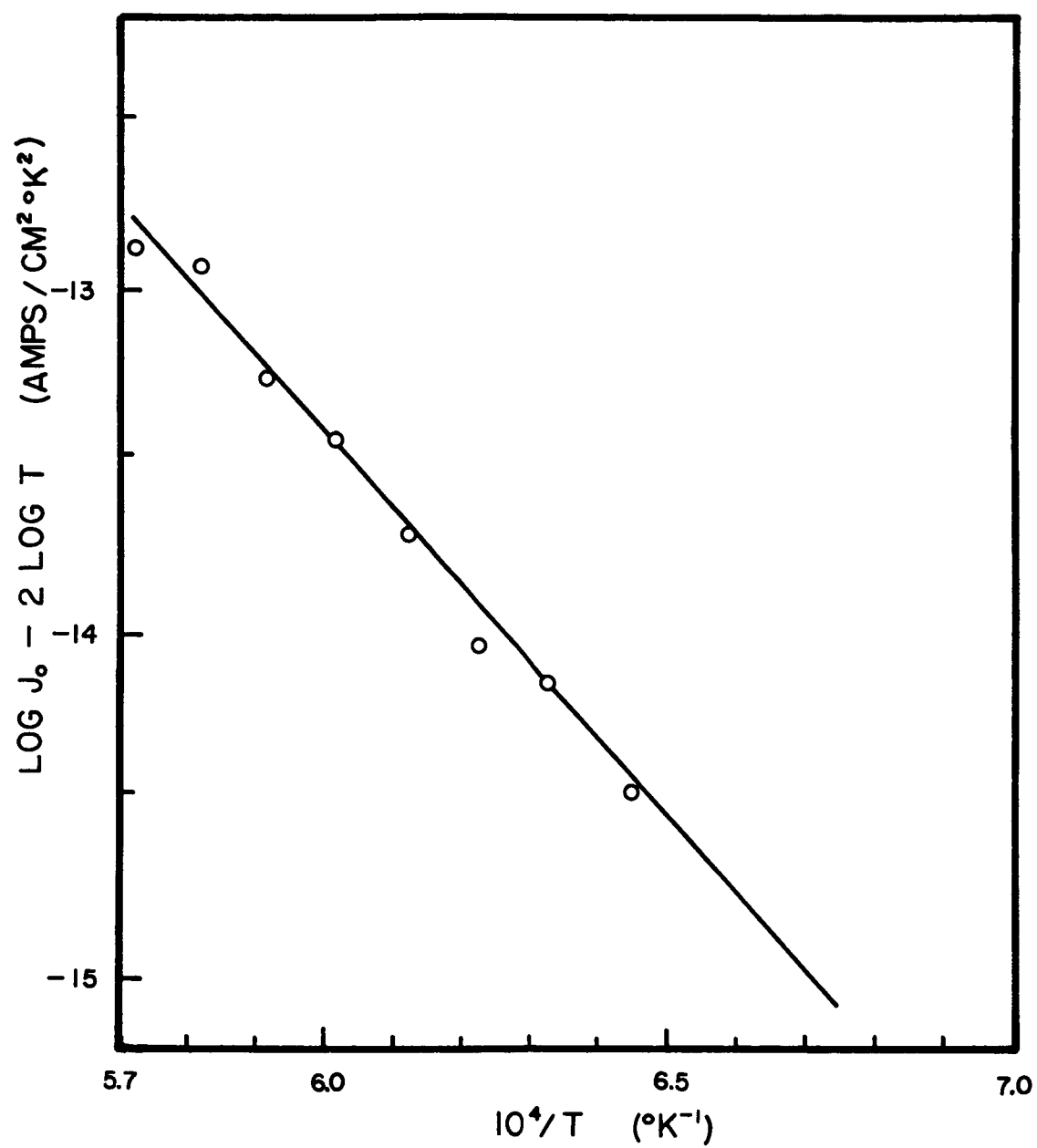
Figure 25. Richardson Plot for Re_3Cr_2

Re$_3$Mo$_2$

Table XI shows the emission currents at various emitter-anode potentials from which the Schottky plots of Figure 26 were constructed.

The intercepts shown in Table XII, obtained by computer extrapolation of the linear regions of the Schottky plots, were in turn used to construct the Richardson plot shown in Figure 27.

The B-5500 computer was again utilized to determine the intercept and slope of the Richardson plot which are related to the coefficient, A_R, and the work function, ϕ_R, in the Richardson-Dushman equation. For this material, the work function was found to be 4.78 ± .07 eV, and the coefficient, A_R, was 9.5 Amps/cm^2°K^2.

The work function is substantially higher than that of pure molybdenum[7], 4.42 eV, but lower than that of rhenium, 5.1 eV.

TABLE XI

VARIATION OF EMISSION CURRENT WITH TEMPERATURE
AND EMITTER-COLLECTOR POTENTIAL FOR Re_3Mo_2

Emitter Radius 0.0343 cm   E = 14.47 V   j = 3.827 I

T_{OBS} (°C)	1546	1509	1447	1394	1352
$\epsilon\lambda,T$	0.581	0.588	0.597	0.606	0.613
T_{BB} (°K)	1919	1876	1805	1745	1697
Current (Amps)	$I \times 10^4$	$I \times 10^5$	$I \times 10^5$	$I \times 10^5$	$I \times 10^6$
Potential (Volts)					
1000	1.78	9.58	2.73	1.10	4.40
900	1.74	9.37	2.67	1.08	4.28
800	1.70	9.14	2.605	1.05	4.16
700	1.64	8.90	2.54	1.02	4.03
600	1.58	8.61	2.47	0.983	3.90
500	1.50	8.29	2.385	0.949	3.74
400	1.42	7.89	2.28	0.908	3.59
300	1.31	7.28	2.155	0.861	3.40
200	1.17	6.51	1.975	0.795	3.14
100	1.00	5.375	1.645	0.678	2.63
75	0.951	5.00	1.51	0.630	2.47
50	0.872	4.55	1.36	0.562	2.22
40	0.828	4.33	1.28	0.526	2.09
30	0.766	4.09	1.18	0.490	1.945
25	0.725	3.91	1.13	0.466	1.855
16	0.625	3.42	1.03	0.413	1.67
9	0.504	2.68	0.869	0.359	1.415
4	0.0342	1.855	0.613	0.265	1.12
0	0.0325	0.0207	0.097	0.0053	0.0293

TABLE XI (Continued)

T_{OBS} (°C)   1303
$\epsilon_{\lambda, T}$ 1.621
T_{BB} (°K)   1642
Current (Amps) $I \times 10^6$

Potential (Volts)

Potential (Volts)	$I \times 10^6$
1000	1.495
900	1.41
800	1.33
700	1.255
600	1.20
500	1.145
400	1.085
300	1.02
200	0.917
100	0.788
75	0.733
50	0.660
40	0.624
30	0.581
25	0.556
16	0.501
9	0.445
4	0.349
0	0.0102
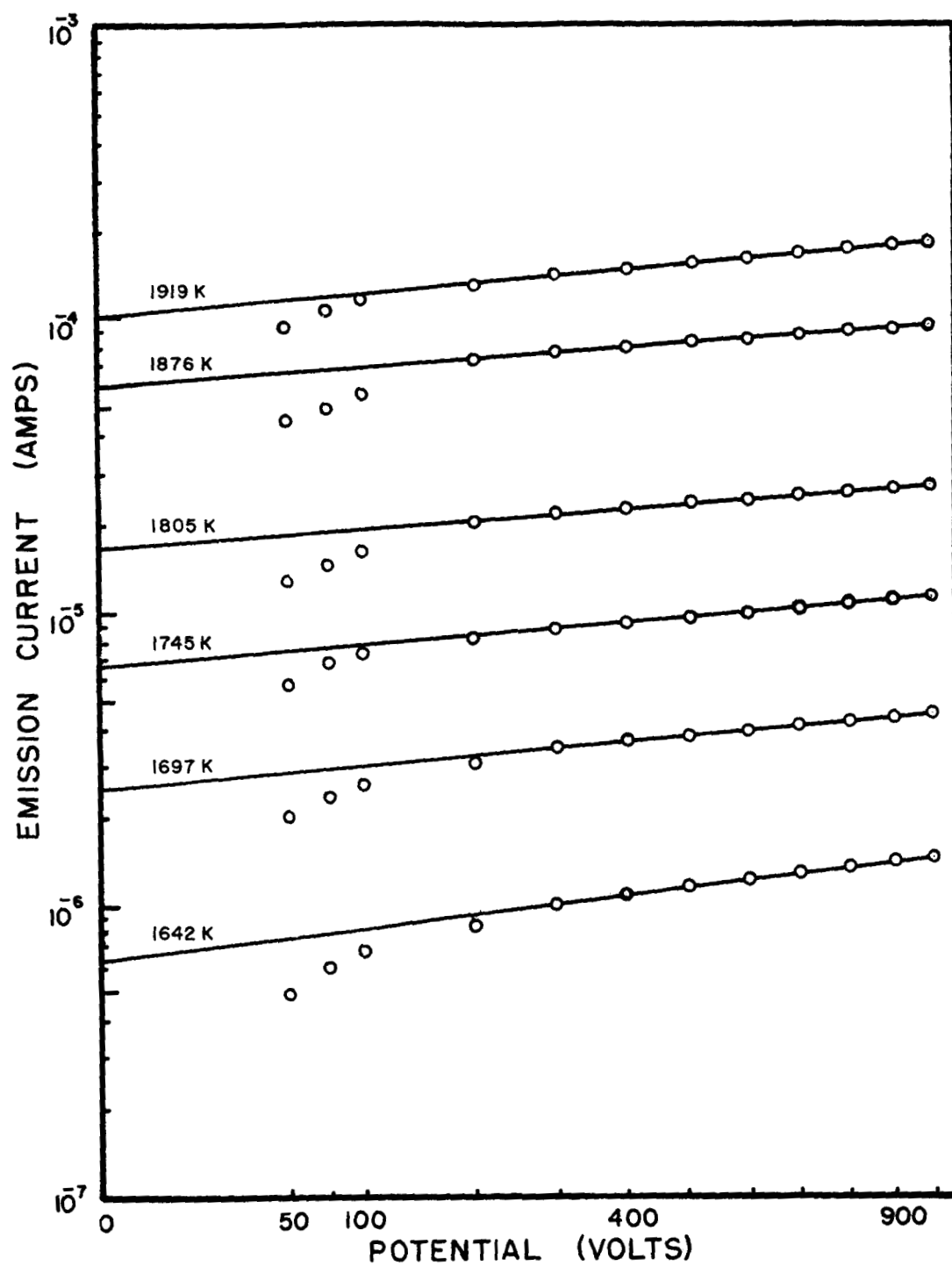
Figure 26. Variation of Emission Current with Emitter-Anode Potential
for Re_3Mo_2

TABLE XII

FUNCTIONS OF ZERO-FIELD CURRENT DENSITY AND TEMPERATURE FOR CONSTRUCTION OF RICHARDSON PLOTS FOR Re_3Mo_2

$T_{BB}(°K)$	$10^4/T_{BB}(°K^{-1})$	$\log j_0$	$\log j_0 - 2 \log T_{BB}$
1919	5.210	$\overline{4}.52298$	$\overline{10}.07264$
1876	5.330	$\overline{4}.28476$	$\overline{11}.86116$
1805	5.539	$\overline{5}.77995$	$\overline{11}.35396$
1745	5.731	$\overline{5}.37790$	$\overline{12}.97492$
1697	5.891	$\overline{6}.97046$	$\overline{12}.58977$
1642	6.088	$\overline{6}.38478$	$\overline{12}.02583$
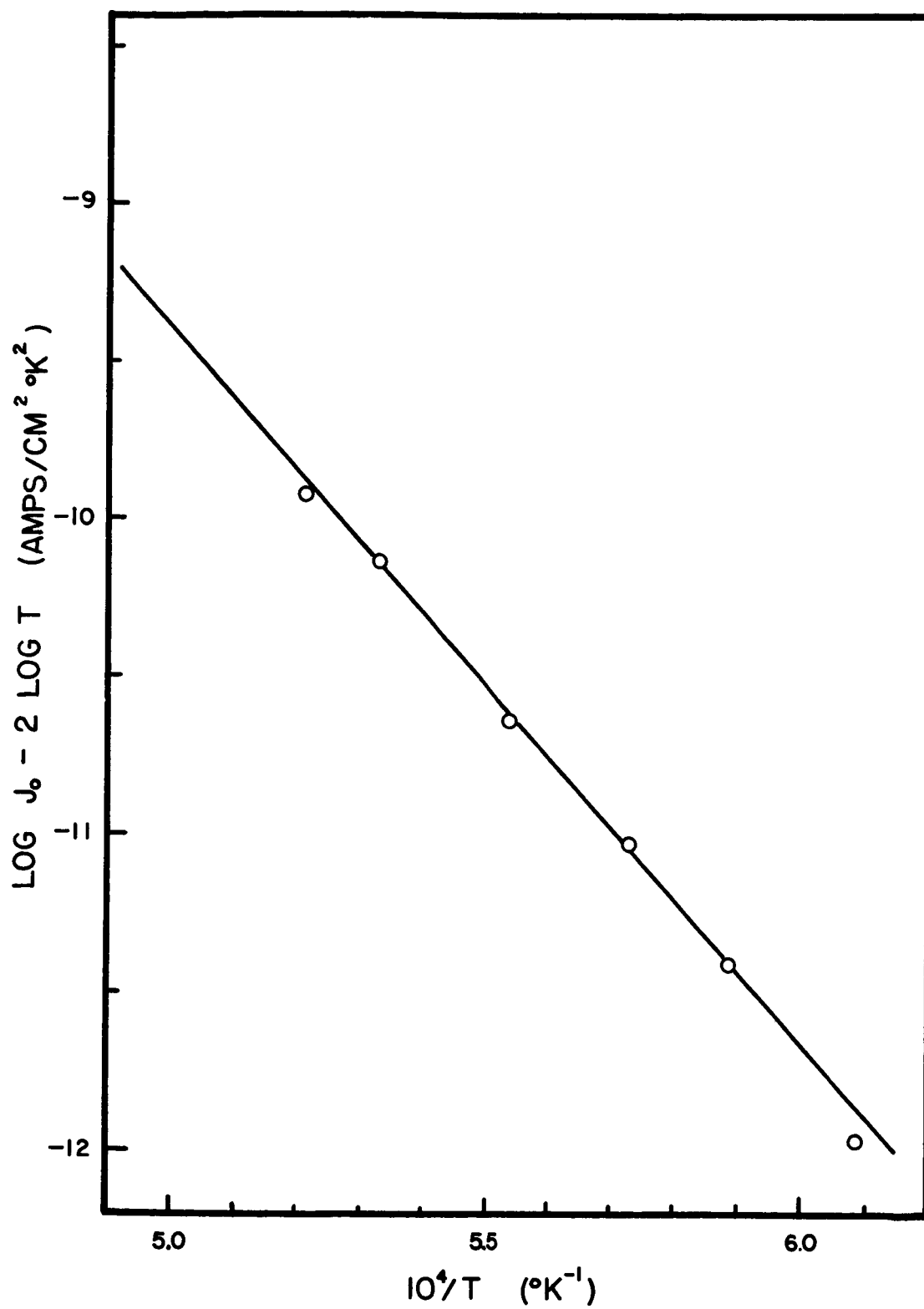
Figure 27. Richardson Plot for Re₃Mo₂

Re_3W_2

The thermionic properties of Re_3W_2 were not measured in the present investigation. Numerous specimens of the material were prepared and sent to the diode manufacturer. Of three diodes that were returned, one did not meet the specifications for concentricity and vacuum, and two were damaged in transit.

It is possible to estimate the work function, however. As discussed in the following chapter, isostructural materials in the Mo-Re and W-Re systems should have identical work functions, based on the number of electrons in the unfilled d-orbitals which determines the screening of the outermost electrons from the nuclear charge. All of the materials here discussed were found to fit this screening scheme very closely. The work functions of the α-Mn phases, Re_3Mo and Re_3W were 4.92 and 4.91 eV, respectively as predicted, which strongly suggests that the work functions of Re_3W_2 should be very nearly that of Re_3Mo_2, or about 4.78 eV.

Re$_3$Mo

Table XIII shows the emission currents, measured at various observed temperatures between 1100 and 1650C and at emitter-anode potentials of up to 1000 Volts. The Schottky plots for these data are shown in Figure 28 and the corresponding Richardson plot, constructed from the Schottky intercepts as in Table XIV is shown in Figure 29.

The slope and intercept of the Richardson plot, determined in a multiple regression analysis by the B-5500 computer, yielded a work function of 4.92 ± .02 eV and a coefficient, A_R, of 102 Amps/cm^2°K^2, respectively.

TABLE XIII

VARIATION OF EMISSION CURRENT WITH TEMPERATURE AND EMITTER-COLLECTOR POTENTIAL FOR Re_3Mo

Emitter Diameter 0.0350 cm   E = 13.77 V   j = 5.579 I

T_{OBS} (°C)	1650	1600	1575	1550	1525
$\epsilon_{\lambda,T}$	0.613	0.621	0.624	0.628	0.631
T_{BB} (°K)	2025	1968	1939	1911	1882
Current (Amps)	$I \times 10^4$	$I \times 10^5$	$I \times 10^5$	$I \times 10^5$	$I \times 10^5$
Potential (Volts)					
1000	1.46	5.46	4.62	2.33	1.58
900	1.42	5.31	4.52	2.23	1.54
800	1.39	5.18	4.41	2.23	1.50
700	1.36	5.03	4.32	2.17	1.47
600	1.31	4.88	4.16	2.10	1.42
500	1.27	4.70	4.00	2.02	1.36
400	1.23	4.50	3.82	1.92	1.30
300	1.15	4.24	3.62	1.81	1.23
200	1.08	4.00	3.36	1.67	1.14
100	1.00	3.48	2.83	1.46	0.982
75	0.951	3.40	2.72	1.38	0.916
50	0.868	3.23	2.51	1.30	0.859
40	0.838	3.10	2.49	1.26	0.830
30	0.815	2.85	2.35	1.23	0.797
25	0.808	2.76	2.29	1.20	0.782
16	0.780	2.67	2.18	1.12	0.740
9	0.658	2.60	2.04	1.08	0.692
4	0.440	2.00	1.40	0.940	0.610
0	0.0745	0.708	0.485	0.400	0.218

TABLE XIII (Continued)

T_{OBS} (°C)	1500	1475	1450	1425	1400
$\epsilon_{\lambda, T}$	0.635	0.639	0.642	0.646	0.650
T_{BB} (°K)	1854	1826	1798	1770	1742
Current (Amps)	$I \times 10^6$	$I \times 10^6$	$I \times 10^6$	$I \times 10^6$	$I \times 10^6$

Potential (Volts)					
1000	9.76	5.12	3.68	2.00	1.26
900	9.56	5.01	3.60	1.96	1.24
800	9.32	4.90	3.52	1.91	1.21
700	9.03	4.74	3.42	1.86	1.17
600	8.74	4.60	3.28	1.78	1.13
500	8.40	4.43	3.18	1.71	1.09
400	8.01	4.22	2.91	1.62	1.04
300	7.53	3.97	2.76	1.53	0.953
200	6.91	3.66	2.53	1.41	0.870
100	6.02	3.20	2.19	1.22	0.750
75	5.68	2.92	2.06	1.15	0.704
50	5.28	2.70	1.92	1.07	0.650
40	5.08	2.60	1.84	1.03	0.624
30	4.84	2.49	1.75	0.959	0.593
25	4.72	2.42	1.71	0.929	0.577
16	4.48	2.27	1.60	0.872	0.540
9	4.19	2.12	1.48	0.792	0.500
4	3.32	1.73	1.28	0.486	0.414
0	1.50	0.879	0.160	0.347	0.238

TABLE XIII (Continued)

T_{OBS} (°C)	1375	1350	1325	1300	1275
$\epsilon\lambda, T$	0.654	0.657	0.661	0.664	0.668
T_{BB} (°K)	1714	1686	1658	1631	1603
Current (Amps)	$I \times 10^7$	$I \times 10^7$	$I \times 10^7$	$I \times 10^7$	$I \times 10^8$
Potential (Volts)					
1000	8.33	4.46	2.49	1.38	6.71
900	8.08	4.33	2.43	1.35	6.59
800	7.86	4.25	2.36	1.32	6.39
700	7.63	4.08	2.28	1.28	6.17
600	7.36	3.96	2.21	1.23	5.91
500	7.04	3.80	2.10	1.18	5.65
400	6.70	3.61	2.00	1.12	5.35
300	6.30	3.40	1.87	1.05	5.00
200	5.74	3.11	1.71	0.914	4.55
100	4.92	2.68	1.46	0.778	3.88
75	4.64	2.53	1.37	0.728	3.64
50	4.34	2.32	1.26	0.667	3.34
40	4.12	2.22	1.21	0.638	3.20
30	3.92	2.11	1.15	0.606	2.97
25	3.82	2.06	1.12	0.586	2.88
16	3.58	1.91	1.05	0.548	2.68
9	3.27	1.75	0.924	0.504	2.49
4	2.50	1.32	0.686	0.382	2.22
0	1.52	0.798	0.417	0.216	1.12

TABLE XIII (Continued)

T_{OBS} (°C)	1250	1225	1200	1175	1150
$\epsilon_{\lambda, T}$	0.672	0.675	0.679	0.683	0.687
T_{BB} (°K)	1576	1549	1521	1494	1467
Current (Amps)	$I \times 10^8$	$I \times 10^8$	$I \times 10^8$	$I \times 10^9$	$I \times 10^9$

Potential (Volts)

1000	3.66	1.97	1.04	4.95	2.39
900	3.56	1.93	0.983	4.83	2.31
800	3.46	1.88	0.958	4.68	2.23
700	3.36	1.82	0.922	4.52	2.15
600	3.23	1.74	0.889	4.33	2.06
500	3.06	1.66	0.848	4.16	1.96
400	2.86	1.57	0.803	3.92	1.84
300	2.67	1.46	0.744	3.64	1.69
200	2.43	1.33	0.670	3.31	1.51
100	2.05	1.12	0.659	2.60	1.26
75	1.92	1.07	0.628	2.43	1.17
50	1.75	0.938	0.481	2.20	1.08
40	1.68	0.896	0.461	2.10	0.970
30	1.58	0.851	0.438	1.98	0.920
25	1.53	0.825	0.424	1.92	0.890
16	1.43	0.772	0.396	1.78	0.827
9	1.33	0.712	0.369	1.63	0.760
4	1.02	0.646	0.338	--	--
0	0.641	0.292	0.144	0.720	0.362

TABLE XIII (Continued)

T_{OBS} (°C)	1125	1100
$\epsilon_{\lambda, T}$	0.690	0.693
T_{BB} (°K)	1440	1413
Current (Amps)	$I \times 10^9$	$I \times 10^{10}$

Potential (Volts)

1000	1.14	5.32
900	1.11	5.09
800	1.08	4.95
700	1.00	4.74
600	0.924	4.55
500	0.883	4.32
400	0.836	4.05
300	0.764	3.72
200	0.679	3.28
100	0.555	2.52
75	0.515	2.34
50	0.465	2.11
40	0.442	2.00
30	0.420	1.89
25	0.410	1.82
16	0.378	1.70
9	0.350	1.59
4	--	--
0	0.155	0.630
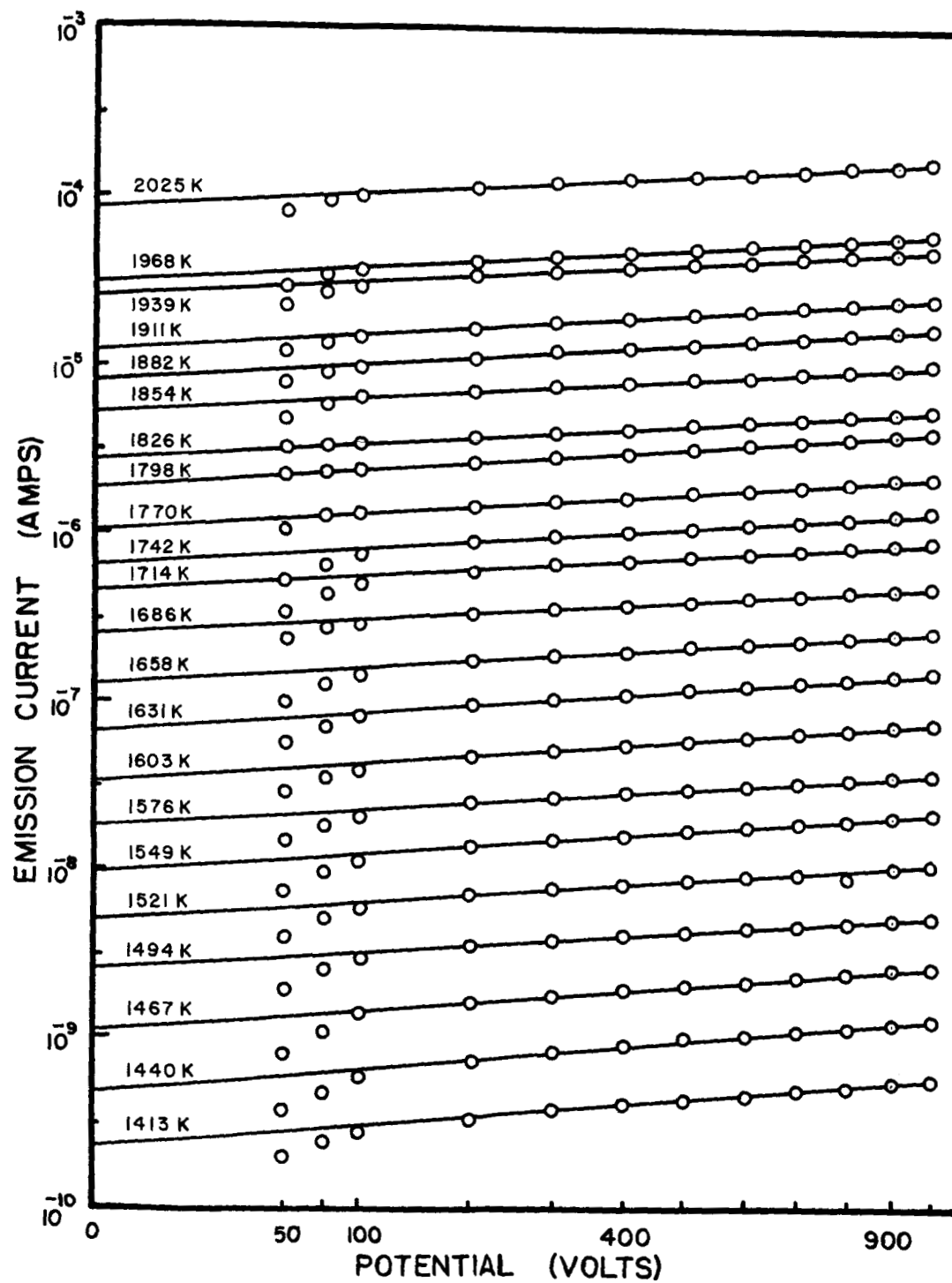
Figure 28. Variation of Emission Current with Emitter-Anode
Potential for Re₃Mo

TABLE XIV

FUNCTIONS OF ZERO-FIELD CURRENT DENSITY AND TEMPERATURE FOR CONSTRUCTION OF RICHARDSON PLOT FOR Re$_3$Mo

T_{BB} (°K)	$10^4/T_{BB}$ (°K^{-1})	log j$_0$	log j$_0$ - 2 log T_{BB}
2025	4.938	$\overline{4}$.47321	$\overline{11}$.86861
1968	5.083	$\overline{4}$.01735	$\overline{11}$.43785
1939	5.157	$\overline{5}$.93086	$\overline{11}$.36399
1911	5.234	$\overline{5}$.63839	$\overline{11}$.08442
1882	5.313	$\overline{5}$.46701	$\overline{12}$.92597
1854	5.394	$\overline{5}$.27360	$\overline{12}$.74575
1826	5.477	$\overline{5}$.00016	$\overline{12}$.48566
1798	5.562	$\overline{6}$.82278	$\overline{12}$.32167
1770	5.651	$\overline{6}$.57727	$\overline{12}$.09587
1742	5.742	$\overline{6}$.36849	$\overline{13}$.89492
1714	5.835	$\overline{6}$.18549	$\overline{13}$.72595
1686	5.931	$\overline{7}$.92227	$\overline{13}$.47684
1658	6.030	$\overline{7}$.65565	$\overline{13}$.22463
1631	6.131	$\overline{7}$.38972	$\overline{14}$.97320
1603	6.237	$\overline{7}$.07506	$\overline{14}$.67335
1576	6.345	$\overline{8}$.79515	$\overline{14}$.40845
1549	6.457	$\overline{8}$.53946	$\overline{14}$.16791
1521	6.573	$\overline{8}$.23489	$\overline{15}$.87881
1494	6.693	$\overline{9}$.93406	$\overline{15}$.59368
1466	6.817	$\overline{9}$.57893	$\overline{15}$.25450
1440	6.944	$\overline{9}$.19912	$\overline{16}$.89081
1413	7.077	$\overline{10}$.91246	$\overline{16}$.62053
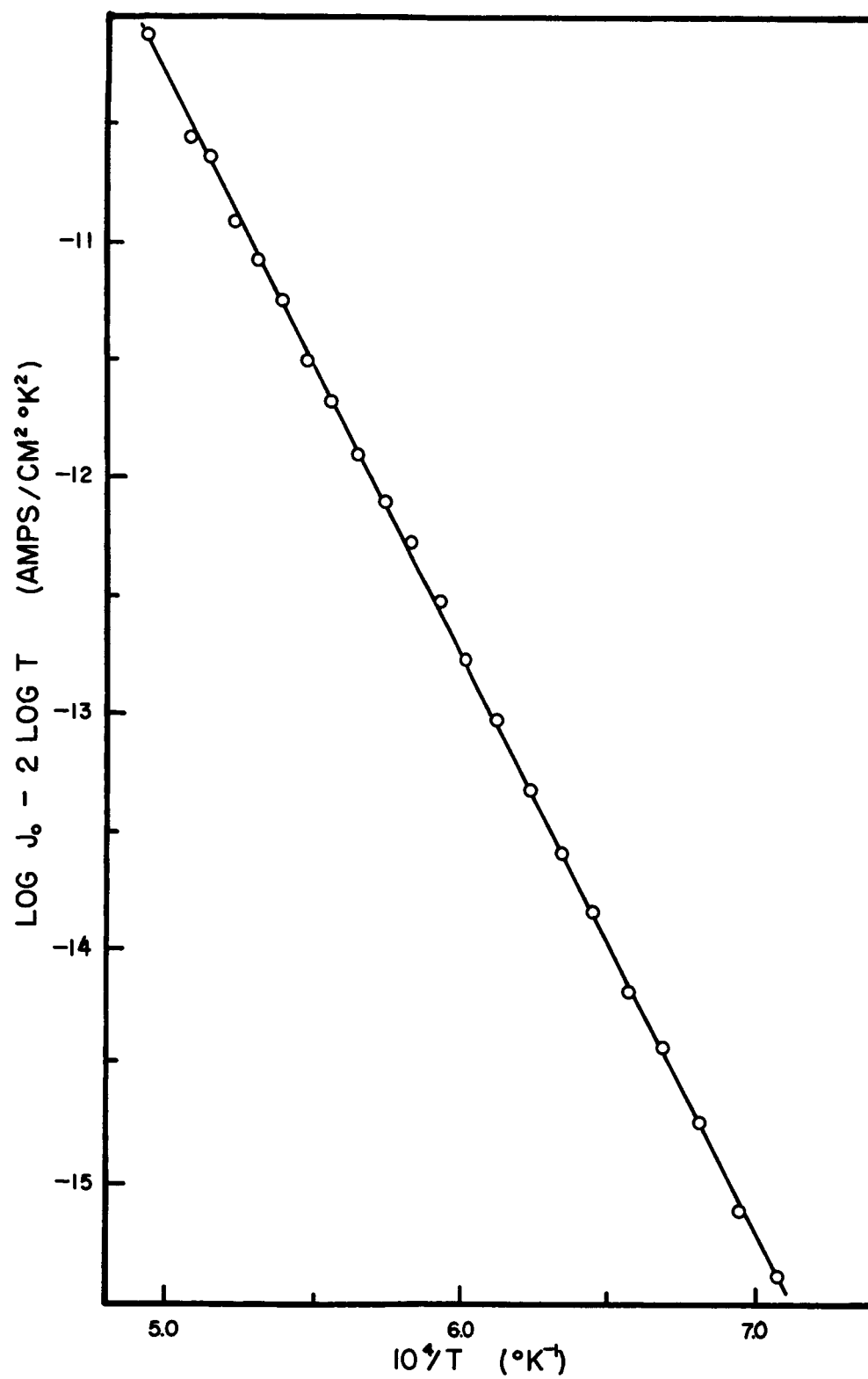
Figure 29. Richardson Plot for Re₃Mo

Re₃W

The emission currents shown in Table XV were used to construct the Schottky plots of Figure 30. The corresponding Richardson plot appears in Figure 31, constructed from Table XVI.

A computer fit of the data in Figure 31 yielded a work function of $4.91 \pm .02$ eV, and a coefficient, A_R, of 110 Amps/cm^{2}°K^{2}.

The abnormally steep slopes in the Schottky plots at the 1898, 1869 and 1840K temperatures in Figure 30 are attributed to contamination by gaseous impurities, and illustrate the necessity for flashing the filament before the series of measurements is begun.

TABLE XV

VARIATION OF EMISSION CURRENT WITH TEMPERATURE AND EMITTER-COLLECTOR POTENTIAL FOR Re$_3$W

Emitter Diameter 0.0356 cm   E = 13.60 V   j = 3.524 I

T_{OBS} (°C)	1603	1575	1550	1525	1500
$\epsilon_{\lambda,T}$	0.553	0.560	0.566	0.572	0.578
T_{BB} (°K)	1992	1958	1928	1898	1867
Current (Amps)	$I \times 10^4$	$I \times 10^4$	$I \times 10^5$	$I \times 10^5$	$I \times 10^5$
Potential (Volts)					
1000	2.05	1.24	8.59	6.84	3.41
900	2.00	1.22	8.42	6.04	3.33
800	1.95	1.16	8.24	5.24	3.23
700	1.90	1.13	7.96	5.11	2.66
600	1.86	1.10	7.54	4.94	2.30
500	1.80	1.05	7.12	4.65	2.22
400	1.70	1.00	6.78	4.30	2.10
300	1.57	0.942	6.38	4.06	1.94
200	1.40	0.848	5.80	3.70	1.73
100	0.956	0.623	4.52	2.92	1.43
75	0.736	0.498	3.76	2.49	1.25
50	0.468	0.328	2.43	1.73	0.980
40	0.388	0.247	1.85	1.14	0.778
30	0.282	0.183	1.35	0.949	0.549
25	0.238	0.153	0.114	0.759	0.426
16	0.155	0.0990	0.0708	0.448	0.252
9	0.0885	0.0552	0.0388	0.232	0.144
4	0.0424	0.0256	0.0176	0.120	0.0760
0	0.0057	0.0037	0.0027	0.0489	0.0342

TABLE XV (Continued)

TOBS (°C)	1475	1425	1400	1375	1350
$\epsilon\lambda$, T	0.584	0.597	0.603	0.609	0.615
TBB (°K)	1840	1781	1752	1723	1695
Current (Amps)	$I \times 10^5$	$I \times 10^6$	$I \times 10^6$	$I \times 10^6$	$I \times 10^7$
Potential (Volts)					
1000	2.54	9.27	5.04	1.09	6.77
900	2.49	9.15	4.98	1.08	6.64
800	2.42	8.99	4.90	1.06	6.54
700	2.32	8.81	4.82	1.05	6.44
600	1.97	8.40	4.72	1.02	6.28
500	1.70	8.08	4.58	1.00	6.16
400	1.64	7.30	4.32	0.977	6.04
300	1.51	5.76	3.88	0.956	5.86
200	1.34	5.19	3.04	0.934	5.68
100	1.12	4.18	2.40	0.790	5.00
75	1.00	3.83	2.15	0.720	4.76
50	0.770	3.12	1.81	0.652	4.28
40	0.625	2.68	1.59	0.598	4.16
30	0.440	2.22	1.30	0.529	3.95
25	0.345	1.99	1.10	0.489	3.72
16	0.196	1.11	0.764	0.398	3.18
9	0.121	0.673	0.394	0.274	1.96
4	0.0715	0.430	0.190	0.156	1.16
0	0.041	0.338	0.0690	0.0194	0.475

TABLE XV (Continued)

T_{OBS} (°C)	1325	1300	1275	1250	1225
$\epsilon_{\lambda, T}$	0.622	0.628	0.634	0.640	0.646
T_{BB} (°K)	1666	1638	1610	1582	1554
Current (Amps)	$I \times 10^7$	$I \times 10^7$	$I \times 10^7$	$I \times 10^7$	$I \times 10^8$

Potential (Volts)

1000	4.02	2.28	1.83	1.26	8.76
900	3.92	2.23	1.78	1.23	8.50
800	3.86	2.16	1.74	1.20	8.08
700	3.76	2.11	1.68	1.16	7.78
600	3.65	2.04	1.62	1.12	7.46
500	3.56	1.98	1.56	1.07	7.14
400	3.45	1.90	1.50	1.04	6.81
300	3.34	1.83	1.44	0.968	6.41
200	3.21	1.74	1.37	0.900	5.98
100	2.96	1.65	1.29	0.842	5.36
75	2.84	1.56	1.24	0.820	5.26
50	2.66	1.49	1.18	0.777	5.04
40	2.52	1.44	1.15	0.757	4.91
30	2.41	1.36	1.10	0.724	4.74
25	2.33	1.33	1.06	0.704	4.58
16	1.96	1.21	0.960	0.628	4.20
9	1.20	0.813	0.730	0.468	2.81
4	0.692	0.452	0.380	0.288	2.03
0	0.440	0.253	0.195	0.189	1.45

TABLE XV (Continued)

T_{OBS} (°C)	1200	1175	1148	1122	1094
$\epsilon\lambda, T$	0.653	0.659	0.665	0.672	0.656
T_{BB} (°K)	1526	1498	1468	1439	1412
Current (Amps)	$I \times 10^8$	$I \times 10^9$	$I \times 10^9$	$I \times 10^9$	$I \times 10^{10}$

Potential (Volts)

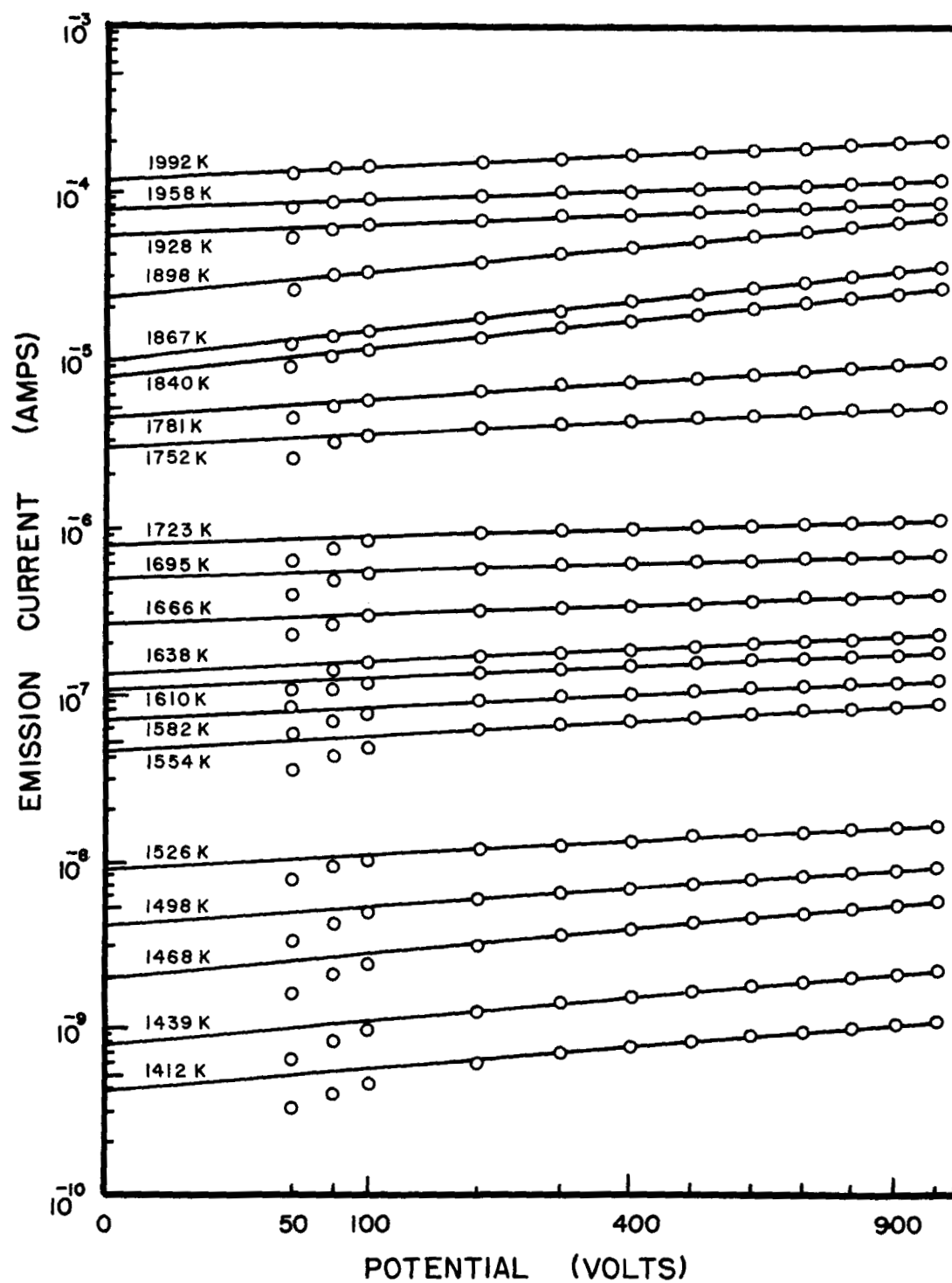|					
1000	1.73	8.98	4.76	2.14	11.0
900	1.64	8.55	4.50	2.01	9.90
800	1.59	8.22	4.35	1.90	9.08
700	1.52	7.85	4.14	1.79	8.42
600	1.46	7.49	3.94	1.67	7.75
500	1.39	7.11	3.72	1.56	7.17
400	1.32	6.73	3.50	1.47	6.49
300	1.24	6.30	3.25	1.34	5.86
200	1.17	5.81	2.92	1.22	5.10
100	1.04	5.20	2.57	1.07	4.29
75	1.01	5.05	2.48	1.03	4.12
50	0.980	4.86	2.37	0.954	3.89
40	0.956	4.78	2.33	0.936	3.78
30	0.932	4.67	2.26	0.910	3.67
25	0.924	4.61	2.23	0.897	3.61
16	0.870	4.42	2.14	0.855	3.42
9	0.829	4.20	2.01	0.802	3.26
4	0.578	3.05	1.28	0.515	2.11
0	0.298	1.68	0.919	0.383	1.50

Figure 30. Variation of Emission Current with Emitter-Anode Potential for Re_3W

TABLE XVI

FUNCTIONS OF ZERO-FIELD CURRENT DENSITY AND TEMPERATURE FOR CONSTRUCTION OF RICHARDSON PLOT FOR Re_3W

| $T_{BB}(°K)$	$10^4/T_{BB}(°K^{-1})$	$\log j_0$	$\log j_0 - 2 \log T_{BB}$
1992	5.021	$\overline{4}.58757$	$\overline{11}.98766$
1958	5.107	$\overline{4}.35904$	$\overline{11}.77397$
1928	5.186	$\overline{4}.17819$	$\overline{11}.60647$
1898	5.267	$\overline{5}.90991$	$\overline{11}.35168$
1869	5.351	$\overline{5}.48348$	$\overline{12}.93886$
1840	5.436	$\overline{5}.40879$	$\overline{12}.87793$
1781	5.615	$\overline{5}.25703$	$\overline{12}.75423$
1752	5.707	$\overline{5}.08203$	$\overline{12}.59344$
1723	5.802	$\overline{4}.45840$	$\overline{13}.98418$
1695	5.900	$\overline{6}.24035$	$\overline{13}.78069$
1666	6.002	$\overline{7}.97367$	$\overline{13}.52883$
1638	6.106	$\overline{7}.69585$	$\overline{13}.26590$
1610	6.213	$\overline{7}.58305$	$\overline{13}.16820$
1582	6.323	$\overline{7}.38989$	$\overline{14}.99033$
1553	6.437	$\overline{7}.18294$	$\overline{14}.79888$
1525	6.555	$\overline{8}.46793$	$\overline{14}.09968$
1498	6.676	$\overline{8}.15739$	$\overline{15}.80509$
1468	6.812	$\overline{9}.83567$	$\overline{15}.50080$
1439	6.948	$\overline{9}.43222$	$\overline{15}.11452$
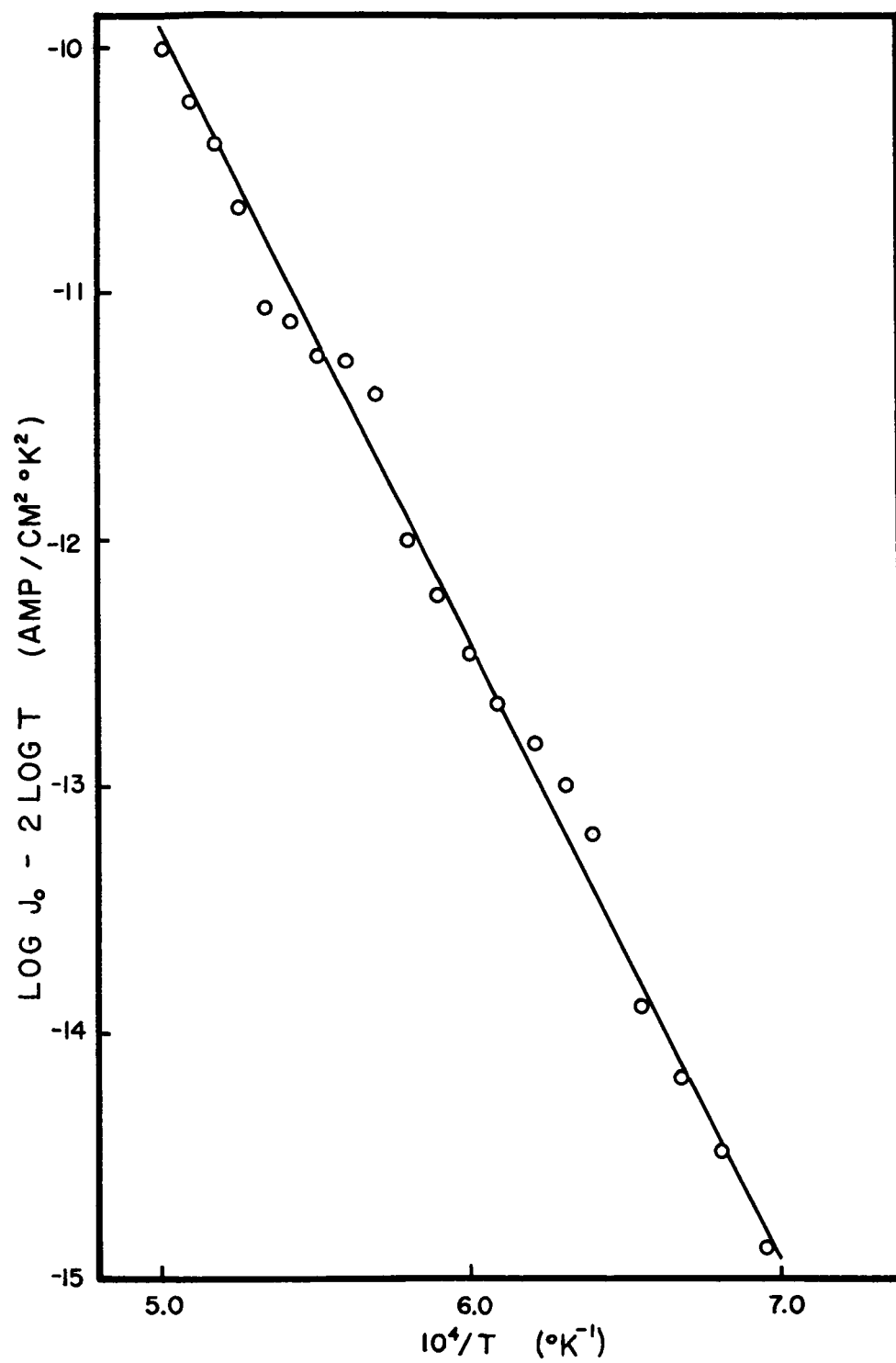
Figure 31. Richardson Plot for Re₃W

Error Analysis

The investigation here described required the independent experimental measurement of temperature, cathode-anode potential and emission current.

The principal source of systematic errors is in the measurement of temperature. Removal of these errors has been discussed in the previous chapter. The following discussion describes the statistical treatment of random errors.

Recall that the current densities at zero field, used for construction of the Richardson plot, are obtained from a linear extrapolation of the Schottky plot, $\log j$ vs. $E^{\frac{1}{2}}$, at various temperatures. A logical first step is to determine the effect of uncertainty in measurement of V and T on the emission current. If the effect is small with respect to the uncertainty of the current measurement, it can be neglected and the uncertainty of the latter used in the final error-propagation calculation.

The preliminary calculation is based on the Schottky equation which was previously derived,

$$\log j = \log j_0 + \frac{1.913}{T} E^{\frac{1}{2}} \qquad (2\text{-}27)$$

where j is the current density, T is the absolute temperature and E is the electric field strength.

As stated previsouly, the high voltage power supply is variable in one-volt increments by decade switching and is regulated to within one percent of the desired value over the entire 0 to 1000-volt range at the rated current. The instrument was calibrated with a 1/2-percent Weston precision voltmeter and found to be somewhat better than the one-percent value.

The Keithley micro-microammeter used to measure current is similarly advertised as a one-percent device, although no calibration equipment was available with which to check this claim.

The Pyro micro-optical pyrometer, used for temperature measurement, has three nonlinear scales with provision for overlap when switching between scales. The smallest scale divisions correspond to 5C, with some experience it is possible to reproduce temperature differences of less than 5C after the method described by Plunkett[43].

For the following worst-case calculation, conservative estimates of the uncertainties were taken to be:

voltage   0.01 (fractional uncertainty)

current   0.01 (fractional uncertainty)

temperature   5K (absolute uncertainty)

In general, if z is a function of x and y, the absolute uncertainty in z, due to uncertainties in x and y, is given by

$$dz = \left[\left(\frac{\partial z}{\partial x}\right)_y^2 dx^2 + \left(\frac{\partial z}{\partial y}\right)_x^2 dy^2 \right]^{\frac{1}{2}} \tag{4-1}$$

From the Schottky equation (2-27)

$$\log j = \log j_0 + \frac{1.913}{T} E^{\frac{1}{2}} \tag{2-27}$$

$$d \log j = \frac{dj}{j} = \left[\left(\frac{1.913}{2T} E^{-\frac{1}{2}}\right)^2 dE^2 + \left(-\frac{1.913 E^{\frac{1}{2}}}{T^2}\right)^2 dT^2 \right]^{\frac{1}{2}} \tag{4-2}$$

Because of the logarithmic nature of the Schottky equation, the absolute uncertainty in log j is equal to the fractional uncertainty in j, that is, $d \log j = dj/j$.

Equation (2-46) of Chapter II relates the electric field strength, E, at the emitter surface to the applied emitter-anode potential. The quantity in brackets is greatest for small emitter radii; its maximum value for the present diodes is 17.6 cm^{-1}, whence

$$E = 17.6 \text{ V}. \tag{4-3}$$

Changing the variable E in equation (4-3) to V, one obtains, with some simplification, the following expression:

$$\frac{dj}{j} = \frac{8.035}{T} \left[\frac{1}{4V} dV^2 + \frac{V}{T^2} dT^2 \right]^{\frac{1}{2}} \qquad (4-4)$$

By inspection of equation (4-4), the fractional uncertainty is apparently greatest for low temperatures and high potentials.

For a worst-case calculation then, one might use the following typical values:

V = 1000 Volts

dV = .01 (1000) = 10 Volts

T = 1000K

dT = 5K

Substituting the above values in equation (4-2), one finds the fractional uncertainty in current density to be 0.0018 or about 0.2 percent. Since this value is much less than the one-percent precision of the electrometer, the larger value must be used in subsequent error propagation calculations. It is important to note that since current and current density are related by a constant factor, the fractional uncertainty in current density is equal to the fractional uncertainty in the current.

$$\frac{dj}{j} = \frac{dI}{I} = 0.01 \qquad (4-5)$$

The same argument is used for the electric field strength and the applied potential which are similarly related by a constant factor; hence their fractional uncertainties must be likewise identical.

$$\frac{dE}{E} = \frac{dV}{V} = 0.01 \qquad (4-6)$$

Having determined the fractional uncertainty in current (or current density) to be 0.01, and knowing the fractional uncertainty of the potential to be 0.01 as well, it is possible to calculate the uncertainty of the zero-field current density. Recall that the zero-field value is

obtained by a linear extrapolation of a Schottky plot, $\log j$ vs $E^{\frac{1}{2}}$, or $\log I$ vs $V^{\frac{1}{2}}$ as in the present investigation.

The best straight line is obtained by the method of least squares, for which Parratt[44] has developed expressions for the uncertainties in the slope and the intercept. Parratt's equations are as follows:

$$\text{slope: } S_m = \left[\frac{n}{n\Sigma x_i^2 - (\Sigma x_i)^2}\right]^{\frac{1}{2}} S_y \tag{4-7}$$

$$\text{intercept: } S_b = \left[\frac{\Sigma x_i^2}{n\Sigma x_i^2 - (\Sigma x_i)^2}\right]^{\frac{1}{2}} S_y \tag{4-8}$$

in the above equations, the x_i's are the abcissal values, S_m and S_b are the uncertainties in the slope and intercept, respectively, S_y is the uncertainty in the ordinal measurement and n is the number of measurements.

A brief explanation of the above equations is required. They are derived by minimizing the sum of the squares of the deviations from the straight line $y = mx, + b$ with respect to the slope, m, and the intercept, b. Strictly speaking, the deviations should be taken normal to the line, but Parratt has explained that the resulting calculation is extremely laborious. He has derived the above equation by measuring the deviations in the y-direction only; uncertainties in the x-direction are considered negligible.

The uncertainties reported in the previous sections were determined by a digital computer which was programed to handle uncertainties in both variables. The following calculations for the Schottky intercepts were in excellent agreement with the computer-fitted values.

Equation (4-8) is utilized to determine the uncertainty of the Schottky intercept. In the following tabular presentations the abcissal values, x_i, are replaced by $V^{\frac{1}{2}}$, and the ordinal uncertainty, S_y, is

simply the maximum fractional uncertainty of the electrometer, which was previously found to be 0.01. The uncertainty of the intercept, S_b, is, of course,

$$\frac{dI_0}{I_0} = \frac{dj_0}{j_0} = d \log j_0 .$$

(4-9)

Table XVII shows how loss of data at the relatively low potentials strongly affects the Schottky intercept. From the discussion in Chapter II, one may recall that the Langmuir-Child Law does not predict that the potential at which the Schottky plot becomes linear increases with decreasing temperature, whereas the effect is so pronounced that it can be observed in almost any series of Schottky plots. Figure 8, for example, shows the effect clearly in Haas and Jensen's[23] measurements on UC. It was primarily for this reason that the Langmuir-Child Law and the effective-work-function method of Hensley were rejected in favor of the present method, although the former method is undoubtedly the more expedient.

As Table XVIII shows, a loss of data at higher potentials has much less effect on the uncertainty of the intercept. The uncertainty is decreased from about two percent to one percent as the maximum potential is increased from 400 to 1000 Volts. However, with only four or five points, it is often difficult to make a decision regarding the extent of the linear region, and how many points should be included for extrapolation purposes. It was for this reason that the equipment was modified, following the initial tungsten measurements, to include a 1000-Volt power supply instead of the 400-Volt prototype.

Having determined the uncertainty of the Schottky intercept, $d \log j_0 = 0.03$, it is necessary to propagate this uncertainty into the

TABLE XVII

EFFECT OF REDUCTION IN NUMBER OF MEASUREMENTS AT LOW* POTENTIALS ON UNCERTAINTY OF SCHOTTKY INTERCEPT

Number of Measurements	Minimum Potential (Volts)	$\Sigma V_i^{\frac{1}{2}}$	ΣV_i^2	$(\Sigma V_i^{\frac{1}{2}})^2$	dj_0/j_0
10	100	224.7	5500	49001	0.0092
9	200	214.7	5400	46096	0.015
8	300	200.6	5200	40240	0.020
7	400	183.3	4900	33599	0.026
6	500	163.3	4500	26667	0.037
5	600	140.9	4000	19853	0.052
4	700	116.4	3400	13549	0.082

* The maximum potential is taken to be 1000 Volts, with measurements made in increments of 100 Volts.

** For the intermediate phase materials here described, the minimum number of points used in the Schottky extrapolation was seven. In most cases, at least 10 could be used, but the maximum uncertainty, 0.03, is used for subsequent uncertainty propagations.

TABLE XVIII

EFFECT OF REDUCTION OF NUMBER OF MEASUREMENTS AT HIGH* POTENTIALS ON UNCERTAINTY OF SCHOTTKY INTERCEPT

Number of Measurements	Maximum** Potential (Volts)	$\Sigma V_i^{\frac{1}{2}}$	ΣV_i	$(\Sigma V_i^{\frac{1}{2}})$	dj_0/j_0
10	1000	224.7	5500	49001	0.0092
9	900	193.1	4500	37288	0.012
8	800	163.1	3600	26602	0.013
7	700	134.8	2800	18171	0.014
6	600	108.3	2100	11729	0.016
5	500	83.8	1500	7022	0.018
4	400	61.4	1000	3770	0.021

* The minimum potential was taken to be 100 Volts with measurements made at 100-Volt increments.

** The maximum potential for the intermediate-phase materials was 1000 Volts in all cases. The prototype equipment used for the thermionic measurements on pure tungsten had a power supply with only a 400-Volt potential capability.

uncertainty of the work function. However, upon inspection of the Richardson-Dushman equation written in logarithmic form,

$$\log j_0 - 2\log T = \log A_R - \phi_R / 2.303 kT, \qquad (4\text{-}10)$$

the left side of the equation is found to contain both of the variables, j_0 and T. There are uncertainties associated with each, and neither of the uncertainties is negligible. A trial calculation using equation (4-7) yielded an uncertainty in ϕ_R of only 0.01 eV, whereas the computer-fitted values were in the range 0.02 to 0.10 eV. The discrepancies are, of course, due to the uncertainty in T, assumed negligible by equation (4-7) but taken into account by the multiple regression analysis of the B-5500 computer.

Summary

Table XIX summarizes the work functions of the various intermediate-phase materials and the constants, A_R, obtained in the present investigation.

TABLE XIX

RICHARDSON WORK FUNCTIONS AND EMISSION
CONSTANTS OF GROUP VIA-Re INTERMEDIATE
PHASE MATERIALS

Material	Structure	ϕ_R (eV)	A_R (Amps/cm^2°K^2)
Re_3Cr_2	σ	4.57 ± .10	2.0
Re_3Mo_2	σ	4.78 ± .07	9.5
Re_3W_2	σ	--	--
Re_3Mo	α-Mn	4.92 ± .02	102
Re_3W	α-Mn	4.91 ± .02	110

CHAPTER V

DISCUSSION

Occurrence of Group VIA-Re Intermediate Phases in the Binary Systems

Cr-Re, Mo-Re and W-Re

In early studies of the constitutional features of binary systems

of transition metals, Hume-Rothery and Raynor[45] noted that in passing

across various binary systems of these metals, intermediate phases

always appeared in the following order by structure:

$$\text{b. c. cube} \rightarrow \beta\text{-W} \rightarrow \sigma \rightarrow \alpha\text{-Mn} \rightarrow \text{c. p. hex} \rightarrow \text{f. c. cube}$$

In individual systems, one or more of the above phases may be absent,

but the characteristic order is always retained.

The Group-VIA metals are all body-centered cubic, and rhenium

is hexagonal, close-packed. On the basis of the above scheme, one

might reasonably expect any of the intermediate phases. In practice,

however, the β-W phase is not observed in any of the systems, the σ

phase is present in all three and the α-Mn phase is found in only the

Mo-Re and W-Re systems as discussed previously in Chapter I (Figures

3, 4, and 5).

The role of electronic factors in the occurrence of σ phases

has been the subject of considerable controversy. As mentioned pre-

viously, the σ-phase materials of the present study are, except for the

Cr-Re system, of rather broad compositional extent. Hence the com-

positions of the σ-phase materials in the Mo-Re and W-Re systems

were arbitrarily selected so as to be of the same stoichiometric com-

position, nominally Re_3M_2, or 60 atomic-percent rhenium.

Hume-Rothery and Raynor[45] have pointed out that the electronic

configuration of the transition metals is not well understood, the exact

number of bonding electrons being in considerable doubt. However, if one uses as the number of electrons those which are outside the inert-gas ion cores, as is common for some of the simpler metals, the Group-VIA elements each have six electrons, and rhenium has seven, occupying the orbitals shown in Table XX.

TABLE XX

ELECTRONIC CONFIGURATION OF OUTERMOST ELECTRONS
IN GROUP-VIA METALS AND RHENIUM

Transition Metal	Electronic Configuration	Number of Bonding Electrons
Cr	$3d^5 4s^1$	6 (Pauling, 5.78)
Mo	$4d^5 5s^1$	6
W	$5d^4 6s^2$	6
Re	$5d^5 6s^2$	7

For the σ phases of composition Re_3M_2 then, the electron/atom ratio would be:

$$\frac{e}{a} = \frac{3(7) + 2(6)}{5} = \frac{33}{5} = 6.60$$

Similarly the σ-Mn phases, nominally Re_3M, would have the following ratio:

$$\frac{e}{a} = \frac{3(7) + 1(6)}{4} = \frac{27}{4} = 6.75$$

If electronic factors govern the presence of these intermediate phases, one might reasonably expect that when rhenium is replaced by another transition metal, so as to alter the number of electrons outside the inert gas core, the intermediate phases would be shifted in composition so as to preserve the e/a ratio. Knapton[46] has studied the occurrence of numerous σ phases and found exactly such a shift in composition

upon substituting osmium and iridium for rhenium, in both Group VA and VIA-metal systems. Unfortunately, the α-Mn phases are not observed when osmium and iridium are substituted for rhenium; therefore a similar prediction for these phases cannot be checked.

The absence of the α-Mn phase in the Cr-Re system is also predictable by the Hume-Rothery and Raynor scheme, if one uses as the valency of chromium 5.78 rather than 6, according to the Pauling hypothesis. There is considerable justification for use of the 5.78 value; it is the difference between the six electrons in the outer shells and 0.22, the number in so-called atomic d-orbitals, which are not available for bonding. Hume-Rothery, Irving, and Williams[47] in their so-called "modified scheme" assigned the 5.78 value to chromium, but retained the value of 6 for molybdenum and tungsten. Using the 5.78 value for chromium, the α-Mn phase would have an e/a ratio of 6.69, just below the 6.7-7.0 range given by Hume-Rothery and Raynor as characteristic of that phase.

From consideration of the complex structure of the σ-phase, shown in Figure 1, it is generally agreed, according to Hume-Rothery and Raynor, that the foregoing treatment is over simplified. Figure 1 shows that atoms in the basal planes, and in the plane c/2 above the basal plane in the unit cell, are located directly one above the other. In between are "rumpled" layers of atoms in a hexagonal array. The upper rumpled layer is rotated 90° from the lower and displaced by half the base diagonal of the unit cell as in Figure 2.

Now if we choose as an example the system Mo-Re, in which the σ phase has a unit cell of dimensions a = 9.54A, c = 4.95A, the plane sheets lie only c/2 apart, or 2.48A. This is much less than the closest approach of atoms in either of the pure metals (Mo, 2.72A, and Re,

2. 73A). Numerous ordering schemes have been proposed for the structure[3], in which there exist five distinct types of sites. The fact remains, however, that whichever atoms occupy these sites, they must be forced much more closely together than they are in either of the pure metals. This abnormal proximity suggests that their electronic constitutions must be different from those of either of the pure constituents. Furthermore, as Bradley and Preston[48] have observed, the valence of atoms in complex crystals depends upon the type of site they occupy, and that different atoms of the same species may assume different valencies within the same crystal if they occupy more than one type of site.

Correlation of Work Functions with Related Properties

The work functions of the various intermediate-phase materials and their temperature dependence were summarized in Table XIX of the previous chapter. As stated previously, the present theories regarding the transition metals are inadequate for prediction of the work functions, even for the pure elements. For this reason, many investigators have attempted to correlate experimentally-determined work functions with a number of related physical and chemical properties of the pure materials, several of which are shown in Table XXI.

TABLE XXI

SELECTED PROPERTIES OF GROUP-VIA
ELEMENTS AND RHENIUM

Element	At. No.	ΔH_S (Kcal/mol)	E_0^0 (eV)	ϕ (eV)
Cr	24	90	6.7	4.51
Mo	42	160	7.4	4.27
W	74	205	8.0	4.50
Re	75	190	7.8	5.1

Wigner and Bardeen[30] first postulated the relationship between the work function and the heat of sublimation in 1935. According to these investigators, the work function consisted of two parts; the binding energy of the lattice, hence ΔH_s, and the energy required to move the electron through the dipole layer at the metal surface, although in their treatment this latter factor was neglected. They did obtain qualitative agreement with experimentally determined work functions, particularly those of the alkali metals. However, as Goodman and Homonoff[1] have pointed out, their treatment depends on the assumption that the electronic structure is one of completely filled inner shells surrounded by a single bonding electron. This is, of course, not the case for transition metals.

Figure 32 shows the work functions of the intermediate-phase materials of the present study and the heats of sublimation of Cr, Mo, and W, both plotted as functions of atomic number.

Since the true work function is defined as the energy necessary for the removal of an electron from the surface of the solid, one wonders immediately how this might compare with the energy required for removal of an electron from a Group VIA atom; hence, a correlation with the first ionization energies is also shown in Figure 32. Because of the great similarity in the increase of both E_0^0 and ΔH_s within Group VIA, the points are practically coincident. The lines connecting the data in Figure 32 are not intended to denote intermediate points since it is well known that both of these properties, the work function, and a great many other properties of the elements vary in periodic fashion with atomic number, usually reaching a maximum at Group VIA or VIIA. Within Group VIA the work functions of the elements change only slightly, and show a slight decrease in passing from chromium to molybdenum.
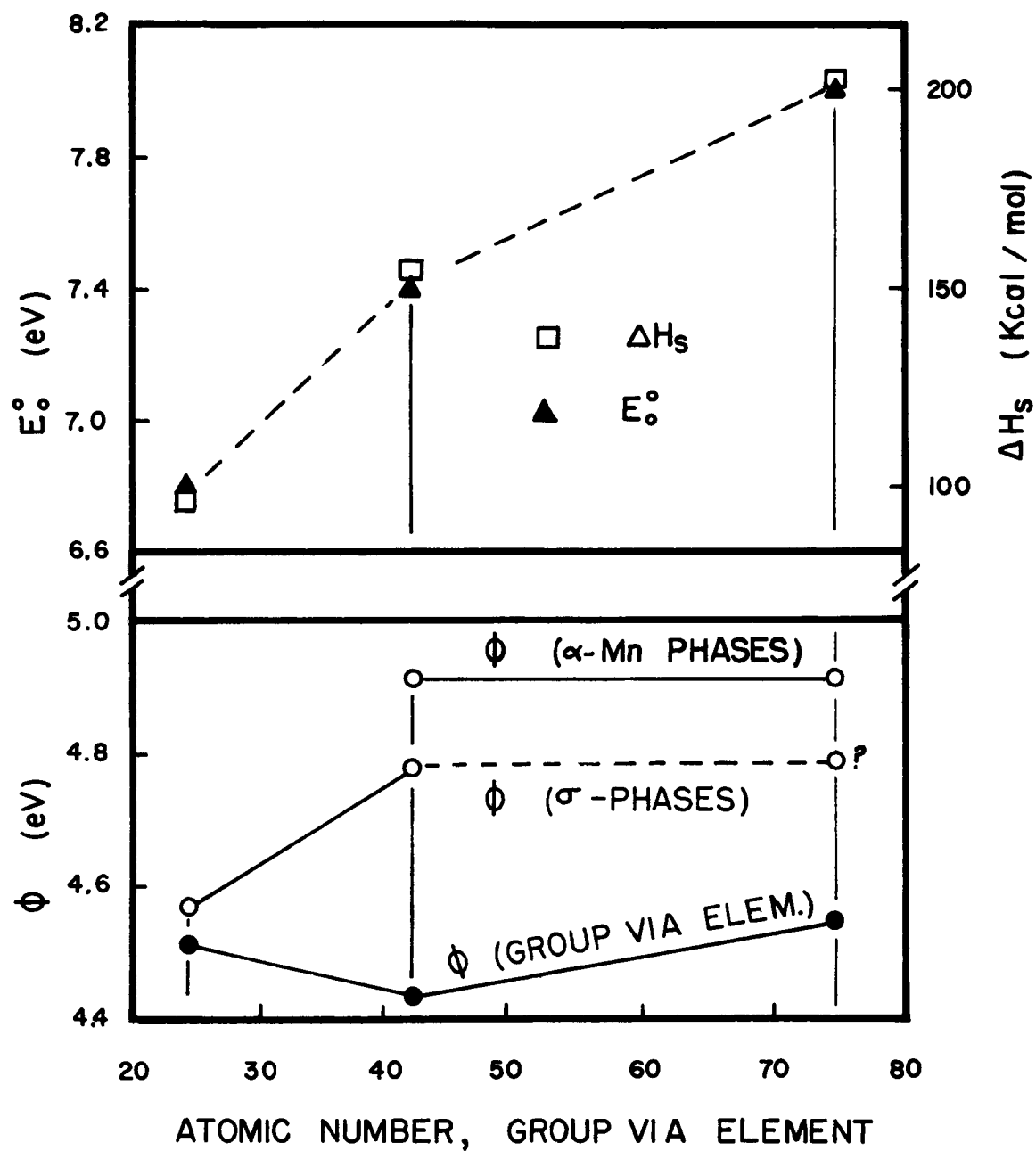
Figure 32. Variation of Work Function with Atomic Number as Compared
with Variation of Heat of Sublimation and First Ionization
Potentials

Upon examination of Figure 32, it is apparent that the Wigner-Bardeen scheme relating the work functions to the heat of sublimation is inadequate not only for the intermediate phase materials of this study but for the pure VIA elements as well. The first ionization potentials, which vary in a manner similar to ΔH_S, seem equally inadequate, therefore.

Samsonov and Neshpor[49] developed a scheme relating the work function of transition metals to the quantity $1/Nn$, where N is the principal quantum number of the incomplete d-orbitals, and n is the number of electrons occupying those levels in the free atom of the transition metal. The quantity $1/Nn$ is interpreted as being a measure of the screening of the s-electrons from the nuclear charge. The work function decreases as the screening increases as shown in Figure 33.

Applying this scheme to the VIA metals, we find that $1/Nn$ for chromium, molybdenum, and tungsten takes the values shown in Table XXII.

TABLE XXII

SCREENING CONSTANTS AND WORK FUNCTIONS OF GROUP VIA
ELEMENTS AFTER THE METHOD OF SAMSONOV AND NESHPOR[49]

VIA Metal	N	n	$1/Nn$	ϕ (eV)
Cr	3	5	0.067	4.51
Mo	4	5	0.05	4.42
W	5	4	0.05	4.53

The intermediate phase materials of the present study seem to fit such a scheme more satisfactorily than even the Group-VIA elements. For example, $1/Nn$ for chromium is 0.067, and one would predict a value for pure chromium lower than those of either molybdenum or
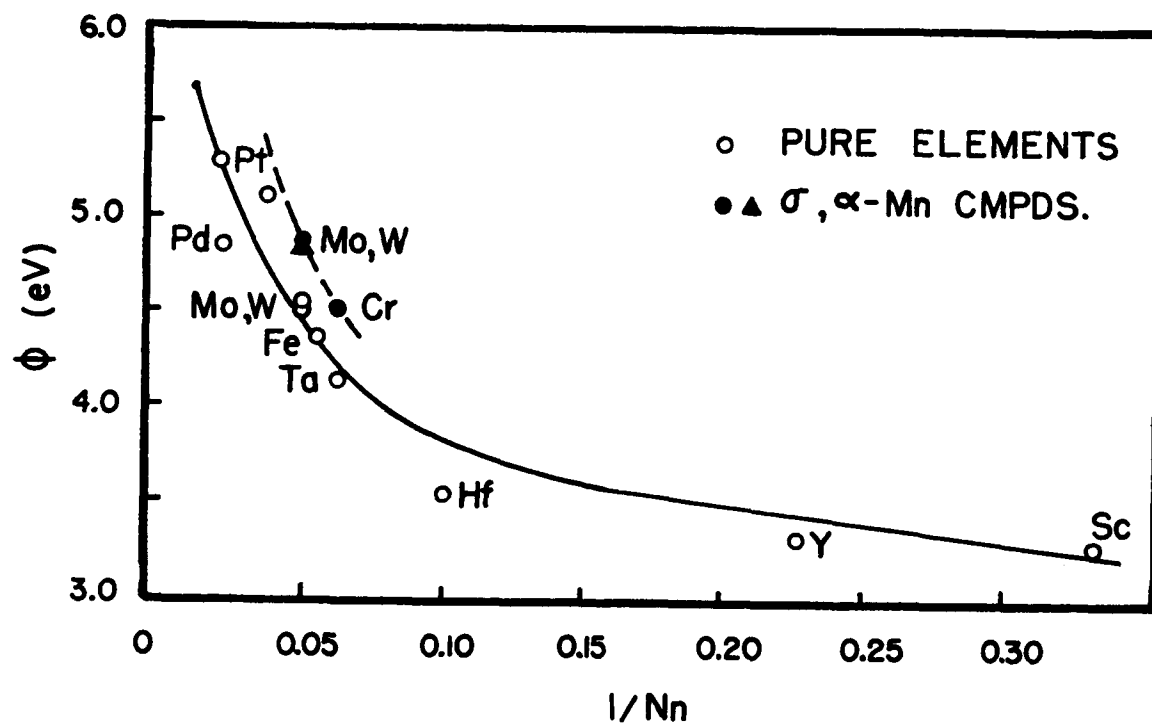
Figure 33. Variation of the Work Function with Screening of Electrons
from the Nuclear Charge in Transition Metals and Group
VIA-Re Intermediate Phases

tungsten, whereas it actually lies roughly midway between, at about
4. 5 eV.

Applying the method to the present intermetallic compounds,
we find that the scheme requires the work functions of isostructural
materials containing molybdenum and tungsten to be substantially the
same, since 1/Nn is 0. 05 for both. The work function of the corre-
sponding chromium compound should be somewhat lower because of the
higher screening constant, 0. 067. The upward displacement of the
curve from that describing the pure metals is attributed to the rhenium
content in each of the compounds, but the form of the curve appears to
be what one might reasonably expect.

The α-Mn phases in the Mo-Re and W-Re systems do indeed
have practically identical work functions, and one would expect the
σ phases to behave in similar fashion; that is, the work function of
Re_3W_2 should be very nearly the same as that for Re_3Mo_2, 4. 78 eV.

Finally, the variation of the work function with composition is
of interest. Figure 33 shows the work functions of the materials of the
present study as a function of rhenium content. Husmann[17] has mea-
sured the work functions of W-Re alloys in the W-rich solid solution
region up to about 26 weight percent rhenium. His work did not include
the intermetallic compounds here described, but he apparently proposed
the continuous change with composition as indicated by the dotted line
in Figure 34.

An alternate solution, based on the thermodynamical model
described in Chapter II, is proposed. The model presumes the metal
to be in equilibrium with the electron vapor and the work function was
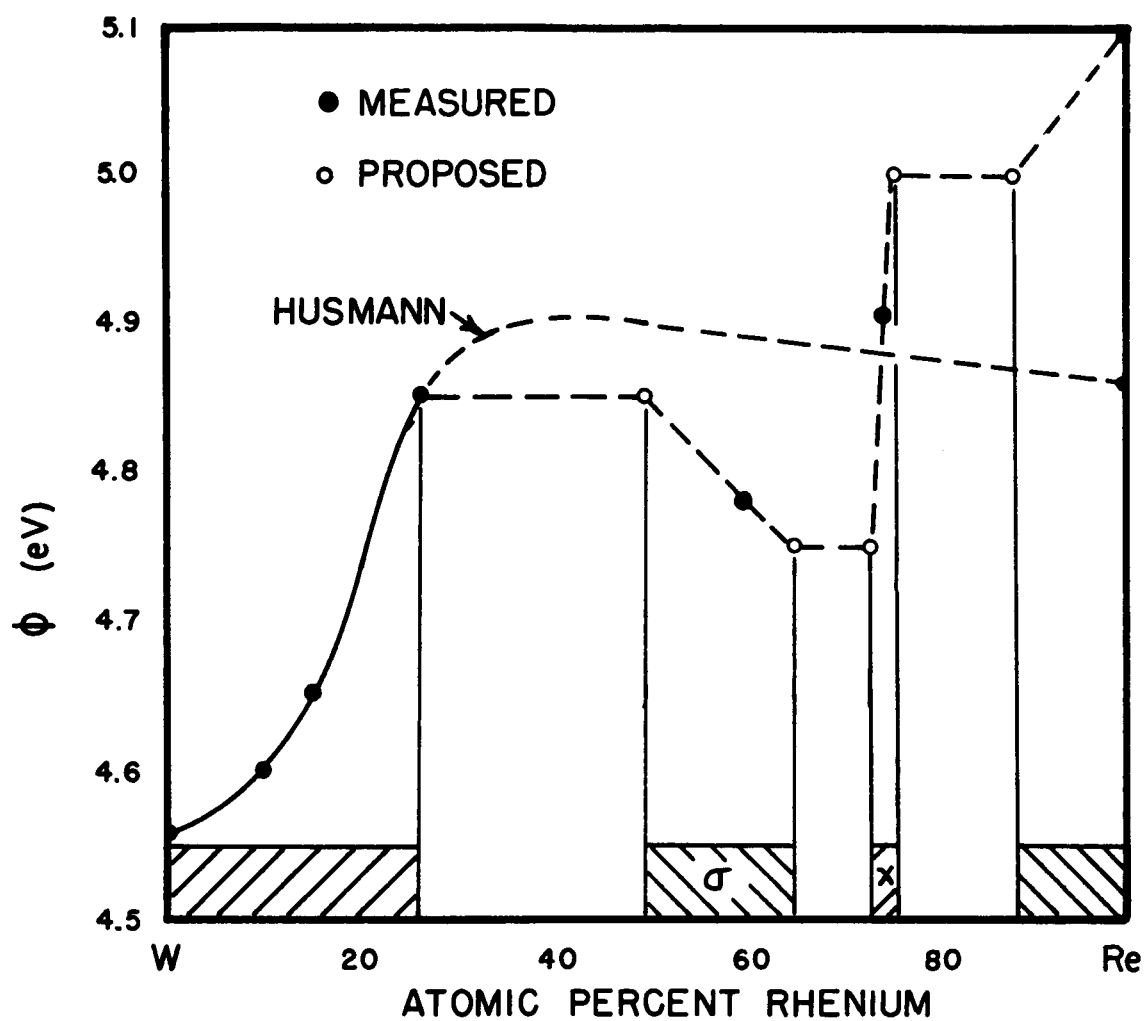found to be the negative of the chemical potential.

Figure 34. Variation of the Work Function with Composition in W-Re Alloys. Shaded Areas Indicate Approximate Extent of Single-Phase Regions Between Which the Work Function Must be Invariant

In regions in which two solid phases are in equilibrium with the electron gas, the chemical potential must be the same for each phase and therefore invariant across the entire two-phase region. Hence, the work function, identified with the negative of the chemical potential, would be similarly invariant within the region.

Combining the data of Husmann with those of the present study then, one may construct a diagram similar to that illustrated in Figure 34.

In the absence of data in the two-phase regions, which would determine the work function at the phase boundaries, a linear variation of the work function with composition is presumed.

Admittedly, the model is greatly simplified. The idealized mathematical treatment of the electron vapor neglects the numerous and complex effects which may modify the surface-potential barrier. For polycrystalline specimens though, the existing patch theories are hardly adequate in any case. Experimentally, one expects an "average" work function containing contributions from numerous patches of random orientation. For such specimens, there is little possibility of predicting the work function except by treatment of the vapor phase which relates to the bulk properties only.

Evaluation of Group VIA-Re Intermediate Phases for Possible Thermionic Converter Applications

None of the materials of the present study displayed particularly low thermionic work functions. In general the work functions of these intermediate-phase materials was in the same range as their respective constituents, all of the work functions falling within the range 4.5 to 5.0 eV. This result was not particularly unexpected, since the materials are purely metallic. They were not expected to behave as some

of the refractory carbides, for example, in which the work function is often substantially lower than either of the constituents,

Despite the fact that the emission levels of metallic emitters are lower than almost all other classes of materials, they have, in the past, enjoyed broad applicability because of their mechanical strength and ruggedness. These very desirable properties were not observed in the materials of this study, however. As for resistance to mechanical shock, all five of the materials can only be described as being brittle in the extreme.

Brittle behavior was to be expected, of course, although possibly not to the extent that it was observed. Particularly in the σ-phase, with its curious arrangement of atoms packed together so tightly, brittleness is practically a hallmark. If, as in the present study, the material were to be used as a coating on a substrate of another metal, as most nonmetallic emitters are generally used, the problem is largely eliminated. However, the mechanical ruggedness argument cannot be invoked for the materials themselves.

As mentioned in Chapter I, radiative heat transfer away from the emitter material is important to the design of a thermionic converter, since it effects heating of the collector, thereby lowering the converter efficiency.

The spectral emittance is, of course, dependent on the temperature of the emitter, generally decreasing as the temperature is increased. As shown in the emission current tables of the previous chapter, the spectral emittances of the materials vary between 0.65 and 0.70 at 1000C to between 0.54 and 0.62 at 1650C, observed.

These values are typical of the comparatively "rough" surfaces obtained by electrophoretic deposition of particles and are generally

higher than one would expect from a polished surface. For example, the emittance of tungsten is about 0.44 in the same range of temperatures. Were the materials to be used in the form of a coating, then, one would expect the converter efficiency to be lower than for a pure metal emitter, say tungsten or rhenium with a polished surface, particularly at the lower temperatures.

With the possible exception of Re_3Cr_2, the materials do seem to display high thermodynamic stability at elevated temperatures. No formal investigation of this nature was undertaken, but noticeable reactions of the coatings with the substrates were never observed, and no measurable loss of constituents in the vapor phase could be detected. The temperature of the Re_3Cr_2 diode was limited to 1400C as a precaution against such losses, however.

Because of the purely metallic nature of the materials, they almost surely would have characteristic long life expectancies as thermionic emitters, being immune from the rigors of donor depletion and not requiring the activation procedures frequently encountered with oxides and numerous semiconductor materials. They appear not to be easily poisoned by gaseous impurities as are some oxides and many refractory coatings.

From the above discussion, then, one may infer that the intermediate phase materials of this study have generally the same thermionic characteristics as the pure refractory metals in Groups VIA and VIIA. However, they are without the notable advantage of mechanical ruggedness that is characteristic of their constituents. The present state-of-the-art seems to require that these materials be handled in the manner of ceramic materials during fabrication, with the attendant spectral emittances which are higher than one might wish. With respect

to thermionic converter applications then, the author is of the opinion that the materials of this study must be considered inferior to either pure rhenium or tungsten, and possibly molybdenum as well.

BIBLIOGRAPHY

BIBLIOGRAPHY

1. P. Goodman and H. Homonoff, "A Study of Materials for Thermionic Converters, " Summary Report No. 1, Document No. ARA-1029, Allied Research Associates, December 31, 1961.

2. G. A. Haas, "Thermionic Electron Sources, " NRL Report 5657, Naval Research Laboratory, October 6, 1961.

3. C. G. Wilson, "Order in Binary σ-Phases, " Acta Cryst. 16, 724, (1963).

4. W. Hume Rothery, Atomic Theory for Students of Metallurgy, The Institute of Metals, London, 387, (1962).

5. J. M. Dickinson and L. S. Richardson, "Rhenium-Molybdenum Alloys, " 'and "Rhenium-Tungsten Alloys" (two articles), Trans. ASM 51, 1055, 758, (1959).

6. E. M. Savitskii and M. A. Tylkina "Alloys of Rhenium with Metals Having High Melting Points," Zhur. Neorg. Khim. 3, 820, (1958).

7. H. B. Michaelson, "Work Functions of the Elements, " J. Appl. Phys. 21, 536, (1950).

8. H. B. Wahlin, "The Thermionic Properties of Chromium, " Phys. Rev. 73, 1458, (1948).

9. A. D. Paddock and C. B. Magee, "Determination of the Work Functions of Selected Metals and Inorganic Compounds, " Summary Report No. 2344, Denver Research Institute, August 5, 1966.

10. W. A. Wood, "Note on the Preferred Orientation of the Crystallites of Electro-deposited Hexagonal Cromium, " Phil. Mag. 24, 772, (1937).

11. H. C. Rentschler and D. E. Henry, "Effect of Oxygen upon the Photoelectric Thresholds of Metals, " J. Opt. Soc. Am. 26, 30, (1936).

12. O. Klein and E. Lange, "Die Elektronenaustrittarbeiten der Metalle, " Zeit. f. Electrochemie 44, 542, (1938)

13. M. H. Nichols, "Average Thermionic Constants of Polycrystalline Tungsten Wires, " Phys. Rev. 78, 158, (1950).

14. R. C. Jerner, "Thermionic Properties of Polycrystalline Zirconium, Beryllium and Selected Zirconium Beryllides, " Dissertation, University of Denver, 28, (1965).

15. C. Agte et al., "Physical and Chemical Properties of Rhenium, " Zeit. f. Anorg. und Allgem. Chemie 196, 137, (1931).

16. R. Levi and G. A. Esperson, "Preparation of Rhenium Emitters and Measurement of their Thermionic Properties, " Phys. Rev. 78, 231, (1950).

17. O. K. Husmann, "Porous Ionizer Evaluation, " Progress Report No. 5, Hughes Research Laboratories, April 16, 1965.

18. C. Herring and M. H. Nichols, "Thermionic Emission, " Revs. Mod. Phys. 21, 22 185, (1949).

19. V. L. Stout, "Thermionic Emission and Thermionic Power Generation, " in Thermoelectricity, P. H. Egli, (Ed.) Wiley, New York, 209, (1958).

20. E. B. Hensley, "Thermionic Emission Constants and their Interpretation, " J. Appl. Phys. 32, 301, (1961).

21. L. V. Azaroff and J. J. Brophy, Electronic Processes in Materials, McGraw-Hill, New York, 305, (1963).

22. W. Schottky, "Cold and Hot Electron Discharge, " Zeit. f. Physik 14, 63, (1923).

23. G. A. Haas and J. T. Jensen, Jr., "Thermionic Properties of UC," J. Appl. Phys. 31, 1231, (1960).

24. I. Langmuir, "The Effect of Space Charge and Residual Gases on Thermionic Currents in High Vacuum," Phys. Rev. 2, 450, (1913).

25. A. D. Paddock, University of Denver, Private Communication. See also reference 9.

26. G. A. Haas, Naval Research Laboratory, Private Communication.

27. D. W. Juenker, "Electron Emission in Moderate Accelerating Fields," J. App. Phys. 28, 1398, (1957).

28. G. F. Smith, "Thermionic and Surface Properties of Tungsten Crystals," Phys. Rev. 94, 295, (1954).

29. E. W. Müller, "Work Function of Tungsten Single-Crystal Planes Measured by the Field Emission Microscope," J. Appl. Phys. 26, 732, (1955).

30. E. Wigner and J. Bardeen, "Theory of Work Functions of Monovalent Metals," Phys. Rev. 48, 84, (1935).

31. G. Herrmann and S. Wagener, The Oxide Coated Cathode Vol. 2, Chapman and Hall, London, 17, (1951).

32. H. Homonoff and S. Ruby, "Study of Materials for Thermionic Converters," Summary Report No. 2, Document No. ARA-T-9159-2, Aracon Laboratories, December 31, 1962.

33. E. P. Wohlfarth, "Thermionic Emission Constants and Band Overlap," Proc. Phys. Soc. 60, 360, (1948).

34. W. B. Nottingham, "Thermionic Emission," Handbuch der Physik Vol. XXI, Springer-Verlag, Berlin, 1, (1956).

35. E. P. Abrahamson and N. J. Grant, "Brittle and Ductile Transition Temperatures of Binary Chromium-Base Alloys," Trans. ASM 50, 705, (1958).

36. C. F. Leitten, Jr., "Pyrolytic and Chemical Vapor Decomposition Studies," ORNL Report No. 3470, Oak Ridge National Laboratory, May 31, 75, (1963).

37. R. Holzl, San Fernando Laboratories, Private Communication.

38. K. B. Blodgett and I. Langmuir, "The Design of Tungsten Springs to Hold Tungsten Filaments Taut," Rev. Sci. Instr. 5, 321, (1934).

39. G. L. Tawney, "Zigzag and Helical Springs; Elastic Properties of Molybdenum," Rev. Sci. Instr. 10, 152, (1939).

40. G. A. Haas and F. H. Harris, "High-Accuracy X-Y Pulse Measuring System," Rev. Sci. Instr. 30, 623, (1959).

41. A. G. Worthing, "The True Temperature Scale of Tungsten and its Emissive Powers at Incandescent Temperatures," Phys. Rev. 10, 377, (1917).

42. M. F. Angell, "Thermal Conductivity at High Temperatures," Phys. Rev. 33, 422, (1911).

43. J. D. Plunkett, "The Total and Spectral Normal Emissivities of Carbon and Graphite," Dissertation, Massachusetts Institute of Technology, 161, (1961).

44. L. G. Parratt, Probability and Experimental Errors in Science, Wiley, New York, 131, (1960).

45. W. Hume-Rothery and G. V. Raynor, The Structure of Metals and Alloys, The Institute of Metals, London, 210, (1962).

46. A. G. Knapton, "An X-Ray Survey of Certain Transition-Metal Systems for Sigma Phases," J. Inst. of Metals 87, 28, (1958-59).

47. W. Hume-Rothery, H. M. Irving and R. J. P. Williams, "The Valencies of the Transition Elements in the Metallic State," Proc. Roy. Soc. 208, 431, (1951).

48. A. J. Bradley and G. D. Preston, apparently unpublished work cited by W. Hume-Rothery and G. V. Raynor, (see reference 45), 85.

49. G. V. Samsonov, et al., "The Relation of Thermo-Emission Constants (and Their Compounds With Some Metalloids) to their Electronic Structure," Radio Engineering and Electronic 2, No. 5, 155, (1957).